Fabrication and Characterization of Diamond Whiskers for Application in Electron Emitter Devices

李朝陽

Chaoyang Li

A dissertation submitted to
Kochi University of Technology
in partial fulfillment of the requirements
for the degree of
Doctor of Philosophy

Graduate School of Engineering
Kochi University of Technology
Kochi, Japan

September, 2006

Fabrication and Characterization of Diamond Whiskers for Application in Electron Emitter Devices

李朝陽

Chaoyang Li

A dissertation submitted to
Kochi University of Technology
in partial fulfillment of the requirements
for the degree of
Doctor of Philosophy

Special Course for International Students
Department of Electronic and Photonic System Engineering
Graduate School of Engineering
Kochi University of Technology
Kochi, Japan

September, 2006

ABSTRACT

This work is the author's doctor's thesis worked at Department of Electronic and Photonic System Engineering of Kochi University of Technology, Japan. This research concerns the fabrication of diamond whiskers on the diamond films and characterized the diamond whiskers by Raman spectroscopy, Cathodoluminescence spectroscopy, and Energy dispersive X-ray spectroscopy. The field emission properties from diamond whiskers were investigated. The following seven chapters institute this thesis.

Chapter 1 Introduction

The general introductions on history and applications of the electron emission are given. The unique characteristics of diamond are illustrated and the advantage of applied diamond as electron emitter is discussed. The novel methods for fabrication of diamond whiskers are demonstrated. The purpose and the significance of this research work are pointed out.

Chapter 2 Synthesis of diamond film using microwave plasma chemical vapor deposition

The history of synthesis of diamond technique is introduced. Synthesis of polycrystalline diamond film using microwave plasma chemical vapor deposition (MWCVD) method is described. Basic deposition theory, experimental apparatus, deposition processes and experimental results are explained in detail.

Chapter 3 Fabrication of diamond whiskers using Ar/O_2 radio frequency plasma etching

The radio frequency plasma etching of CVD diamond film has been investigated in Ar, O_2 and Ar/O_2 mixtures, with an emphasis to elucidate the effects of reacting gases on the fabrication of diamond whiskers. The concerning apparatus (sputter device and radio frequency reactor) and their operation principles are illustrated. Diamond whiskers are formed on diamond films which previously coated with aluminum. It is found that diamond whiskers preferentially formed at the diamond grain boundaries, then on the diamond crystal surface with increasing of volumetric ratio of O_2 to Ar. The relationship between the distribution of diamond whiskers and the O_2 ratio is discussed in detail. The plasma etching mechanism is analyzed. The function of Al coating on fabrication of diamond whiskers is also considered.

Chapter 4 Effects of metal mask on formation of diamond whiskers in O_2 radio frequency plasma etching

As-grown and metal-coated CVD diamond films are etched in an oxygen (O_2) radio frequency plasma. In this study, Molybdenum (oxidizable) and Nickel (non-oxidizable) are used as coating materials represents. The distributions of the whiskers are investigated and compared for different samples. A Field Emission Scanning Electron Microscopy (FESEM) is used to inspect the diamond surfaces before and after etching. It is found that the coating metal with oxidizability contributes efficiently to the anisotropic etching. The effects of different metals(oxidizability and nonoxidizablity) on fabrication of diamond whiskers are compared in details.

Chapter 5 Characterization of diamond whiskers

In order to characterize obtained diamond whiskers, Raman spectroscopy, Energy dispersive X-ray spectroscopy and Cathodoluminescence spectroscopy are used to analysis after etching processes. The basic theories of these 3 devices are illustrated. Raman spectroscopy is used to analysis the qualities of diamond and whiskers. It shows that the structural quality of nanowhiskers is almost as same as that of non-etched diamond film, sp^3 bonding structure in the whiskers is dominated.

Energy dispersive X-ray spectroscopy is used to analysis the components of the obtained whiskers. It clearly showed the metal oxide capped on the diamond whiskers, serving as mask during the etching process, contribute to the formation of diamond whiskers. There is no metal found on the over-etched area. The EDX mapping measurement also confirmed that the metal oxide, following as the shape of the diamond particles, formed on the diamond surface.

Cathodoluminescence spectroscopy (CL) measurement is carried out using a Topcon 350 type scanning electron microscope (SEM). The CL spectra are taken at 21 points along a line crossing the boundary between whiskers and diamond on each sample, an interval of 20 μm between the investigated points is considered. The results showed the average luminescent intensity of the whiskers obtained on oxidizable metals coating diamond surface is almost the same as that of the as-grown diamond film. However, the significantly decreased luminescent intensity is observed on whiskers obtained on non-oxidizable metal coating diamond films.

Chapter 6 Electron field emission characteristics of diamond whiskers

The field emission theory and measured method are introduced. Electron field emission

characteristics of nanowhiskers are investigated in a specially designed field emission system installing in an SEM vacuum chamber. The emission site can be defined precisely to micro area and anode-cathode (samples) distance can be precisely set up.

I-V characteristics of whiskers obtained from different metal coated diamond surface are investigated in details. All of the whiskers showed field emission behavior, demonstrating as good linearity in the Fowlor-Nordheim (F-N) diagram.

Diamond whiskers showed improved field emission property and better thermal conductivity comparing non etched diamond film which had damaged surface when apply the same voltage on them.

Chapter 7 Conclusions

The main results obtained from this research work are summarized.

ACKNOWLEDGEMENTS

TABLE OF CONTENTS

LIST OF FIGURES

LIST OF TABLES

ACKNOWLEDGEMENT

The research work for this thesis was performed in the Hatta Laboratory, Department of Electronic and Photonic System Engineering, Kochi University of Technology during the years 2003 to 2006.

I would like to express my deepest gratitude to my supervisor, Professor Akimitsu Hatta, for providing me the possibility to join his group for three years. In addition, I owe him my sincere appreciation for his guidance and encouragement during this work. I would also like to thank him for support me to join in several international conferences to get more helpful information for writing this thesis.

I would like to thank Professor Hiroshi Kanbe, Professor Takashi Katoda, Professor Tadashi Narusawa, Associate Professor Michio Watamori for their helpful discussions and encouragement.

Professor Hisao Kanda, director of diamond group in Advanced Materials Laboratory, National Institute for Materials Science, Japan, is sincerely acknowledged for the help to analysis samples as well as for his advice and guidance during this work.

I would like to thank all my colleagues at the Hatta group for the innovative and pleasant working environment. Especially I owe my thanks to Mr. Hiroaki Yoshimura, Mr. Hiroaki Kanakusa, Mr. Yusuke Aoki for their help. I am most grateful to Dr. Nan Jiang for his encouragement, friendship, and for the numerous discussions.

Finally, I owe warm thanks to my parents, my brother for their love and encouragement during these years.

My sincerely thanks belong to my dear husband and my daughter, for all of love, patience, and encouragement. Thank you for standing by me during both good and bad times.

Chaoyang Li

August 2006

Caption of Figures

Caption of Tables

CHAPTER 1

INTRODUCTION

Diamond has been considered as a special material due to its wide range of extreme properties, which make it possible to use in many potential applications as an engineering material. Apart from the applications of cutting tools, thermal management, optics, diamond is gradually beginning to appear in electronic applications. Especially, one potential application which is causing a great deal of interest at the moment is the idea of using diamond nanostructure (nanometer scale tip emitter) as an electron emitter in flat panel displays. It has been found that the tip emitters will produce highly efficient emission. This research concerns a very important issue of the field emitters: Tailor diamond into nano-sized needle-like structures which we named them as whiskers. In this research, one kind of novel technique was used to fabricate diamond nano-whiskers and the characteristics of diamond whiskers were analyzed.

1.1 History and perspective of diamond electron emitter

1.1.1 History of study on electron emission

Electron emission from solid is a fundamental process underlying electrical transmission in a gas or vacuum, and as such, was among the earliest phenomena to be observed scientifically. In the middle of eighteenth century, Jean-Antoine Nollet and William Morgan conducted experiments showing that the passage of electrical discharge in partially evacuated tubes produced a glow between the electrodes. In the nineteenth century, Johann Hittorf and Sir William Crookes independently investigated the radiation produced by a cathode in a vacuum tube, demonstrating that an invisible “light” was produced which caused glass to fluoresce and cast shadows.

In 1884, Thomas Edison obtained a patent for a thermionic emission device, consisting of an incandescent wire in an electric field within an evacuated envelop, which was the forerunner of amplifier tubes. In 1897, Joseph John Thompson demonstrated that these cathodic rays were actually beams of negatively charged particles (electrons).

In 1905, Albert Einstein used a quantum theory to explain the sharp threshold value for photoemission with respect to wavelength.

In 1922, Lilienfeld [1] demonstrated that an X-ray tube with a pointed cold cathode passed a current of a few milliamperes when subjected to a strong electric field.

A first attempt to explain the emission of electrons from cold metal at high field strengths was

made by Schottky [2] who attempted to correlate the various electron emissions, including the thermionic and field emission. The Schottky effect is accompanied by quantum tunneling, because of the finite width of the barrier. In 1928, field emission effects were summarized in the Fowler-Nordheim relation equation which became a classical theory in the field emission study by Fowler and Nordheim [3].

In 1923 and 1935, Zworykin invented ionoscope and multiplier phototubes, respectively, which set the stage for television and video camera.

The cathode ray tube (CRT), equipped with a phosphorescent screen, become the basic device for translating electronic signals into visual displays. Modern CRT devices rely on electron guns based on field emission, which provided greater life, brightness, and focusing ability than the thermionic or photoemission sources. The electron source in CRT incorporated a magnetic deflector, which moves the electron beam across the phosphorescent background at a constant rate to create a two dimensional images from an essentially one dimensional electronic signal. The electron beam technology was developed after 1945 and widely application in the 1950's and early 1960's. A conventional display is shown in Fig. 1.1

Since the flat display monitor appeared in 1991, one of the technologies being tipped as representing the future of flat panel displays was the FED or Field Emission Display. The schematic of FED display is shown in Fig. 1.2. In field emission displays, electrons come from millions of tiny microtips passing through gates and lighting up pixels on a screen. The principle is similar to that of cathode-ray-tubes in television sets. The difference is: Instead of just one "gun" spraying electrons against the inside of the screens faces, the FED uses multiple electrons emitters to excite phosphors pixel in the display. There are as many as 500 million of microtips inside. The first generation of FEDs uses tiny, conical electron emitters (known as a "Spindt tip") which need very complex technique to fabricate. Therefore, in the future there would be visions using nanostructure materials as electron emitters which have a more efficient electron emission than the Spindt tip [4]. Nonastructural diamond is considered as a potential candidate for application in this field.

At present, many research groups in the world are working at fabrication of the different types of electron emitter with efficient electron emission.

1.1.2 Electron emitter using diamond

Diamond is a crystalline form of carbon, a group-IV element in the periodic table. The diamond cubic structure is shown in Fig. 1.3 [5]. It may be seen as two interpenetrating face–centered cubic (fcc) sublattices with one displaced from the other by one-quarter of the distance along a diagonal of the cube. The measured cubic edge is 3.567 Å.

Diamond can be used in various fields due to its different properties. Diamond has an

exceptional hardness that suggests it being a suitable material to be used in ultrasound technology [6-10]. Diamond is chemically inert at the room temperature and pressure. Therefore diamond is biologically compatible and could be used in sensors in biological and medical environment [11-14]. Optical using of diamond for different wavelength regions is due to its transparent over a wide spectral range [15-20]. The using of diamond as a heat sink for electronic equipment is because diamond has the highest thermal conductivity coefficients [21-23]. The properties of diamond were concluded in Table 1.1.

Since the success of low temperature and low pressure diamond film deposition, diamond is considered to be used in electron device, especially, employed as a field emitter which has been studied in many groups [24-28].

As mentioned above, many groups in the world are working at discovering new materials and methods which can be used in the field emission device. Most of materials can not be used since they are insulator owing to low charge-carrier concentrations, low mobility, and high trap densities. However, diamond can be doped either n-or p-type and grown with low trap densities and high carrier mobility, making it a semiconductor. Another reason is the unique properties of chemical vapor deposition (CVD) diamond films, which was mentioned before. Among the various applications of diamond, the field emission from diamond was considered as one interesting study area. [29-32], in which diamond is called a cold cathode which means that field emission is the emission of electron from a solid under an intense electric field, usually at ambient temperature [33]. The diamond can be used in the cold cathode device due to the unique property of diamond. The negative electron affinity (NEA) property of diamond first mentioned by Himpsel [34], unlike other materials, is stable in a residual gas ambient. In addition, the strongly bonded diamond crystal structure allows the realization of diamond field emission devices operating with maximum stability and reliability. The comparison of the diamond structure and graphite is shown in Fig. 1.4. Diamond shows a much more stable structure. Furthermore, diamond can operate at high temperature or high power because of its very high electrical breakdown field and high thermal conductivity, properties highly beneficial to field emission applications. The most attractive property might be its presentation of a rather small barrier to the emission of electrons into a vacuum.

Recent study paid more attention to nanostructure materials. One interesting example is nano-sized diamond structures that may have interesting properties like better optical transmission, high density of defect cores, enhanced quantum electronic conduction, and good field electron emission [35-38]. Therefore, the nanometer structure of diamond is pursued in this research. It is expected that diamond nanostructures will be used as field emitter replacing the conventional metal electron emitter.

1.1.3 State-of-the-art of diamond as electron emitter

Duo to its unique characteristics, diamond is an excellent material for electron field emitter. Extensive studies of electron emission from diamond have been carried out by different groups since the first report of electron emission from diamond in 1991 [39-43].

The most widely considered device is the field emission displays (FEDs). Because FEDs require a reliable and efficient cold cathode material as electron field emitter. Earlier field emitters typically employed metal (such as Mo) or semiconductor (such as Si) with nanometer-sized sharp tips. They have demonstrated reasonable emission characteristics with stability and reproducibility necessary for practical application. However, the control voltage required for emission from these materials is relatively high (~100 V) because of their high work functions. The high voltage operation increases the damaging instabilities due to ion bombardment and surface diffusion of the emitting tips and necessitates high power density to be supplied from an external source to produce required emission current. In addition, fabrication of the uniform sharp tips over a large area proves to be a difficult and expensive process. All of the disadvantages evoke researchers to find an alternative emitter material. Diamond films are regarded as one of such candidates because of its high thermal conductivity, chemical stability and robustness, and negative electron affinity.

From the early cold emission studies of diamond, two approaches were formulated that originated from different research fields [42]. The first approach, developed by the “diamond” community, assumed that only the material properties (low work function, negative electron affinity, etc.) were keys for controlling emissivity. This approach resulted in the development of “planar” cold cathode that would become revolutionarily next generation electron emission devices replacing “classical” field emission tips. It was postulated that flat structures could be manufactured cheaply and an efficient electron source could be produced by a process not requiring submicron scale techniques, a drawback of sharply pointed field emitters. The other approach came from the “field emission” community. The cathode geometry was always considered a key factor and the cathodes were fabricated by deposition of thin coating onto the ends of sharply pointed field emission tips.

At present, there comes a new idea of directly using nanostructure diamond to replace the electron emitter, the schematic of the diamond nanostructure used in the field electron emitter is shown in Fig. 1.5. There are now a lot of evidences that the very low switch-on field reported for the electron emission from diamond film appears to be geometric field enhancement. Based on the observation in the diodes of high current electron accelerators developed by Parker *et al.* [44] and Mesyats [45], respectively, it was found that as the field emission process at a cathode point develops to explosion of the point and plasma formation, the current moves from pure field emission to a space charge limited flow governed by the Child-Langmuir equation. However, the ions produced, together with those from the anode or elsewhere, act to reduce the space charge in the gap, and hence a greater current, which further heats the electrodes to cause yet more plasma

with its ions; *i.e.* a “runaway” situation is created. A potential difference of several tens of volts then develops over the Debye length between the metal of the cathode emitting site and the plasma. The resulting electric field is sufficient to produce further intense electron emission. The principle is shown in Fig. 1.6 [46]

However, the potential merits of diamond cold cathode may not be utilized without control of electron emission sites on the diamond surface. Successful definition of electron emission sites and concomitant effective emission have been achieved by way of shaping diamond films into micro- or microtips [47] either by a transfer mold technique using (100) Si inverted pyramidal mold [48, 49] or by dry etching of diamond via sputter faceting of silicon oxide dot mask on the diamond film [50]. Single crystal diamond emitter with very sharp tips [51] and whiskers of less than 5 nm [52] were already fabricated by using a reactive ion etching system [53]. However, polycrystalline diamond is far from realization by the microtechnique.

1.2 Scope and objective of this work

As described above, CVD film is an excellent material which can be used in electron field emitter. Micro- or nano-fabrication of diamond is one of the most important techniques in fabrication of electron emission device for the coming generation. However, the high hardness and chemical inertness of diamond make it difficult to fabricate the diamond with an arbitrary shape. So far, many efforts have already been made to fabricate various structures on diamond for application. Considering the requirement of the electron emitters in FED display, nano-structure diamond is pursued in this research. Two main points are focused on in this work: (1) Fabrication of diamond nanowhiskers and (2) characterization of diamond nanowhiskers for field emission application.

In order to obtain nano-structural diamonds (named as diamond nanowhiskers), one novel method, in opposition to the growing up technique (like fabrication of nanotube), of using radio frequency (RF) plasma etching diamond film to fabricate diamond nanowhiskers was considered.

Although the synthesis technique of diamond film is extensively developed, up to date, practically using of polycrystalline diamond in devices is still far from the expected goals. In this research, CVD was chosen to synthesis polycrystalline diamond for using due to considering of the lower fabrication cost in the future market.

Three steps, as shown in Fig. 1.7, are critical processes to fabricate diamond whiskers:

1) The first step: Polycrystalline diamond films are deposited on Si substrate using microwave plasma chemical vapor deposition (MWPCVD) technique. Although the MWPCVD is a feasible method to deposit diamond film, deposition conditions are very important for diamond film growth. Therefore, the optimum conditions should be investigated.
2) The second step: Coating of diamond films with different metals using sputtering

technique. According to the etching requirement, different coating conditions should be applied by adjusting the sputtering conditions.

3) The third step: Etching diamond films in O_2 or Ar/O_2 radio frequency plasma reactor. Until now, the mechanism of the etching is still unclearly, so that the effective factors on fabrication of diamond whiskers should be investigated in detail, for instance—working gas composition, coating metals, and etching time. In our research, the etching conditions and influence factors were examined systematically.

The characteristics of diamond nanowhiskers were analyzed in Raman spectroscopy, Energy dispersive X-ray spectroscopy (EDX), and Cathodoluminescence spectroscopy (CL). These analysis results help to explore the mechanism of the radio frequency plasma etching of diamond films, as well as to elucidate the function of fabricating techniques such as metal coating.

It is also necessary to investigate the field emission property for application as emission emitter. In the last part of the thesis, I-V characteristics of diamond nanowhiskers were presented. The possibility of using nanowhiskers in the emission emitter was confirmed.

In this research, the size of diamond crystallites was controlled. Different CH_4 ratios were introduced during the deposition system. In chapter 2 of this thesis, a detailed description about depositing polycrystalline diamond film using MWCVD is given.

The surface treatment or shaping diamond into micro, nano size shapes remains a bottle-neck in this field. In this work, radio frequency plasma reactive ion etching (RIE) was performed to tailor the diamond crystallites. In this technique, the etching rate, anisotropy, aspect ratio, control of the lateral size and roughness of the etched surface were usual criteria for the quality nanowhiskers.

In this research, the nano diamond whiskers (with 20 nm diameter) were initially obtained under the optimum etching conditions [54]. The effective factors on formation of diamond nanowhiskers were determined. The functions of metal coatings were investigated firstly in this work, and oxidizable metals were found to remarkably inhibit the etching rate during the etching process [55].

The organization chart of this thesis is shown in Fig. 1.8.

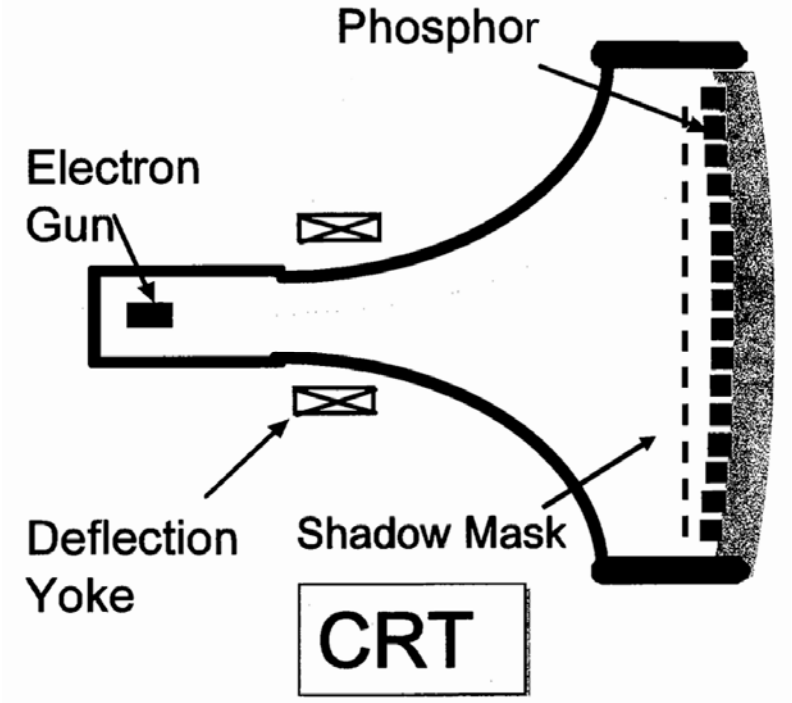

Fig. 1.1. Traditional CRT display.

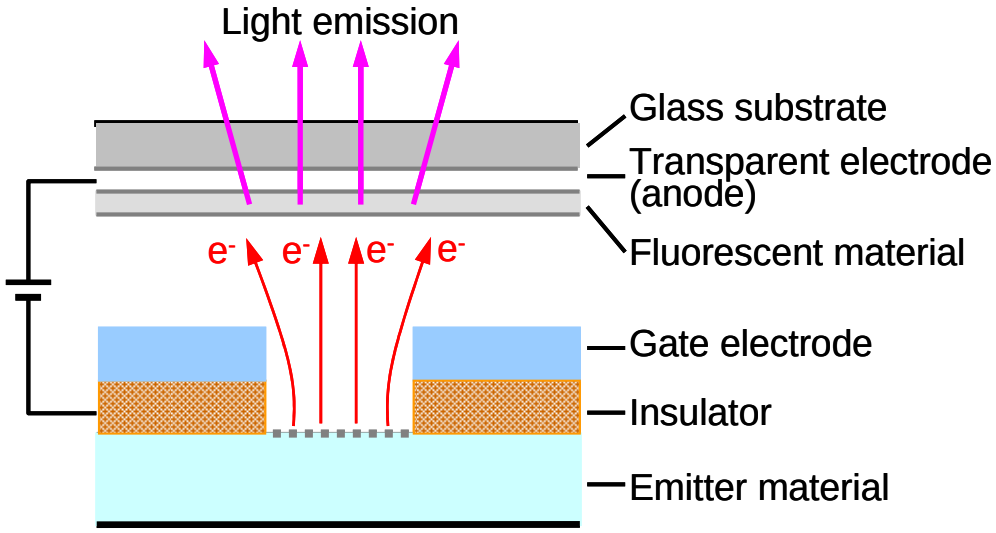

Fig. 1.2. Schematic of FED display.

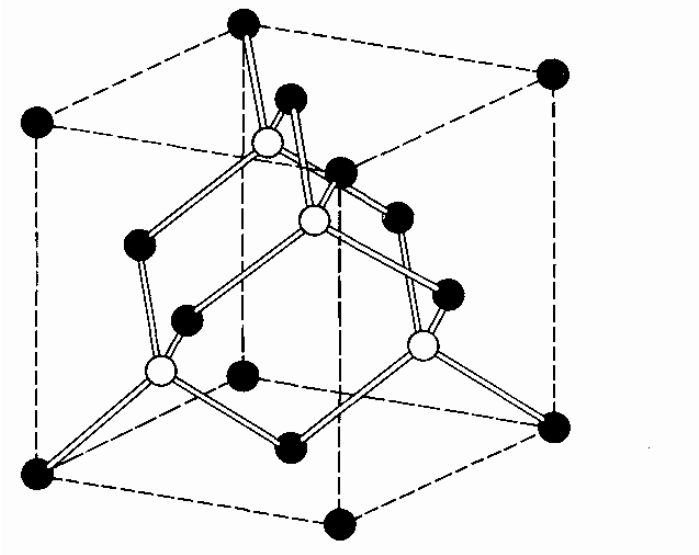

Fig. 1.3. Diamond cubic structure [5].

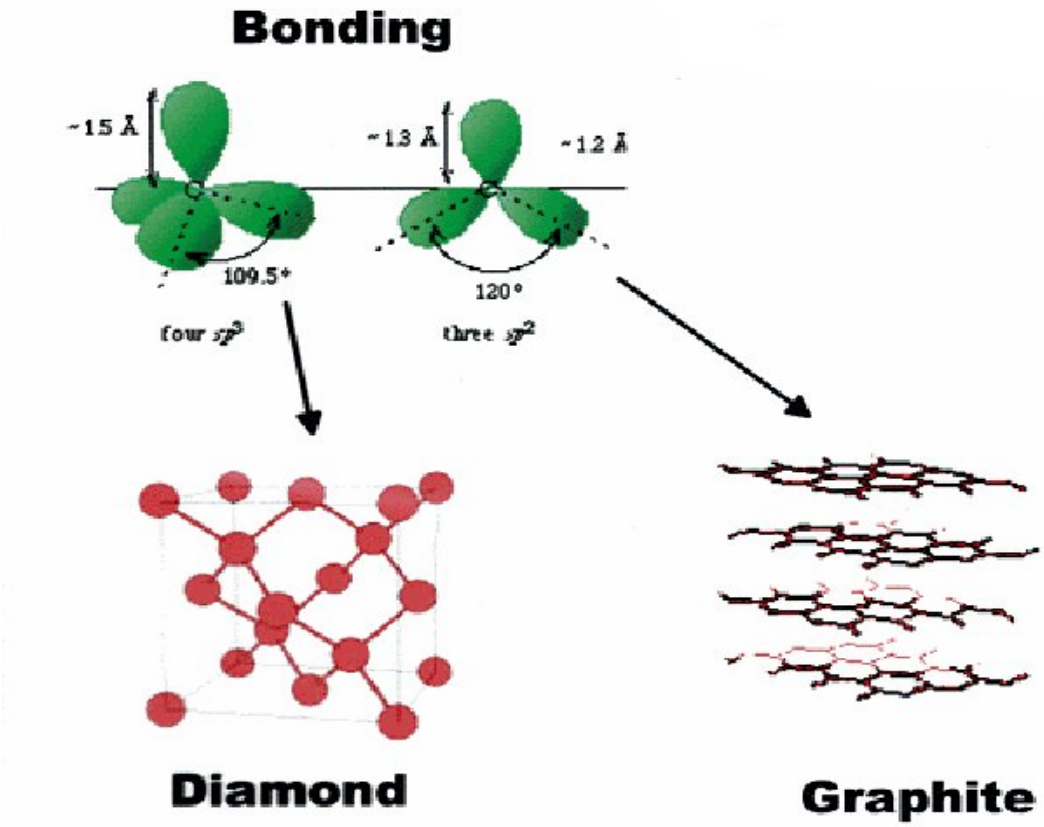

Fig. 1.4. Comparison of diamond and graphite bonding structures.

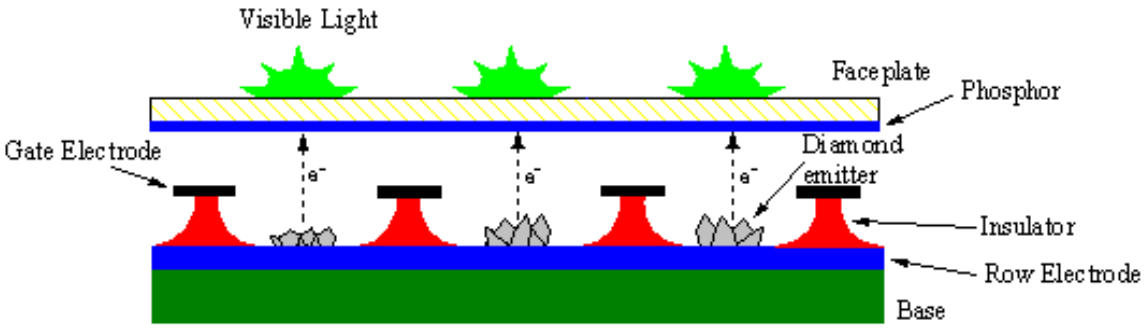

Fig. 1.5. Field emission display using nanostructure diamond as emitters.

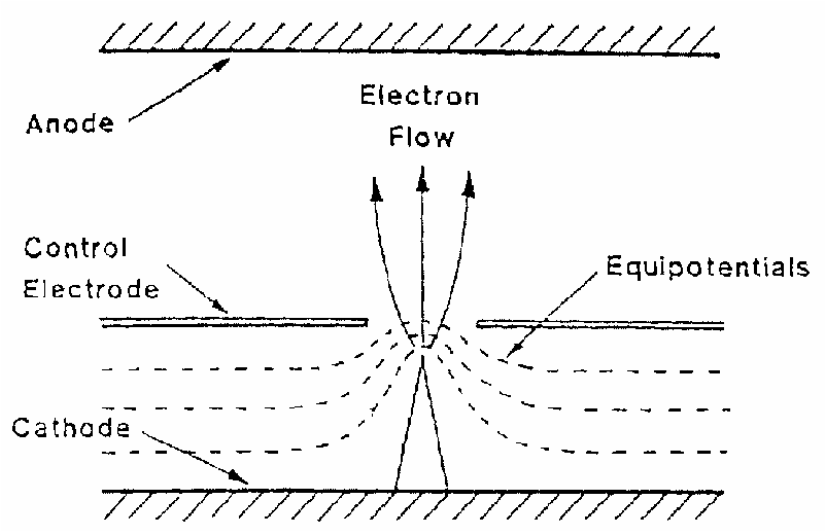

Fig. 1.6. Illustration of field enhancement and electron emission from a needle-shaped emitter.

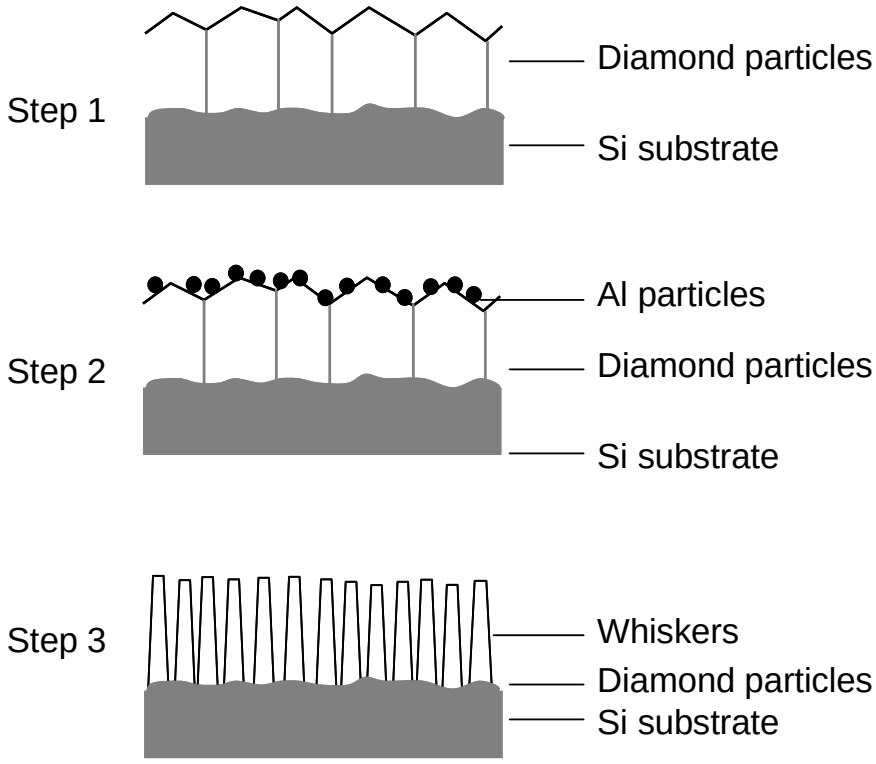

Fig. 1.7. Schematic of the diamond whiskers fabrication process (a) deposit diamond film on the Si wafer, (b) coating metal on the diamond film by DC sputter device, and (c) diamond whiskers obtained by etching diamond film in the radio frequency plasma.

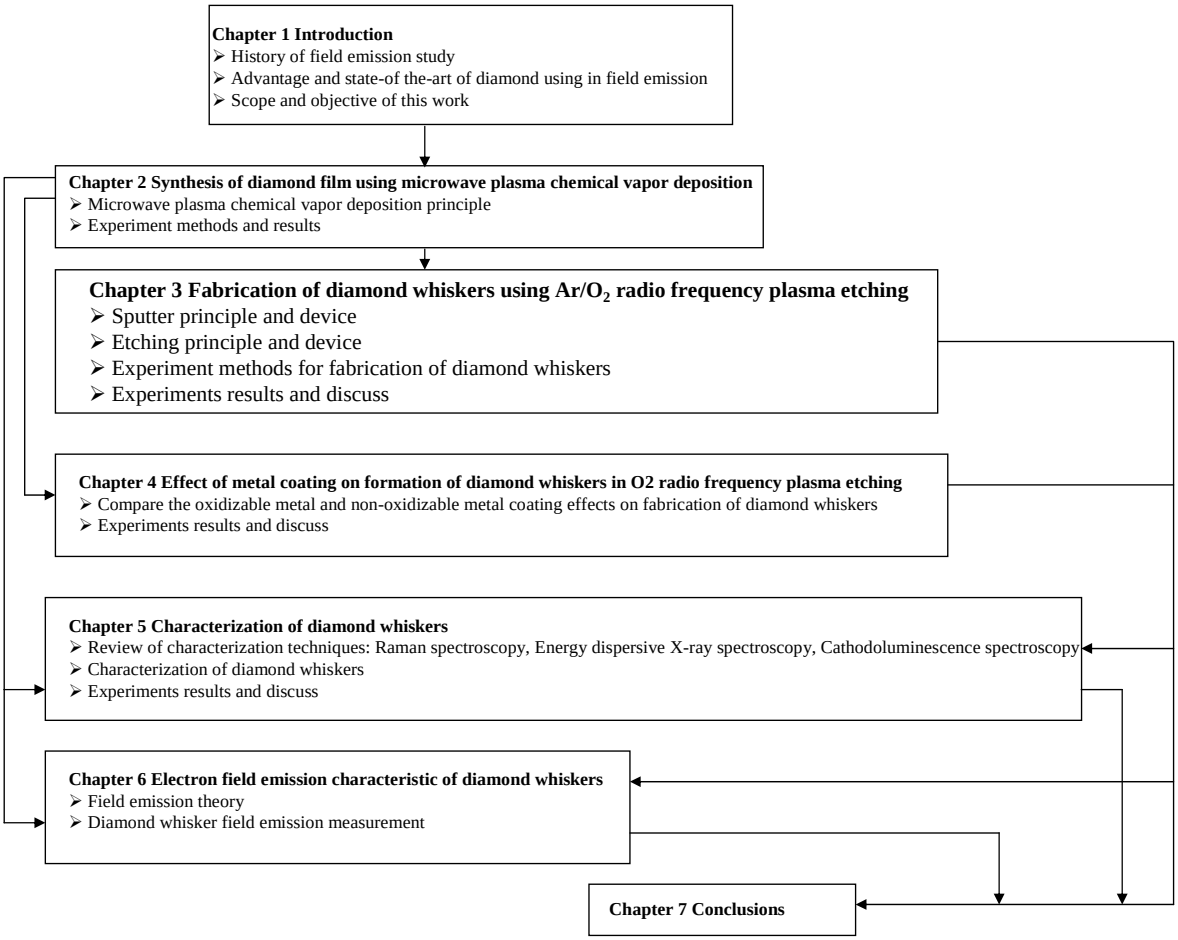

Fig. 1.8. Organization chart of the thesis.

References

[1] J. E. Lilienfeld, Phys. Z., **23**, 506 (1922).

[2] W. Z. Schottky, Phys., **14,** 80 (1923).

[3] R.H. Fowler and L.W. Nordheim, Proc. Roy. Soc. A, **119,** 173 (1928).

[4] C. A. Spindt, I. Brodie, L. Humphrey, and E. R. Westerberg, J. Appl. Phys., **47**, 5248 (1976).

[5] J. Wilks, E. Wilks, "Properies and Applications of Diamond" Butterworth-Heinemann Ltd 1991, p.28-29

[6] C. H. Goeting, F. Marken, R. G. Compton and J. S. Foord, Chem. Commun., **17**, 1697 (1999).

[7] C. H. Goeting, J. S. Foord, and R. G. Compton, Diam. Relat. Chem., **8**, 824 (1999).

[8] A. J. Saterlay, S. J. Wilkins, C.H.Goeting, J. S. Foord, R. G. Compton, and F. Marken, J. Solid State Electrochem., **4**, 383 (2000).

[9] K.B. Holt, J. Del Campo, J.S. Foord, F. Marken, J. Electronal Chem., **94,** 513 **(**2001).

[10] E. Pace, A. Pini, G. Corti, F. Bogani, A. Vinattieri, C.S.J. Oickles, and R. Sussmann, Diam. Relat. Chem., **10**, 736 (2001).

[11] T. N. Rao, I. Yagi, T. Miwa, D. A. Tryk, and A. Fujishima, Anal. Chem., **71**, 2506 (1999).

[12] A. Denisenko, A. Aleksov, and E. Kohn, Diam. Relat. Chem., **10**, 667 (2001).

[13] N. Spataru, B.V. Sarada, E. Popa, and A. Fujishima, J. Electrochem. Soc., **E112,** 148 (2001).

[14] K. Ohnishi, Y. Einaga, H. Notsu, C. Terashima, T. N. Rao, S. G.. Park, and A. Fujishima, Electrochem. Solid State Lett., **D1**, 5 (2002).

[15] J. K. Zak, J. E. Butler, and G. M. Swain, Anal. Chem., **73**, 908 (2001).

[16] C. S. J. Pickles and T.D. Madgwick, Diam. Relat. Chem., **9,** 1726 (2000).

[17] S. E. Coe and R.S. Sussmann, Diam. Relat. Chem., **9,** 1726 (2000).

[18] K. Hayabashi, S. Yamanaka, H. Watanabe, T. Sekiguchi, H. Okushi, and K. Kajimura, J. Appl., **81,** 744 (1997).

[19] R. Locher, J. Wagner, F. Fuchs, M. Maier, P. Gonon, and P. Koidl, Diam. Relat. Chemi., **4**, 678 (1995).

[20] G. Piantanida, A. Breskin, R. Chechik, O. Katz, A. Laikhtman, A. Hoffman, and C. Coluzza, J. Appl. Phys., **89**, 8259 (2001).

[21] A. Vlasov, V. Ralchenko, S. Gordeev, D. Zakharov, I. Vlasov, A. Karabutov, and P. Belobrv, Diam. Relat. Chem., **9**, 1104 (2000).

[22] J. L. Davidson, W. P. Kang, Y. Gurbuz, K. C. Holmes, L. G. Davis, A. Wisitsora-at, D.V. Kerns, R. L. Eidson, and T. Henderson, Diam. Relat. Chem., **8**, 1741 (1999).

[23] J. Lee, D. A. Tryk, A. Fujishima, and S. M. Park, Chem. Commun., 486 (2002).

[23] H. Murakami, M. Yokoyama, S. M. Lee, and T. Ito, Appl. Surf. Sci., **175**, 474 (2001).

[24] J. Ristein, Diam. Relat. Chem., **9,** 1129 (2000).

[25] J. B. Cui, J. Ristein, and L. Ley, Phys. Rev. Lett., **81,** 429 (1998).

[26] P. K. Baumann and R. J. Nemanich, J. Appl. Phys., **83**, 2072 (1998).

[27] T. P. Humphreys, R. E. Thomas, D. P. Malta, J. B. Posthill, M. J. Mantini, R. A. Rudder, G. C. Hudson, R. J. Markunas, and C. Pettenkofer, Appl. Phys. Lett., **70,** 1257 (1997).

[28] J. Vanderweide and R. J. Nemanich, Phys. Rev. B., **49**, 13629 (1994).

[29] R. U. Martinelli and D. G. Fisher, Proc. IEEE, **62**, 1339 (1974).

[30] J. L. Dye, Science, **247**, 663 (1990).

[31] E. S. Kohn, Appl. Phys. Lett., **18**, 272 (1971).

[32] M. O. Aboelfotoh and J. A. Lorenzen, J. Appl. Phys., **48**, 4754 (1977).

[33] J. R. Nonmember, IEICE Trans Electron., VOL. E 86-C, NO.5 May 2003.

[34] F. J. Himpsel, J. A. Knapp, J. A. Vanvechten, and D. E. Eastman, Phy. Rev. B **20**, 624 (1979).

[35] T-S. Yang, J-Y Lay, M-S Wong, and C-L Cheng, J. Appl. Phys., **92**, 2133 (2002).

[36] V P Mammana, TEA Santos, A Mammana, V Baranauskas, H J Ceragio and A C Peterlevitz, Appl. Phys. Lett. **81**, 3470 (2002).

[37] D M Gruen, MRS Bull, **9,** 32 (1998).

[38] B M Jin, J Kim and C C Kim, Appl. Phys, A **65**, 53 (1997).

[39] N.S. Xu, R. V. Latham, and Y. Tzeng, Electron. Lett., **29,** 1596 (1993).

[40] M. W. Geis,, J. C. Twichell, and T. M. Lyszczarz, J. Vac. Sci. Technol. B **14**, 2060 (1996).

[41] V. V. Zhirnov, E. I. Givargizov, and P. S. Plekhanov, J. Vac. Sci. Technol. B **13**, 418 (1995).

[42] V. V. Zhirnov and J. J. Hren, MRS Bull. **23**, 42 (1998).

[43] T. A. Railkar, W. P. Kang, H. Windischmann, A. P. Malshe, H. A. Naseem, J. L. Divison, and W. D. Brown, Crit. Rev. Solid State Mater. Sci. **25**, 163 (2000).

[44] R. K. Parker, R. E. Anderson and C. V. Duncan, J. Appl. Phys., **45**, 2463 (1974).

[45] G. A. Mesyats, IEEE Transactions on Plasma Science, **19**, 684 (1991).

[46] R. V. Latham “High Voltage Vacuum Insulation”, Academic Press INC., 377 (1995)

[47] T. Asano, Y. Oobuchi, and S. Katsuma, Technical Digest of 7th International Vacuum Microelectronics Conference, Grenoble, France, July 4-7, p.100, 1994.

[48] K. Okano, K. Hoshima, S. Koizumi, and J. Itoh, IEEE Electron Device Lett. **16**, 239 (1995).

[49] E-S. Baik, D. Jeon, and Y-J. Baik, Diamond Relat. Mater. **8**, 89 (1999)

[50] E-S. Baik, D. Jeon, and Y-J. Baik, Diamond Relat. Mater. **8**, 2169 (1999)

[51] Y. Ando, Y. Nishibayashi, H. Furuta, K. Kobashi, T. Hirao, K. Oura, New Diamond Front. Carbon Technol. **12**137 (2002)

[52] Y. Nishibayashi, Y. Ando, H. Furuta, K. Kobashi, K. Meguro, Mol. Cryst. Liq. Cryst. **386**, 183 (2002).

[53] Y. Nishibayashi, H. Saito, T. Imai, N. Fujimori, Diamond Relat. Mater. **9**, 290 (2000).

[54] C.Y. Li and A. Hatta, Diamond and Related Materials **14**, 1780 (2005).

[55] C.Y. Li and A. Hatta, Diamond and Related Materials **15**, 357 (2006).

CHAPTER 2

SYNTHESIS OF DIAMOND FILM USING MICROWAVE PLASMA CHEMICAL VAPOR DEPOSITION

2.1 Historical perspective of diamond synthesis technique

Diamond was considered to use in industrial processes not only using as gemstones since 1870 when extensive deposits were discovered in South Africa. By the beginning of last century geological evidence clearly implied that diamonds were formed deep in the earth where both the pressure and temperature were very high. In 1955, high pressure and high temperature are obtained in a type of pressure developed by Bridgeman [1]. At the same year, the announcement of the successful general electric synthesis was followed by a period of considerable activities [2]. Although it was now possible for many laboratories to make diamond there was a long way to go to obtain sizeable crystal of high quality.

High pressure and high temperature (HPHT) diamond growth techniques have been used in commercial synthesis for the last 40 years [3]. Much effort has been spent during 60's and 70's to investigate diamond growth at low pressure [4-7]. Diamond synthesis was first successfully achieved by chemical vapor deposition (CVD) techniques at low pressures, reported by Eversole in 1962 [8]. Most of the scientific research effort into CVD diamond technology has been concentrated within the past decade [9-16]. The CVD diamond shows mechanical, tribological, and even electronic properties comparable to those of natural diamond. Therefore, synthesis of diamond is a basic step for its further application.

2.2 Chemical vapor deposition process

Chemical vapor deposition process can be simply described as below: Precursor gases (often diluted in carrier gases) are delivered into the reaction chamber at approximately ambient temperatures. As they pass over or come into contact with a heated substrate, they react or decompose, forming a solid phase which will be deposited onto the substrate. The substrate temperature is critical and can influence what reactions will take place.

The requirement for precursors is that materials are deposited from the gaseous state during CVD. Thus the precursors for CVD processes must be volatile, but at the same time stable enough to be delivered to the reactor. Generally precursor compounds will only provide a single element to

the deposited material, with others being volatilized during the CVD process. However sometimes precursors may provide more than one.

CVD method is a general name which actually includes many different methods, as shown in Fig. 2.1. CVD covers processes such as: Atmospheric Pressure Chemical Vapor Deposition (APCVD), Low Pressure Chemical Vapor Deposition (LPCVD), Metal-Organic Chemical Vapor Deposition (MOCVD), Plasma Assisted Chemical Vapor Deposition (PACVD) or Plasma Enhanced Chemical Vapor Deposition (PECVD), Laser Chemical Vapor Deposition (LCVD), Photochemical Vapor Deposition (PCVD), Chemical Vapor Infiltration (CVI), Chemical Beam Epitaxy (CBE) [17].

All CVD techniques for producing diamond films require a means of activating gas-phase carbon-containing precursor molecules. This generally involves thermal (e.g. hot filament) or plasma (DC, RF, or microwave) activation, or use of a combustion flame (oxyacetylene or plasma torches). A CVD apparatus consists of several basic components:

1) Gas delivery system – For the supply of precursors to the reaction chamber.
2) Reaction chamber – Chamber within which deposition takes place.
3) Substrate loading mechanism – A system for introducing and removing substrates, mandrels *etc*.
4) Energy source – Provides the energy/heat that is required to get the precursors to react/ decompose.
5) Vacuum system – A system for removal of all other gaseous species other than those required for the reaction/deposition.
6) Exhaust treatment systems – In some instances, exhaust gases may not be suitable for release into the atmosphere and may require treatment or conversion to safe/ harmless compounds.
7) Process control equipment – Gauges, controls *etc*. to monitor process parameters such as pressure, temperature and time. Alarms and safety devices would also be included in this category.

CVD process consists of the following basic steps:

1) A predefined mix of reactant gases and diluents inert gases are introduced at a specified flow rate into the reaction chamber;
2) The gases are excited or decomposed to reactants;
3) The reactants get adsorbed on the surface of the substrate;
4) The reactants undergo chemical reactions with the substrate to form the film; and
5) The gaseous by-products of the reactions are desorbed and evacuated from the reaction chamber.

2.3 Principle of microwave plasma CVD

In the plasma chemical diamond synthesis (PDS), the following kinds of discharge are applied: a direct current and its updating (arc-jet), RF (preferably, induction), microwave, and ECR. Among them microwave plasma CVD is a widely used technique for synthesizing diamond thin films because of its comparatively simple equipment, higher growth rate and high stability and repeatability. The microwave discharge is electrodeless and can be carried out in a reactor with quartz [18] or cooled metal wall [19]. The schematic of deposition of diamond film using MWCVD method is shown in Fig. 2.2. On the basis of discharges with frequency of 2.45 and 0.915 GHz, an industrial production of PDS reactors and working costs (replacement of magnetrons, etc.) are high. Therefore, for some of the practical purpose the PDS in reactors with direct current plasmatron is used [20].

As a starting gaseous mixture, 0.5-5% CH_4 in H_2 will usually by utilized at pressure in the range of tens and hundreds Torr. After starting in the mixture of an electric discharge, the conversion of stable CH_4 molecules into neutral and charged hydrocarbonaceous particles: C_2H_2, C_2H_4, CH_3, C_2H_2, CH^+, CH_2^+, *etc.* proceeds. A considerable fraction (from several % up to 90%) of H_2 molecules dissociates to H atoms, and also to ions H^+, H_3^+, H^-. The plasma ionization degree in the majority of the plasma reactors is ~ 10^{-7}. The Diamond film crystallization temperature is 700 to 950 ℃, and the average temperature of the activated gas phase is much higher (from 2000 up to 5000 ℃).

In the CH_4/H_2 plasma system, the four most dominative decompose reactions are:

$CH_4 \rightarrow CH_3 + H$

$CH_4 \rightarrow CH_2 + H_2$

$CH_4 \rightarrow \mathbf{CH + H_2 + H}$

$CH_4 \rightarrow \mathbf{C + 2H_2}$

From the above reactions, it is easier to find that there is a big amount of methyl radicals (CH_3). This CH_3 can be a dominant carbon source for diamond growth, as shown in following reaction:

$CH_4 + CH_2 \rightarrow \mathbf{2CH_3}$

2.4 Experimental apparatus

A MWPCVD system (ASTeX-6350) used in this work is shown in Fig. 2.3. The microwave generated by a 2.45GHz microwave generator goes through isolators and turner, and directs toward an applicator. The applicator is composed of an aluminum waveguide. The applicator is cooled by circulating water. The substrate is put on a steeliness substrate holder which can be moved up and down.

2.5 Diamond film deposition

2.5.1 Substrate preparation

Many substrates can be used for growth of diamond thin films such as Silicon (Si), Molybdenum (Mo), Aluminum (Al), SiC and graphite, etc. In which Si (100) and (111) wafers are widely used to synthesis polycrystalline diamond films. In this work, n-type low resistance (0.02 Ω cm) Si (100) wafer was chosen as a substrate.

An ultrasonic generator (Yamoto 3210), as shown in Fig. 2.4, was used in the cleaning processes.

As shown in Fig. 2.5, the processes of preparation of substrates are the following steps:

Firstly, the Si wafer is cut into several 1.5×1.5 (cm^2) wafer pieces, then

1) Rinse wafers in acetone with ultrasound for 5 min and N_2 blow dry.
2) Rinse wafers in methanol with ultrasound for 5 min and N_2 blow dry.
3) Oxide removal: A 1-2 min dip in 1:10 HF: DI water will remove the native oxide layer and any contamination in the oxide from the wafer surface. HF is extremely dangerous and must be handled with great care. Strong rinse in DI water is required after this cleaning step.
4) Rinse wafers in 5-12 μm diamond powder with ultrasound for 30 min and cleaning by methanol, N_2 blow dry.
5) Rinse wafers in methanol with ultrasound for 300 s and N_2 blow dry for 2 or 3 times.

2.5.2 Deposition process

After cleaning, a Si substrate was put onto the center of the stage in the chamber. The chamber was evacuated by a diffusion pump. A mixture of gases (CH_4 and H_2) with proper ratio was induced into the chamber. A rotary pump was continued after the stop of the diffusion pump to get a suitable pressure. The microwave was then induced and the plasma was generated. The deposition process was timed from the instant when the substrate was heated to a proper temperature. The pressure, microwave power and the temperature could be slight adjusted when they were not stable during the deposition process. After the deposition time reached a prescribed duration, the microwave power and the flow rate of the supplied gases were gradually decreased, allowing for the substrate temperature to decrease to the room temperature. Then air was induced to the chamber, and the samples were taken out from the chamber.

The polycrystalline diamond films were deposited on Si (100) substrates. The working gases were a mixture of CH_4 and H_2. The typical deposition conditions by microwave plasma chemical vapor deposition method were shown in Table. 2.1.

Table 2.1: Typical diamond film deposition conditions by microwave plasma CVD method.

Sources gases	$CH_4 + H_2$ (CH_4 in H_2 : 1%, 3%, 5%, 10%)
Microwave power	5 kW
pressure	100-124 Torr
Substrate temperature	800- 950 ℃

2.6 Experimental results

The diamond films were formed at a microwave power 5 kW and a substrate temperature 800-950 ℃ by the MWPCVD system. The effect of different gas ratios (CH_4 in H_2) and different deposition time on the formation of diamond were investigated. The morphologies of the diamond films were observed with a Scanning Electron Microscope (SEM).

Figs.2.6 (a), (b) and (c) show the diamond films obtained in CH_4 diluted with H_2 and a CH_4 molar concentration is 3%. The diamond films were grown up in 0.5 h, 1 h and 2 h.

It is found that, comparing the images of these 3 different samples, the formation of diamond particles was dependent on the deposition time. In the 0.5 h deposition, the diamond particles grew up to about 1 μm, with most (100) and (111) facet structures. After continuing to grow for 1 h, the particles became 2 μm in size. Two hours later, the diamond became continuous film with particles size about 3 μm.

Figs. 2.7–10 show the diamond films obtained from different CH_4 ratios under the same operating conditions for a 2-hour deposition. The CH_4 concentration in the CH_4/H_2 mixture was 1, 3, 5 and 10%. It is clearly noticed that the quality of the diamond decreased with increasing CH_4 concentration. The diamond with a good crystal orientation is found in the case of the lowest CH_4 concentration (1%).

There are different applications using different quality diamonds. It is found the diamond with the graphite will enhance the emission from the surface. Therefore, moderate quality CVD diamond films (obtained from 3% to 5% CH_4) were considered as samples which would be used in further treatment.

2.7 Summary

Diamond films were deposited on Si substrates using microwave plasma chemical vapor deposition method. The deposition temperature and the CH_4 concentration were the critical factors influencing the quality of the diamond. The quality of CVD diamond film could be controlled by adjusting the CH_4 concentration in H_2. The quality of the diamond was improved with decreasing CH_4 concentration. Much high quality diamond film could be obtained in CH_4 less than 1% and in optimum deposition conditions.

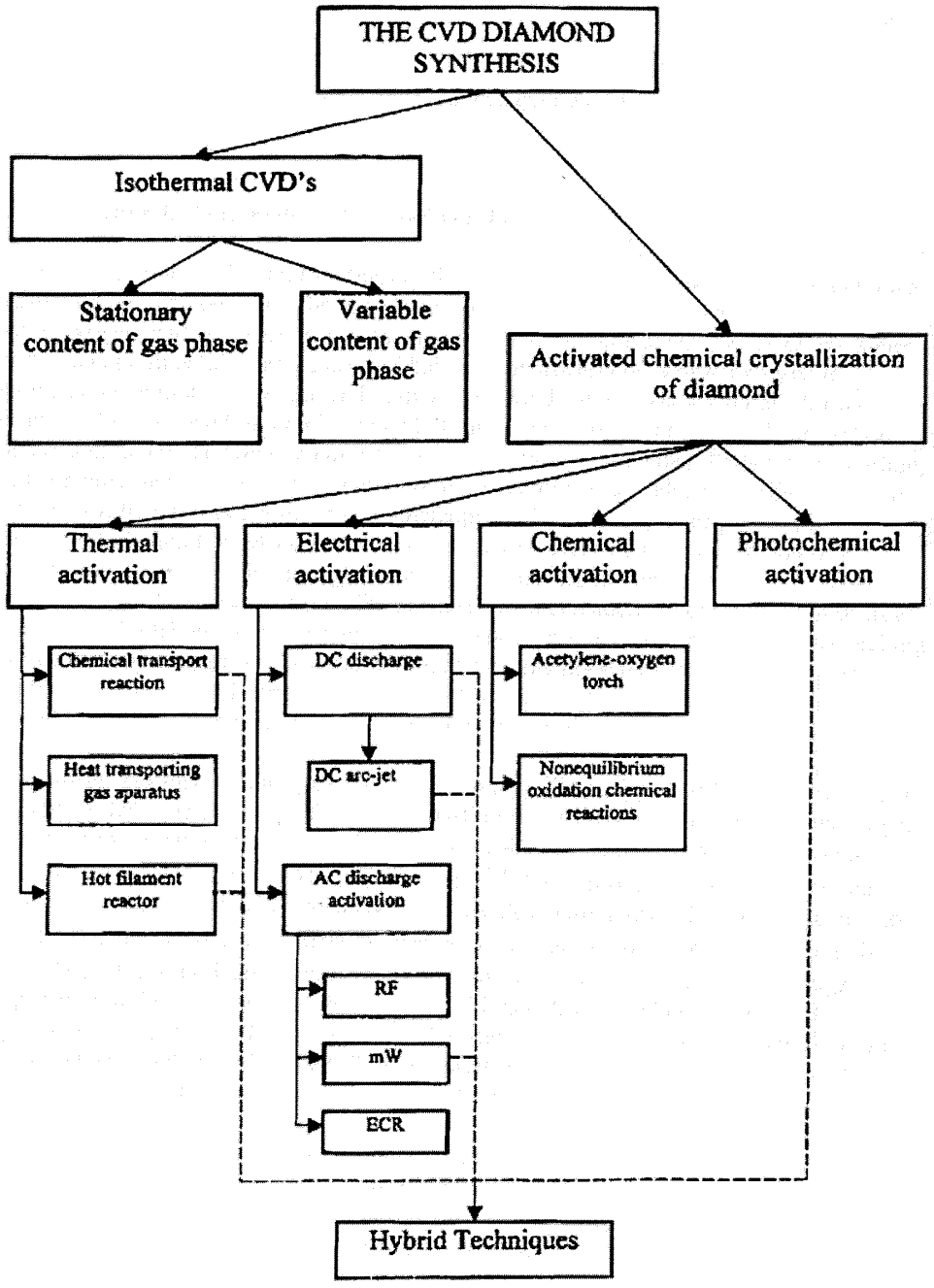

Fig. 2.1. Different methods of chemical vapor deposition.

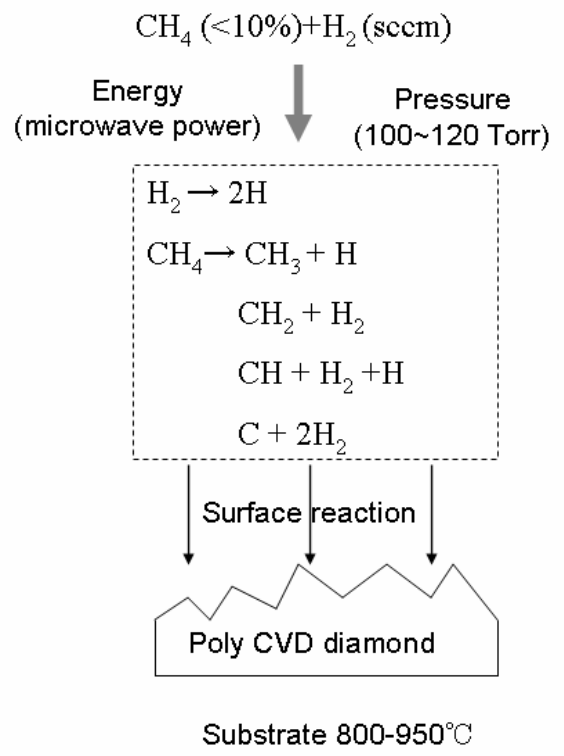

Fig. 2.2. The simple schematic of synthesis diamond film by MWCVD system.

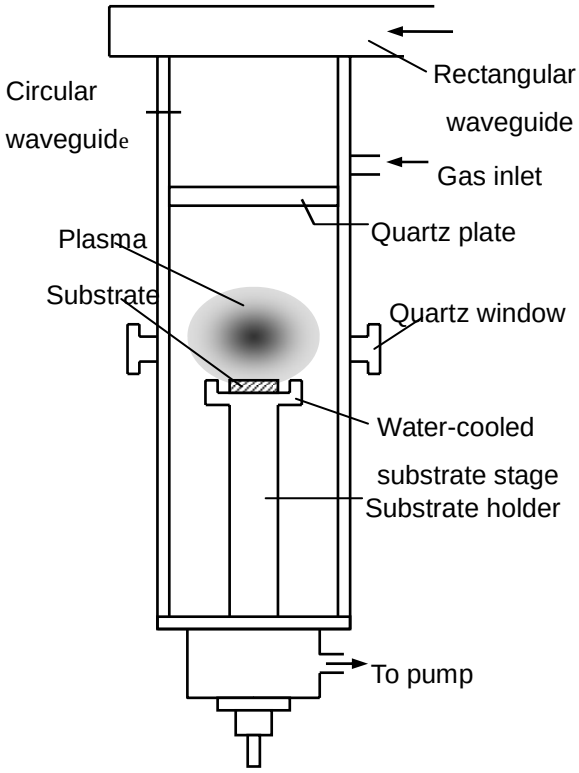

(a) (b)

Fig. 2.3. (a) The microwave plasma chemical vapor deposition system (ASTeX-6350), and (b) a schematic diagram of micro wave plasma chemical vapor deposition system.

Fig. 2.4. The ultrasonic generator used for cleaning.

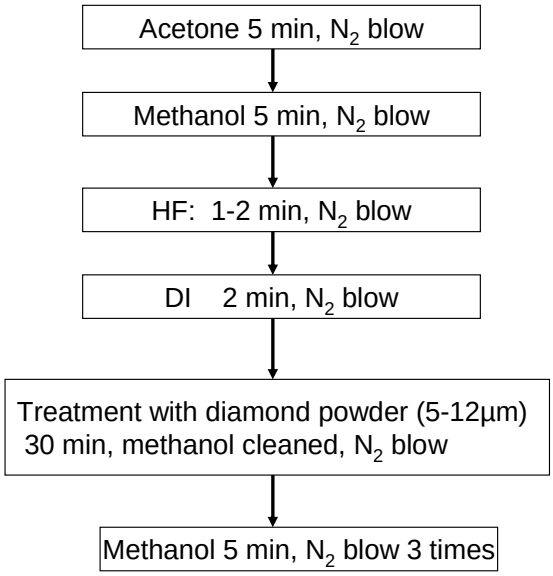

Fig. 2.5. Block figure of processes for preparation of substrates.

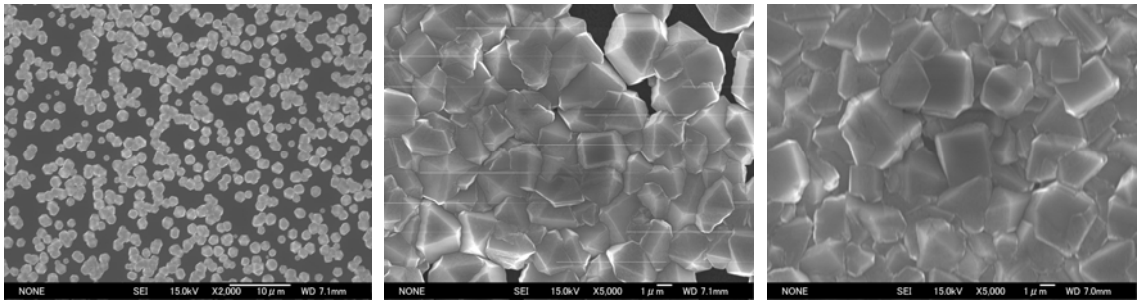

(a) (b) (c)

Fig. 2.6. Diamond films obtained in CH_4 diluted with H_2 and the CH_4 molar concentration is 3 %. The diamond films were grown up in 0.5 h (a), 1h (b) and 2h (c), respectively.

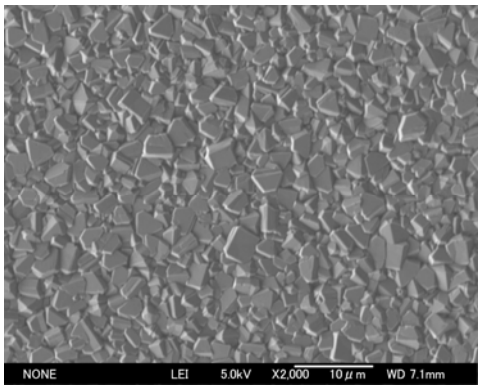

Fig. 2.7. Diamond films obtained in CH_4 diluted with H_2 and CH_4 dilute in H_2 (CH_4 molar concentration is 1 %).

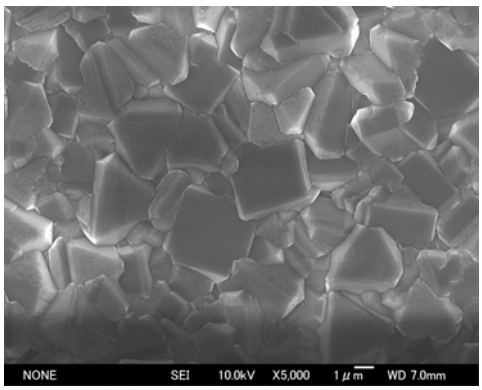

Fig. 2.8. Diamond films obtained in CH_4 diluted with H_2 and CH_4 dilute in H_2 (CH_4 molar concentration is 3 %).

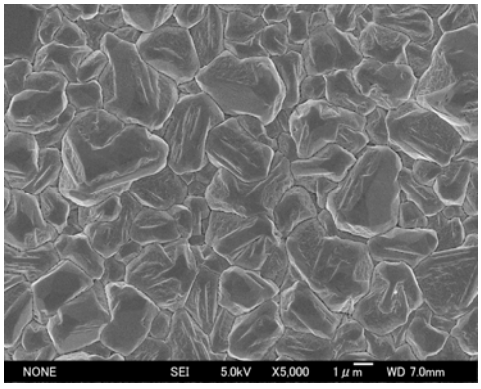

Fig. 2.9. Diamond films obtained in CH_4 diluted with H_2 and CH_4 dilute in H_2 (CH_4 molar concentration is 5 %).

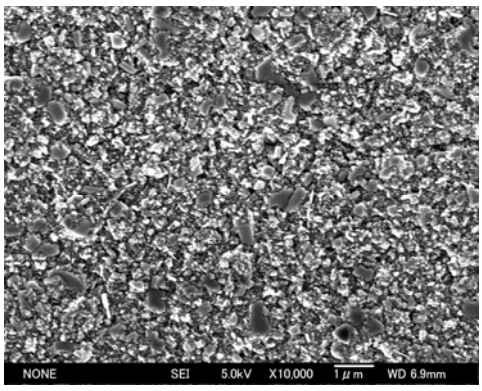

Fig. 2.10. Diamond films obtained in CH_4 diluted with H_2 and CH_4 dilute in H_2 (CH_4 molar concentration is 10 %).

References

[1] R. Berman and F. E. Simon, Zeitschrift fur Elektrochemie, **59**, 333-338 (1955).

[2] P. W. Bridgman, Scientific American, **11**, 42-46 (1955).

[3] F. P. Bundy, and J. S. Kasper, J. Chem. Phys., **46**, 3437-3446 (1967).

[4] J. C. Angus, H. A. Will, and W. S. Stanko, J. Appl. Phys., **39**, 2915-2922 (1968).

[5] R. J. Wedlake, The Properties of Diamond, Academic Press, London, 501-535 (1979).

[6] B. V. Derjaguin, D. V. Fedoseev, and V. M. Lukyanovich, J. Crystal Growth, **2,** 380-384 (1968).

[7] B. V. Spitsyn, L. L. Bouilov, and B. V. Derjaguin, J. of Crystal Growth, **52,** 219-226 (1981).

[8] W. G. Eversole United States Patent **No: S,** 3030188, (1962).

[9] S. Mastumoto, Y. Sato, M. Tsutsumi, and N. Setaka, J. Mater. Sci., **17,** 3106-3112 (1982).

[10] M. Murakawa, S. Takeuchi, Y. Hirose, Surface. Coat. Technol., **39/40**, 235-240 (1989).

[11] K. Suzuki, A. Sawabe, H. Yasuda, and T. Inuzuka, Jpn. J. Appl. Phys., **29**, 153 (1990).

[12] S. Matsumoto, J. Mater. Sci. Lett., **4**, 600 (1985).

[13] D. E. Meyer, R. O.Dillon, J. A. Woolham,. J. Vav. Sci. Technol., **7,** 2325 (1989).

[14] M. Yuasa, Y. Yara, , A. Hatta,, T. Ito, ,and A. Hiraki, Proc. 3rd Internat. Sym. On Diamond Mater., 565 (1993).

[15] C. R. Eddy, Jr. Youchison, D. L. Sartwell, Proc. 3rd Internat. Sym. On Diamond Mater., 365-371 (1993).

[16] W. Piekarzayk,, R.Messier, R. Roy, C. Engdahl, , J. Crystal Growth, **106**, 279-293 (1990).

[17] P. K. Bachmann, A. Lettington, and J. W .Steeds, Thin Solid Film, **1,** 35 (1994).

[18] M. Kamo, Y. Sato, S. Matsumoto, and N. Setaka, J. Cryst. Growth, **62**, 642 (1983).

[19] P. K. Bachmann, M. A. Prelas, M. Dekker, Handbook of Industrial Diamond Films, N.Y., 821 (1998).

[20] K. Kurihara, K. Sasaki, M. Kawarada, and N. Koshino, Appl. Phys. Lett. **52,** 437 (1998).

CHAPTER 3

FABRICATION OF DIAMOND WHISKERS USING Ar/O_2 RADIO FREQUENCY PLASMA ETCHING

3.1 Introduction

Since last decade, diamond was identified as one of the best materials which can be used in various vacuum microelectronic applications mainly due to its outstanding electrical and thermal properties [1-6]. The negative electron affinity (NEA) of diamond surface is more attractive because only low energy or no energy at all is necessary to extract electrons from the diamond surface to a vacuum environment [7]. This property opens up potential applications for the use of diamonds materials as cold cathode for vacuum microelectronics, high luminescent flat panel displays, and so on [8]. However, the concentration of intrinsic electrons in the conduction band of diamond is very low and it is difficult to dope diamond crystals with electron donor impurities to produce n-type diamonds. Therefore, even with favorable NEA, crystalline diamonds are poor field emitter as the transport of electrons through the bulk for emission at the diamond vacuum interface is difficult [9].

Current scientific and technological interest in preparing nanostructured materials stems the fact that they may have new, or better properties than those in the bulk state. Especially, nano-size diamond structures which have better optical transmission, high density of defect cores, enhanced quantum electronic conduction and good field electron emission are different from the micro-size diamond [10-13]. Among them using nano-size diamond as electron field emitter in field emission display (FED) is one of the most promising applications [14-18]. It has been reported that electron field emission would be enhanced at the micro or nano-tips of diamond [19]. Up to present, many efforts have been made to shape diamond film into nano-tips [20-25]. For instance, Ando *et al*. [21] fabricated single crystalline diamond nano-rods using reactive ion etching (RIE) method. Okano [26] successfully used a transfer mold technique to invert pyramidal mold on silicon (100) substrate. Baik *et al*. [20] reported a method to fabricate diamond nano-whiskers by etching a polycrystalline diamond film using air plasma.

However, fabrication of sharpened field emission tips is still a challenging issue until now because it is difficult to control the nano-sized structures arbitrarily. Among the various approaches reactive ion etching is considered as an efficient method to tailor diamond [27].

In this work, a novel method for fabrication of whiskers by reactive ion etching in O_2 and

O_2/Ar plasmas is reported. This method combines deposition, sputtering with etching techniques together. The effect of different gas ratios on the formation of diamond nanowhiskers was investigated. Furthermore, a comparison of the morphologies of diamond surfaces before and after etchings demonstrated the relationship between whiskers and reacting gases.

3.2 Experimental principle

3.2.1 Sputtering coating principle

In physical sputtering deposition, ions incident on a target physically sputter target atoms, which ballistically flow to and are deposited on a substrate. Argon ions at 500-1000 V are usually used. Because sputtering yields are of order unity for almost all target materials, a very wide variety of pure metals, alloys, and insulators can be deposited. Physical sputtering, especially of elemental targets, is a well-understood process, enabling sputtering systems for various applications to be relatively easily designed. Reasonable deposition rates with excellent film uniformity, good surface smoothness, and adhesion can be achieved over large areas.

When an ion approaches the surface of a solid (target), one or all of the following phenomena may occur, as shown in Fig. 3.1. Among these interactions the ion may set up a series of collisions between atoms of the target, possibly leading to the ejection of one of these atoms. This ejection process is known as sputtering.

Assuming that all the sputtered material is deposited on the substrate, the deposition rate for physical sputtering is

$$D_{sput} = \frac{\gamma_{sput}\Gamma_i}{n_f}\frac{A_t}{A_s} \text{ (cm/s)}, \tag{3.2.1}$$

where Γ_i is the incident ion flux ($cm^{-2}\cdot s^{-1}$), n_f is the density of the deposited film (cm^{-3}), A_t (cm^2) is the target area sputtered, A_s (cm^2) is the substrate area on which the films is deposited, and γ_{sput} is the sputtering yield. For 1 kV argon ions with A_t/A_s=1, the deposition rate is 750 Å/min [29].

DC driven planar magnetron discharges are usually used for sputtering, the operating pressure is generally 10^{-3}-10^{-2} Torr, which is low enough that the mean free path for sputtered atoms is larger than the separation between target and substrate.

Sputtered atoms are emitted with a cascade-type energy distribution [30]:

$$F(\varepsilon) \propto \frac{\varepsilon_t \varepsilon}{(\varepsilon_t + \varepsilon)^3}, \tag{3.2.2}$$

where ε_t is the surface binding energy of the target material. The maximum of this distribution

occurs at $\varepsilon = \frac{\varepsilon_t}{2}$. Since ε_t ~1-4 V, the characteristic sputtered atom energies are 0.5-2 V. Atoms striking the substrate with these energies can produce some mixing and diffusion between incoming atoms and substrate materials, leading to enhanced bonding and adhesion.

A conventional DC sputtering system is shown in Fig. 3.2. The material which will be sputtered is made into a sputtering target which becomes the cathode of an electrical circuit, and has a high negative voltage V (DC) applied to it. The target is always solid in this experiment. The substrate which will be coated is placed on an electrically grounded anode a few inches away. These electrodes are housed in a chamber which is evacuated. Argon gas is introduced into the chamber to some specified pressure. The action of the electric field is to accelerate electrons which in turn collide with argon atoms, breaking some of them up into argon ions and more electrons to produce the glow discharge. The charged particles thus produced are accelerated by the field, the electrons tending towards the anode (causing more ionizations on the way) and the ions towards the cathode, so that a current I flows.

When striking the cathode, the ions may sputter some of the target atoms off. They may also liberate secondary electrons from the target and it is these secondary electrons which are responsible for maintaining the electron supply and sustaining the glow discharge. The sputtered atoms from the target fly off in random directions, and some of them land on the substrate (on the anode). Condense there, and form some small islands, then coalescent to a thin film.

3.2.2 Radio frequency plasma etching

3.2.2.1 Radio frequency reactor

The effect of radio frequency discharge is suitable for using in plasma etching [28]. A RF power system is shown in Fig. 3.3. In practice, glow discharge processes are almost always driven by high frequency power supplies, usually in the megahertz range. To ionize and heat a plasma, electrical power is applied at a radio frequency usually assigned of 13.56 MHz. The output into a 50 Ω cable is usually 2 kW or less. The cable then goes into a matching network, or matching box, which performs the important function of transforming the impedance of the antenna-plasma system to the 50 Ω impedance of the rest of the circuit. Before passing through the matching network, the power goes through directional couplers which measure the power flowing into the antenna and back from it. This reflection has to be kept low (<1%) to protect the amplifier and to make best use of its power. The main elements of the matching network are two (physically) large, adjustable vacuum capacitors. The tuning is done by varying the capacitance of these two elements. Since the RF current in the capacitors is displacement current in vacuum, there is very little power loss in such a circuit.

The frequency generator and power amplifier are usually in one chassis, while the matching

circuit and the meters that measure the input and reflected power are in another chassis. In practice balance is achieved by adjusting impedance matching box, resulting at the forward power reaches a maximum as the reflected power drops to a minimum

Etching in this type of reactor can be both anisotropic and isotropic. The reactor is a cylindrical container which can be evacuated. Forward power and reflected power levels are monitored. The forward power is the power into the work chamber, whereas the reflected power is the power reflected back into the power supply.

3.2.2.2 Reactive ion etching principle

At present, plasma etching is a key process for removing material in microfabrication technique [29]. In this research work, O_2 was introduced into the radio frequency vacuum using as an etchant gas. Inside of the chamber, it is an ion energy-driven process for O atom etching of a diamond film (carbon substrate). We assume that the only reactions that occur are

$$\text{O (g)} + \text{C (s)} \xrightarrow{K_a} \text{C : O,} \tag{3.2.3}$$

$$\text{C : O} \xrightarrow{K_d} \text{CO (g), and} \tag{3.2.4}$$

$$\text{Ion} + \text{C : O} \xrightarrow{Y_i K_i} \text{CO (g)} \tag{3.2.5}$$

Let θ be the fraction of surface sites (area density $n_0^{'}$) covered with C: O bonds. We assume Langmuir kinetics, as shown in Fig. 3.4.

All O atoms from the gas phase incident on the surface not covered with C : O are assumed react immediately to form C : O. The rate-limiting etch step is assumed to be desorption of CO (g). The steady-state surface coverage is then found from

$$\frac{d\theta}{dt} = K_a n_{OS}(1-\theta) - K_d\theta - Y_i K_i n_{is}\theta = 0\,, \tag{3.2.6}$$

where n_{os} and n_{is} are the neutral and ion densities at the surface and the plasma-sheath edge, respectively,

$$K_a = \frac{1}{4}\frac{\bar{v}_O}{n_0^{'}} = \frac{1}{4}\left(\frac{8kT_O}{\pi M_O}\right)^{\frac{1}{2}}\frac{1}{n_0^{'}}, \tag{3.2.7}$$

is the O-atom adsorption rate constant, K_d is the rate constant for thermal desorption of CO, Y_i is the yield of CO molecules desorbed per ion incident on a fully covered surface in the absence of other desorption mechanisms, and $K_i = u_B/n_0' = (eT_e/M_i)^{1/2}/n_0'$ is the rate constant for ions incident on the surface. For high ion energies, Y_i is typically much greater than unity. A crude mode is that $Y_i \sim \eta\varepsilon_i/\varepsilon_b$ for ion energies $\varepsilon_i \gg \varepsilon_b$, where ε_b is the energy that binds the molecule to the surface, and where $\eta \leq 1$ is a factor giving the efficiency of bond breaking by the incident ion. Solving equation (3.2.7) for θ, we obtain

$$\theta = \frac{K_a n_{OS}}{K_a n_{OS} + K_d + Y_i K_i n_{is}}. \tag{3.2.8}$$

The flux of CO molecules leaving the surface is

$$\Gamma_{CO} = \left(K_d + Y_i K_i n_{is}\right)\theta_{n0}'. \tag{3.2.9}$$

The vertical etch rate is

$$E_v = \frac{\Gamma_{CO}}{n_e} \text{ (m/s)}, \tag{3.2.10}$$

where n_c is the carbon atom density of the substrate. Inserting equations (3.2.8) and (3.2.9) to equation (3.2.10),

$$E_v = \frac{n_0'}{n_c}\frac{1}{\dfrac{1}{K_d + Y_i K_i n_{is}} + \dfrac{1}{K_a n_{OS}}}. \tag{3.2.11}$$

Assuming that ions strike the substrate at normal incidence, then the ion flux incident on a vertical trench sidewall is zero. In this limit, we obtain a purely chemical horizontal etch rate:

$$E_h = \frac{n_0'}{n_c}\frac{1}{\dfrac{1}{K_d} + \dfrac{1}{K_a n_{OS}}}. \tag{3.2.12}$$

The normalized etch rates $(n_c/n_o')\, E_v/K_d$ are plotted versus the normalized neutral atom density $K_a n_{os}/K_d$ in Fig. 3.6 in the rigime $Y_i K_i n_{is} \gg K_d$, which is the usual regime for ion energy driven

etching. For $K_a n_{os} \le K_d$, the surface is starved for etchant atoms and both E_h and E_v are determined by the rate of arrival of O atoms to the surface, with $\theta \ll 1$. As $K_a n_{os}$ is increased beyond K_d, the normalized horizontal (sidewall) etch rate saturatesis is at 1 and $\theta \to 1$, while the vertical etch rate continues to increase linearly with n_{os}, with $\theta \ll 1$. This is the neutral flux limited regime of ion energy-driven etching. In turn, the normalized vertical etch rate saturates as $K_a n_{os}$ is increased beyond $Y_i K_i n_{is}$. In this ion flux limited regime, both vertical and horizontal surfaces are flooded with O atoms ($\theta \to 1$ for both surfaces), and the vertical etch rate is determined by the rate of arrival of energetic ions to the surface.

The etch anisotropy in the regime $K_a n_{os}$, $Y_i K_i n_{is} \ge K_d$ is

$$a_h = \frac{E_v}{E_h} = \frac{Y_i K_i n_{is}}{K_d} \frac{1}{1 + \frac{Y_i K_i n_{is}}{K_a n_{OS}}}, \tag{3.2.13}$$

and has its maximum value $Y_i K_i n_{is}/K_d$ when $\theta \to 1$ for both horizontal and vertical surfaces; i.e., $K_a n_{os} \gg Y_i K_i n_{is} \gg K_d$. In this ion flux limited regime, high anisotropies can be achieved for high ion energies and fluxes (Y_i and n_{is} large) and low substrate temperatures (K_d small) provided n_{os} is large enough. In the neutral flux limited regime $K_d \ll K_a n_{os} \ll Y_i K_I n_{is}$, the anisotropy is independent of ion energy and flux.

$$a_h = \frac{K_a n_{os}}{K_d}. \tag{3.2.14}$$

During the etching process, actually, there are two processes: associative and normal desorption of O atoms,

$$\begin{aligned} C : O &\rightarrow C + O\ (g) \\ 2C : O &\rightarrow 2C + O_2\ (g) \end{aligned}$$

Ion energy driven desorption of O atoms, the reaction

$$Ions + C : O \rightarrow C + O\ (g)$$

leads to the formation and desorption of CO_2 as an etch product; and the effect of non-zero ion angular bombardment of side wall surfaces.

3.3 Experimental Methods

3.3.1 Sputtering coating

Diamond films were deposited by MWPCVD method using ASTeX (AX-6350) which we had completed described in Chapter 2. The diamond films which were chosen to use in this experiment were deposited with a high CH_4 ratio (CH_4 diluted in H_2 5%). After growing up to about 3 μm in thickness, diamond films were examined with an SEM, then prepared to use for coating. Al was used as coating metal.

The DC sputtering deposition system which was used in this research work is SANYUDENSHI, SC 701 HMC QUICK COATER, as shown in Fig. 3.6 (a). The schematic of the device with parallel target is shown in Fig. 3.6 (b).

The sputtering system is a vacuum chamber, which after pumped out, is re-filled with a low-pressure argon gas. A high voltage ionizes the gas, and creates what is known as the Crookes dark space near the cathode, which in our case, consists of a metal target made out of the metal we want to deposit. Almost all of the potential of the high-voltage supply appears across the dark space. (The glow discharge consists of argon ions and electrons which have been stripped off of them. Since there are about equal number of ions and electrons, the net charge density is about zero, and hence by Gauss's law, so is the field.) The electric field accelerates the argon atoms which slam into the aluminum target. There is an exchange of momentum, and an aluminum atom is ejected from the target, as shown in Fig. 3.2, and heads to the substrate and builds up a metal film. The coating conditions of using a sputtering device with parallel target holder in this research are shown in Table 3.1.

Table 3.1. Coating conditions of using sputtering device with parallel target holder.

	Parallel target holder
Voltage	1200 V
Current	5 mA
Pressure	12 Pa

3.3.2 Radio frequency plasma etching

After a 3 min Al coating in the DC sputtering device, samples were then used in etching process. A radio frequency plasma reactor with frequency of 13.56 MHz was assembled for etching application. The reactor picture and corresponding schematic figure are shown in Figs. 3.7 (a) and (b).

In the RF reactor, in general, the gaseous plasma is excited in a chamber. The etching gases are fed into the vacuum chamber (discharge zone). The plasma is induced in the discharge zone by applying inductively coupled RF excitation. The plasma acts to dissociate the molecular species into ions and neutral atoms as well as ionizing the molecules. During etching process, important parameters such as the RF power, the gas flow rate and the etching time were monitored.

After the Al-coated diamond sample was mounted on the substrate holder, then the reactor chamber was sequentially evacuated by a rotary pump and a turbo molecular pump. When the pressure of the chamber reached 0.1 Pa, etching gases were introduced through individual mass flow controller, the plasma was generated. During RF plasma etching processes, the chamber pressure was maintained at 22~26 Pa. In this study, the gas compositions examined were pure O_2 (100 sccm), mixture of Ar and O_2 in different ratios: O_2 (10sccm)/Ar (90 sccm), O_2 (20 sccm)/Ar (35 sccm) and pure Ar (100sccm). The RF power was 100 W, corresponding to a DC self-bias voltage of around -510 V for each sample. The substrate was cooled by a water-cooling system and its temperature did not rise. The detailed etching conditions are shown in Table 3. 2.

Table 3.2. Operating conditions for RF plasma etching of diamond film.

RF power (W)	Self-bias Voltage (V)	Pressure (Pa)	Working gases	Etching time (min)
100	-510	22	Ar, O_2, Ar/O_2	40, 60, 90

We firstly would like to consider the O_2 etching situation. Diamond film (carbon) can be etched by the formation of volatile reaction products in an O_2 glow discharge. To focus attention on the basic principles of electronegative discharge equilibrium, we consider an oxygen plasma in which only three charged species are included: O^{2+}, created by electron impact ionization, O^-, created by dissociative attachment, and electrons. Negative ions are trapped within the discharge by the positive potential of the plasma with respect to all wall surfaces, and are assumed to be lost only by recombination with positive ions in the volume. Positive ions are lost to the walls by diffusion and in the volume by recombination with negative ions. The simplified set of volume reactions is:

$$e + O_2 \rightarrow O_2^+ + 2e \quad \text{(ionization)}$$
$$e + O_2 \rightarrow O^- + O \quad \text{(dissociative attachment)}$$
$$O_2^+ + O^- \rightarrow O_2 + O \quad \text{(recombination)}$$
$$O_2^+ + O_2 \rightarrow O_2^+ + O_2 \quad \text{(elastic scattering)}$$
$$O_2^+ + O_2 \rightarrow O_2 + O_2^+ \quad \text{(charge transfer)}$$
$$O^- + O_2 \rightarrow O^- + O_2 \quad \text{(elastic scattering)}$$

The latter three reactions lead to ion-neutral momentum transfers that result in effective diffusion coefficients for positive and negative ion species [29].

In plasma etching, shown schematically in Fig. 3.8, the plasma produces both highly reactive neutrals (e.g. atomic oxygen) and ions that bombard the surface being etched. The combined effect of both etchant atoms and energetic ions in producing etch products can be much large. The neutral react with the surface to produce volatile species (CO_2) which will be pumped away. Ion bombardment from oxygen ions increases the etching rate by removing surface contaminants that block the etching or by directly enhancing the kinetics of the etching. As the aspect ratio (depth/width) of the feature increases, shadowing effect of the neutral species due to their non-zero reaction probabilities on the sidewall of the feature can cause concentration gradients within the feature and significantly alter the etching profiles and the etching uniformity. Moreover, shadowing of the isotropic electrons and positive charging on the diamond surface in etching high aspect ratio (width/depth) features can built up an electrical field on the formed oxide surface (Al_2O_3) to distort the ion trajectory. The reaction rate will be determined by the energetic ion bombardment. The etching rate generally increases with increasing ion energy.

3.4 Experimental results and discussion

Morphological analyses of the diamond film before and after etching process were made by a field emission scanning electron microscope (FESEM) using a JEOL JSM-6400F operated at 5 kV, 20 μA.

Figure 3.19 presents the FESEM image of a diamond surface covered with Al coating. It is clear that most texture orientations of diamond crystals were (100) but with no uniform size because the quality of the diamond film was not good due to the higher CH_4 ratio (5%) introduced during the deposition process. The samples were coated with Al for 3 min in the DC sputtering device. However, it was difficult to recognize the mask by SEM examination because the very lower sputtering rate resulting in formation of very few Al islands or thin film on the diamond surface.

After etching process, the surface color of the sample was changed from grey (diamond film) to dark black (whiskers), which can be observed by naked eyes. Observing under SEM in detail, whiskers were found to appear on the diamond surface.

Figure 3.10 illustrates the result for etching in O_2/Ar plasma with 10% O_2 (vol/vol) concentration. The SEM image, Fig. 3.10 (b), displays diamond whiskers spiking outward from the remaining diamond film as a result of etching for 1 h. The whiskers have sizes of about 150 nm in height, 80 nm in diameter and, apparently, they appear at a lower number density about 10 μm^{-2} not randomly distributed over the film surface. From Fig. 3.10 (a), representing a top view of the film (whiskers appear as white dots), one can clearly notice a network-like pattern tracing out preferential location of whisker formation. On closed inspection, the average size of an individual area enclosed by

white dots stands on a par with that of a diamond grain on the etched film surface, suggesting that whiskers might form preferentially at grain boundaries between diamond crystals.

With regard to this phenomenon, one should also note that fairly uniform removal of film material should be in process during RF plasma etching unless it was disturbed by the presence of foreign materials masking the film surface regionwise. In order to check this possibility, we carried out EDX measurements including a dot measurement and a mapping measurement. The result is: there were Al_2O_3 capped on the tips of the diamond whiskers. This measurement and results will be explained in detail in Chapter 5. Another possibility of the whiskers formation might be due to the grain boundary decoration hypothesis [20] which means that the Al atoms would be preferential adsorbed by grain boundaries. This was, most probably, due to the presence of non-diamond sp^2 inclusions (e.g., graphite) between the diamond boundaries during the diamond film deposition process.

Figure 3.11 shows the result for etching in O_2/Ar plasma with 36% O_2 (vol/vol) concentration for 40 min. It was found that, obviously, the density of the whiskers was remarkably increased (about 30 μm^{-2}), as shown in Fig. 3.11 (a). The roots of the whiskers extended gradually into the diamond grains. The height of the whiskers was slightly increased to about 200 nm but with a diameter decreased to 50 nm. As mentioned earlier, there were two processes during the mixture of O_2/Ar RF plasma etching. Whiskers obtained in this situation could be ascribed to the processes of ion-enhanced chemical etching and physical bombardment etching. O_2 would dissociate into O radicals accompanied by the formation of volatile products CO and CO_2 (reactive ion etching), and O ions also bombarded the diamond surface acting as physical etching but the reactive ion etching is dominant. However, Ar (an inert gas which can not react with carbon) would only contribute to bombarding the diamond surfaces, functioning as physical etching. A suitable Ar/O_2 proportion would increase the etching rate [32], accordingly the whiskers were formed this time only in 40 min.

When the etching gas was pure O_2 (100%), the whiskers reached the highest population density (about 50 μm^{-2}), as shown in Fig. 3.12 (a). The average diameter of the whiskers reduced to 20~30 nm with a height of 1 μm, as shown in Fig. 3.12 (b). As mentioned before, during the pure O_2 etching process, O_2 will contribute to both reactive ion etching and physical bombard etching. The total physical etching would become weaker comparing to the reactive ion etching of O_2 without Ar introduced. Although the quality of the whiskers was increased, the etching procedure took longer time (80 min).

Pure Ar (100 sccm) was also used to etched Al-coated diamond film in RF plasma for 40 min. Inert gas Ar (100 sccm) can not be dissociated and it also can not react with carbon. Therefore, the whiskers could not be formed on the surfaces in a pure Ar etching process. As a result, the surface was damaged due to the Ar physical bombardment etching.

Table 3.3. Comparison of diamond whiskers obtained in different Ar and O_2 ratios.

	Diameter (nm)	Height (nm)	Density (μm^{-2})
O_2 in Ar (10%)	80	150	~10
O_2 in Ar (36 %)	50	200	~30
O_2 100%	20	1000	~50
Ar 100%	No whiskers formation, the surface is damaged		

Comparing the whiskers formed in different gas ratios, it was found that the density and the height of the whiskers increased with increasing concentration of O_2. However their diameters were decreased. It is conceivable that the formations of whiskers could be controlled by changing the concentration of O_2 in the reacting gases.

Aluminum oxide was etched slowly, possibly only caused physical bombardment, so that reasonably high Al: C etching rate ratios can be obtained. The ion flux did not fall down on the top of the surface, Al_2O_3 served as inhibitor, protecting the surface to be exposed to the chemical etchant during the etching process.

3.5 Summary

Diamond whiskers were firstly fabricated by etching diamond films in O_2 and O_2/Ar RF plasma. The effect of different etching gas ratios on the formation of whiskers was compared. It was found that the number density of the whiskers relied on the O_2 concentration. The number density of the whiskers increased with the O_2 concentration. During the etching process, O_2 contributed to both reactive ion etching and physical etching but Ar only contributed to physical etching. A suitable Ar and O_2 molar ratio can efficiently increase the etching rate. Whiskers with 20 nm in diameter and 1 μm in height were formed in the pure O_2 etching process. It also found that Al coating was an important factor contributing to anisotropic etching. Al would react with O_2 to produce Al_2O_3, remaining on the top of the diamond surface and serving as mask to protect further etching of the diamond surface.

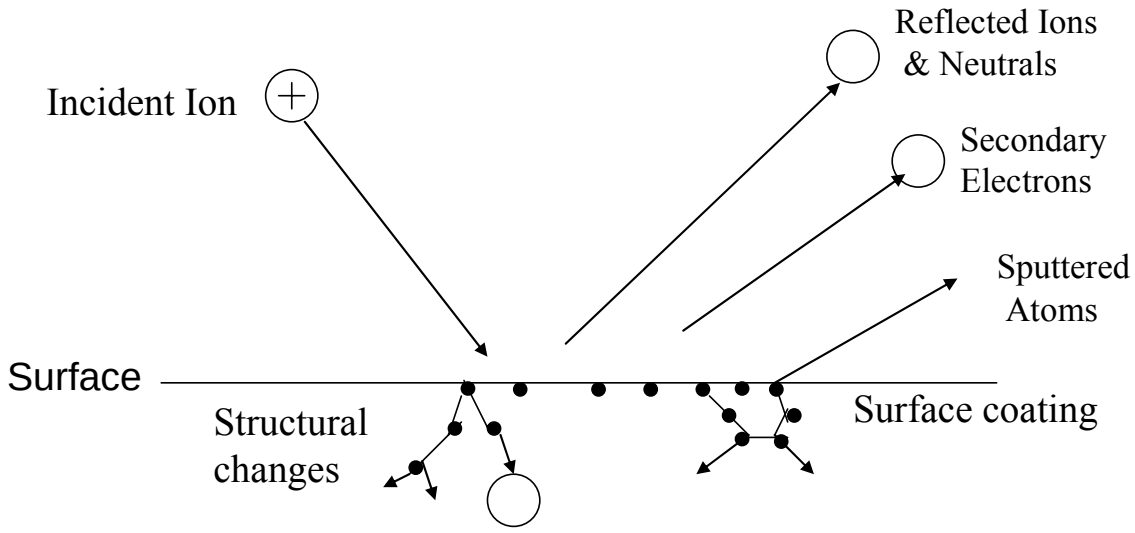

Fig. 3.1. Interactions of ions with surfaces [28].

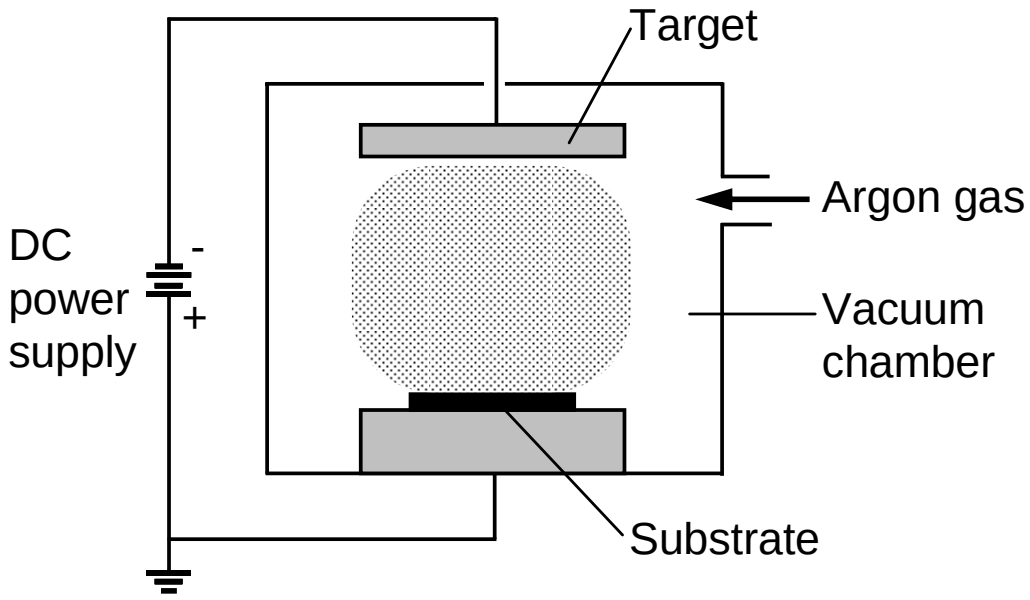

Fig. 3.2. The schematic of a conventional DC sputter system.

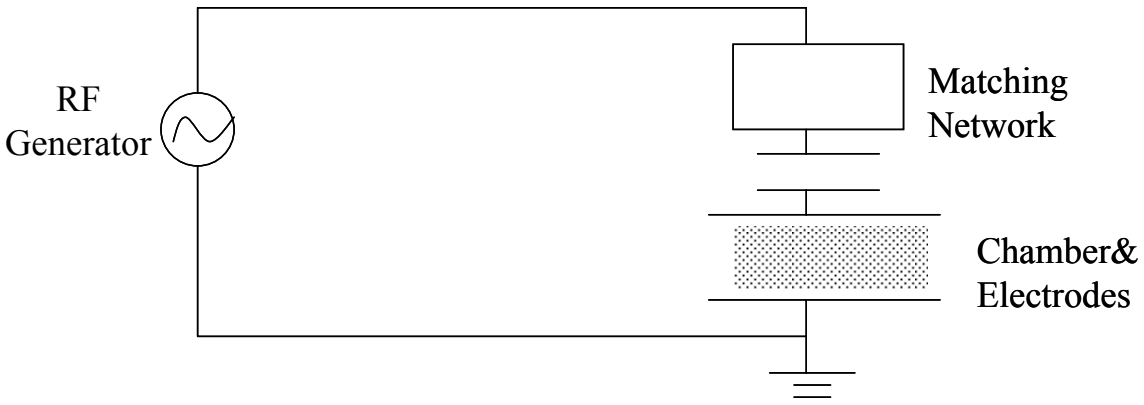

Fig. 3.3. A schematic of a RF reactor [28].

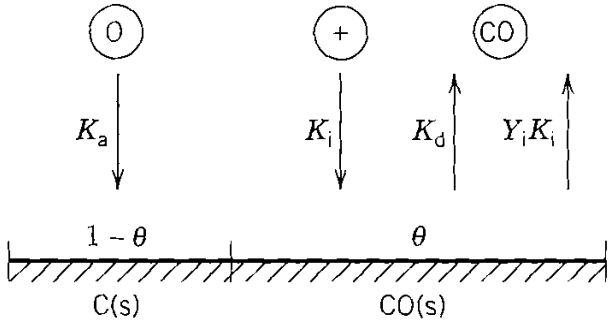

Fig. 3.4. Surface etching model assuming Longmuir kinetics and rate limiting desorption.

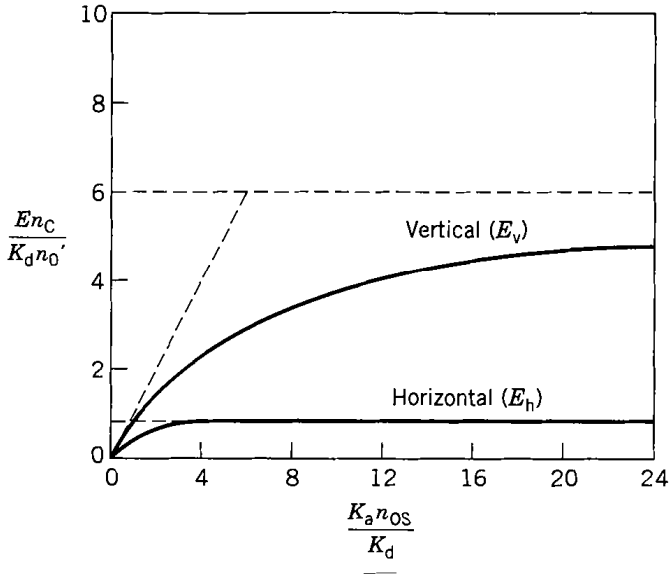

Fig. 3.5. Normalized vertical (E_v) and horizontal (E_h) etch rates versus normalized gas-phase density n_{os}, for $K_i Y_i n_{is}/K_d = 5$.

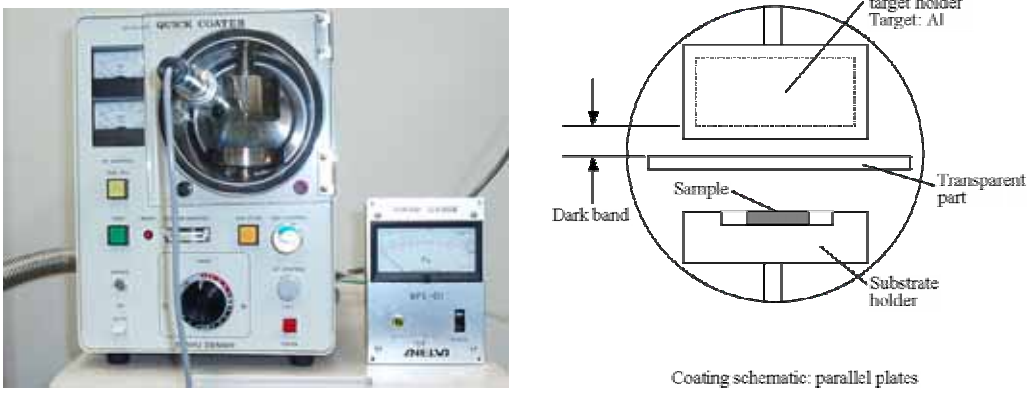

(a) (b)

Fig. 3.6. (a) A Quick coater (SC-701 HMC) sputtering device, and (b) a schematic of the device with parallel target.

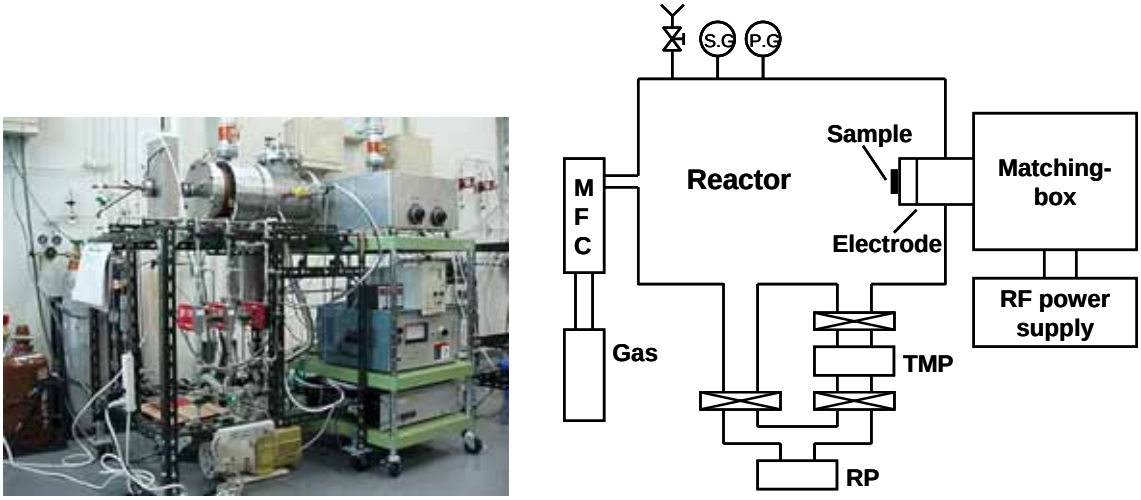

Fig. 3.7. (a) The radio frequency (13.56 MHz) plasma reactor, and (b) its schematic.

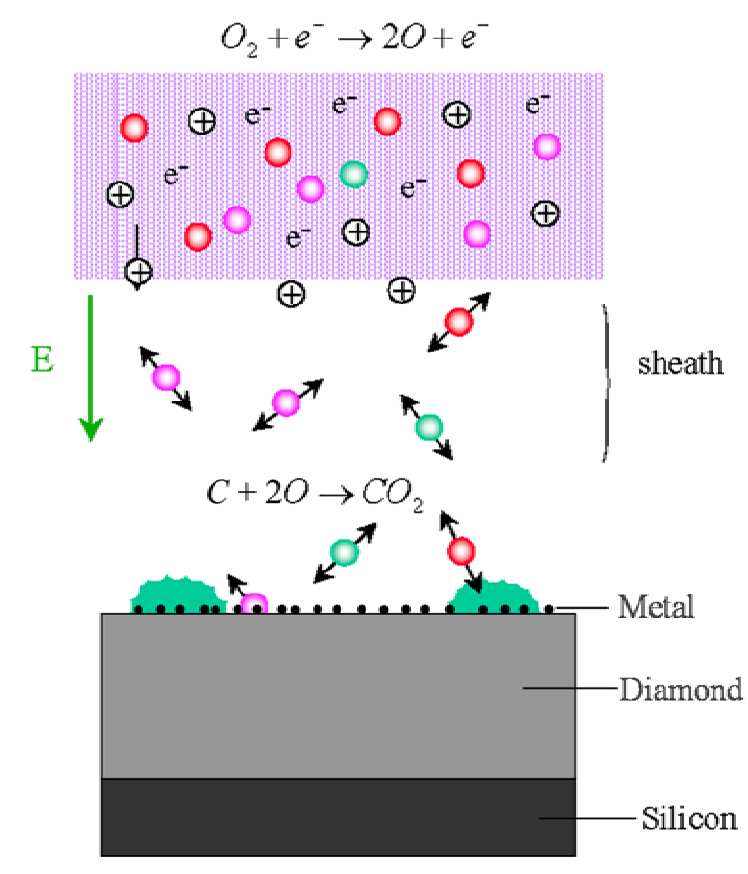

Fig. 3.8. A schematic of oxygen plasma etching diamond film process.

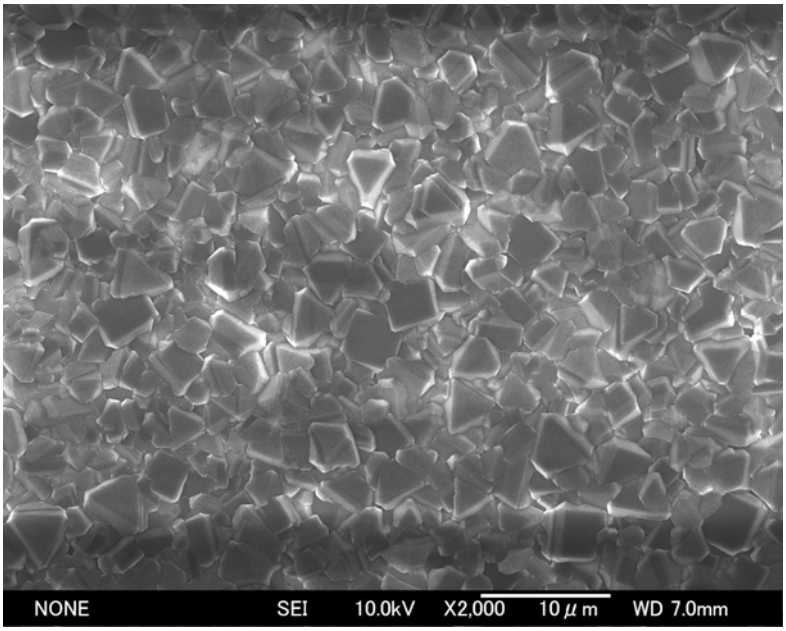

Fig. 3.9. Diamond film deposited by MWPCVD system (CH_4 in H_2 5%) and coated with Al (3 min).

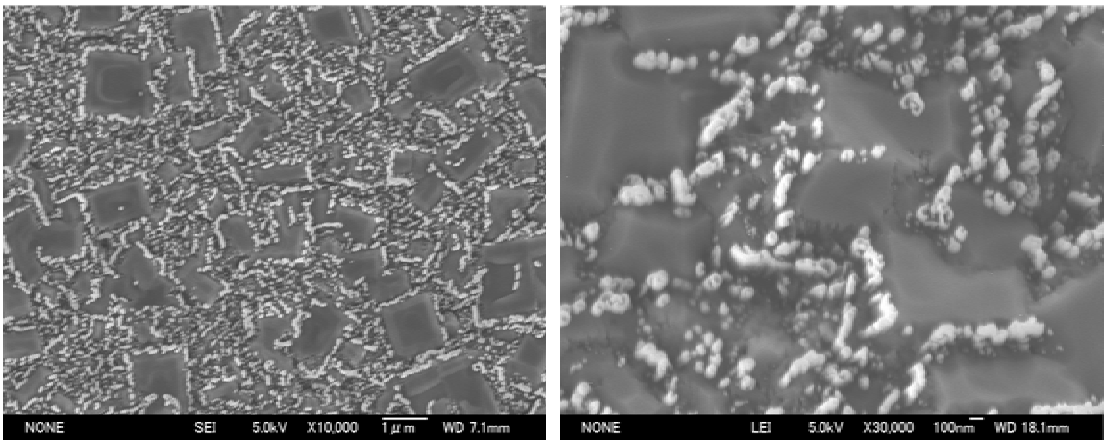

(a) (b)

Fig. 3.10. Illustrations of the result for etching in O_2/Ar plasma with 10% O_2 (vol/vol): (a) top view and (b) perspective view.

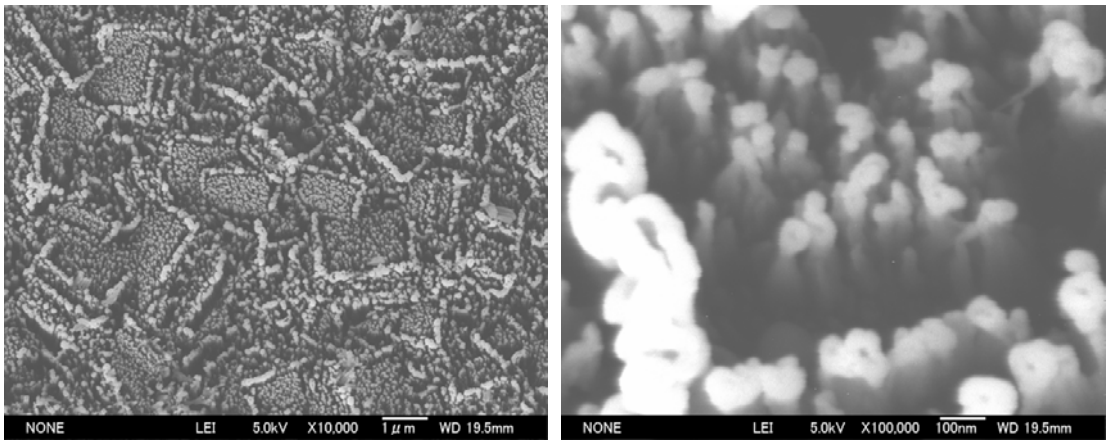

(a) (b)

Fig. 3.11. Illustrations of the result for etching in O_2/Ar plasma with 36 % O_2 (vol/vol), (a) top view and (b) perspective view.

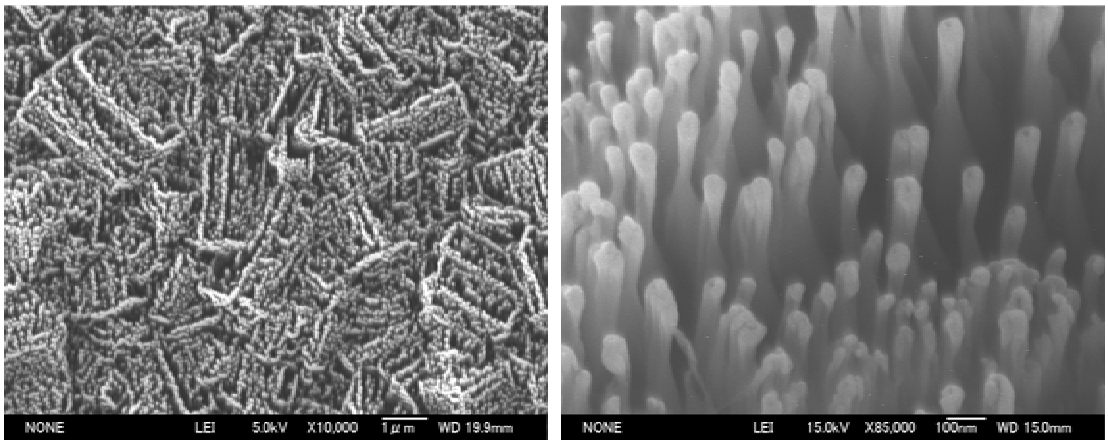

(a) (b)

Fig. 3.12. Illustrations of the result for etching in pure O_2: (a) top view and (b) perspective view.

References

[1] R. F. Davis, Z. Sitar, B. E. Williams, et al., Mater. Sci. Eng. **1**, 77 (1988).

[2] C. Nuzenadel, O. Groning, and L. Schlabach, American Institute of Physics **3**, 02644-7 (1996).

[3] P. W. May, Endeavour Magazine **19**, 101 (1995).

[4] P. Vaudaine, R. Meyer, IEEE IEDM Tech. Dig. 197 (1991).

[5] C. A. Spindt, C. E. Holland, A. Rosengreen, I. Brodie, J. Vac. Sci. Technol. **11,** 468 (1993).

[6] H .H. Busta, D. W. Jenkins, B. J. Zimmerman, J. E. Progeller, IEEE IEDM Tech. Dig. 213 (1991).

[7] F. J. Himpsel, J. A .Knapp, J. A. Vechten and P. E. Eastman, Phys. Rev. **20,** 624 (1979).

[8] V. Baranauskas, M. Fontana, H. J. Ceragioli and A. C. Peterleviz, Nanotechnology **15,** 683 (2004).

[9] C. Bandis and B. B. Pate, Appl. Phys. **A 65,** 53 (1996).

[10] T-S Yang, J-Y Lay, M-S Wong and C-L Cheng, J. Appl. Phys. **92** 2133 (2002).

[11] V P Mammamana, T E A Santos, A Mammama, V Baranauskas, H J Ceragioli and A C Peterlevitz Appl. Phys. Lett. **81**, 3470 (2002).

[12] D M Gruen, MRS Bull. **9,** 32 (1998).

[13] B M Jin, J Kim and C C Kim, Appl. Phys. **A 65,** 53 (1997).

[14] M.-Y. Teng, K.-S. Liu, H.-F. Cheng, I.-N. Lin, Diamond and Relat. Mater., **12**, 450 (2003).

[15] Y. Nishibayashi, H. Saito, T. Imai, N, Fujimori, Diamond Relat. Mater. **9,** 290 (2000).

[16] A. Vescan, W. Ebert, T. H. Borst, E. Kohn, Diamond Relat. Mater. **5,** 747 (1996).

[17] M. Adamschik, M. Hinz, C. Maier, Diamond Relat. Mater. **10**, 722 (2001).

[18] M. Yoshimura, K. Honda, R. Uchikado, Diamond Relat. Mater. **10**, 620 (2001)

[19] T. Tyler, V. V. Zhinov, A. V. Kvit, D. Kang, and J. J. Hren, Appl. Phys. Lett., **82**, 2901 (2003).

[20] E-S. Baik, Y.-J. Baik, J. Mater. Res. **15**, 923 (2000).

[21] Y. Ando, Y. Nishibayashi, A. Sawabe, Diamond Relat. Mater. **13**, 633 (2004).

[22] P. W. Leech, G.K. Reeves, A.S. Holland, F. Shanks, Diamond Relat. Mater. **11**, 4532 (2002).

[23] H. Shiomi, Jpn. J. Appl. Phys. **36**, 7745 (1997).

[24] G. S. Sandhu, W. K. Chu, Appl. Phys. Lett. **55,** 437 (1989).

[25] V. V. Zhirnov and J. J. Hren, MRS Bulletin, **9**, 42 (1998).

[26] K Okano, T Yamada, A Suave, S Koizumi and B B Pate, Appl. Surf. Sci. **146**, 274 (1999).

[27] A. S. Barnard, S. P. Russo, and I. K. Snook, Phys. Rev., **68**, 235407 (2003).

[28] B. Chapman, Glow Discharge Processes, John Wiley& Sons, INC, 139-177 (1980).

[29] M. A. Lieberman, A. J. Lichtenberg, Principles of Plasma Discharges and Materials Processing, John Wiley& Sons, INC, 315,483, 523 (1994)

[30] H. F. Winter, and J. W. Cobun, Surface Sci. Rep. **14**, 161 (1992).

[31] F. F. Chen, and J. P. Chang, Lecture Notes on Principles of Plasma Processing, Kluwer

Academic/ Plenum Publishers, 29 (2003).
[32] P. W. Leech, J. Mater. Sci. **36**, 3457 (2001).

CHAPTER 4

EFFECTS OF METAL MASK ON FORMATION OF DIAMOND WHISKERS IN O_2 RADIO FREQUENCY PLASMA ETCHING

4.1 Introduction

Since 1991, diamond field emitters have attracted a great deal of attention in cold cathode devices as robust field electron emitters having low effective work function [1-4]. Early field emitters typically employ metal (such as Mo) or semiconductor (such as Si) with nanometer-sized sharp tips [5]. Later, one improved method was found that was to deposit diamond coating on the tips [6, 7]. Although these kinds of emitters have demonstrated reasonable emission characteristics with stability and reproducibility necessary for practical application, the control voltage required for emission from these materials is relatively high due to their high work function. The high voltage operation increases the damaging instabilities due to ion bombardment and surface diffusion of the emitting tips and necessitates high power densities to be supplied from an external source to produce the required emission current. In addition, the fabrication of uniform sharp tips over a large area proves to be a difficult and expensive process. Field emission studies have been performed with both film and tip objects. However, diamonds with sharp tips which have significant currents at relatively low voltage, are more attractive to be used as field emitter.

As mentioned in Chapter 3, up to present, although many efforts had been done to try to shape diamond film into nano-tips [8-11], there are only a few successful experiments because of the special characteristics of diamond.

In our research work [12, 13], diamond whiskers has been fabricated using the Ar/O_2 radio frequency plasma etching and the relationship between the number density of the diamond whiskers and the different the gas ratios has been investigated. However, there is no reference to analyze the etching mechanism completely until now. In order to understand well the mechanism of whiskers formation, this chapter will highlight the effects of coating metals, different etching time.

4.2 Experimental details

Prior to the coating process, polycrystalline diamond films were deposited on silicon (Si) wafers by MPCVD using a mixture of hydrogen (95%) and methane (5%), under the operating conditions

mentioned in Chapter 2.

Different kinds of metals: molybdenum, aluminum, iron representing oxidizable metals, and nickel, gold representing non-oxidizable metals, were selected as coating metals for investigation. For comparison, as-grown diamond film without coating was also prepared for etching. The coating was performed in a DC sputtering device with the same conditions of the Al coating in Chapter 3. The coating time for each sample was 10 min. The as-grown and metal-coated CVD diamond films were etched in O_2 radio frequency plasma, under the same conditions as those of the Al-coated etching in O_2 plasma which were mentioned in Chapter 3.

The field emission scanning electron microscope (FESEM) (JEOL JSM-7400F), as shown in Fig. 5.13, was used for imaging the surface structures before and after etching.

4.3 Results and discussion

Figures 4.1 (a) and (b) show the top and perspective views of the SEM image of the as-grown diamond film after etching for 60 min, respectively. It is obvious that whiskers of 400 nm in height and 50 nm in diameter were formed with high population density on the diamond surface. The density of the whiskers was about 80 μm^{-2}, as shown in Fig. 4.1 (a). With close inspection in Fig. 4.1 (b), it is found that the grain boundaries of the diamond were much more etched, which might be because that there were the sp^2 non-diamond bonding structures existence among the boundaries which were easier to be etched away by O_2 than the diamond (sp^3) structures.

The situation was quite different for the metal-coated diamond films compared to the as-grown diamond. Fig. 4.2 shows the whiskers originated from 10 min Mo-coated diamond surface. From their top views, as shown in Fig. 4.2 (a), it is easier to find that the distribution of the whiskers which appeared as white dots was remarkably different from the etched as-grown diamond film, showing a pattern resembling the diamond crystal shapes. In contrast to the as-grown diamond film, the whiskers were mostly present at the grain boundaries with about 1 μm in height, as shown in Figs. 4.2 (b) and (c). Considering the properties of Mo, this phenomenon could be explained as grain boundary decoration [7] that during sputter process the Mo particles were preferentially adsorbed at the grain boundaries where sp^2 bonding existed. When the O_2 plasma was generated in the RF chamber, the Mo particles would react with O_2 to produce stable molybdenum oxide (MoO_3) quickly and remain mostly at grain boundaries. The molybdenum oxide of chemical stability (melting point 795 ℃) was expected to act as micro-masks which have incomparably lower etching rate comparing to that of the substrate carbon. Therefore, the diamond crystal surfaces with fewer protect metal oxide islands were much more etched than the diamond grain boundaries.

In order to confirm the function of this oxidizable metal again, the 10 min Al-coated diamond film was also used for this investigation. The sputtering and etching conditions for Al were the

same as those for the case of Mo. The etched results, as shown in Figs. 4.3 (a) and (b), were very similar to those of the Mo-coated. Whiskers with 50 nm in diameter and 1 μm in height were formed on the diamond film with population density about 35 μm^{-2}. For etching in O_2 plasma, the reactive product Al_2O_3 was more stable and served as micro-masks during etching, functioning similar to MoO_3. The EDX measurement results confirmed that the aluminum oxide remained on the tips of the diamond whiskers, which will be discussed in detail in Chapter 5.

In the case of Ni (non-oxidizable) coated diamond film, as shown in Fig. 4.4, disordered whiskers were found appearing tussock-like on the diamond surface (Fig. 4.4 (a)) with an average diameter of 50 nm and a height of 100 nm (Fig. 4.4 (b)). Unlike the Mo-coated surface, the distribution of the whiskers did not follow the location of the diamond crystal forms. One reason might be the poor crystallinity of Ni. Another might be due to that the significant decrease of its melting point produced nano-balls which had higher flow ability to move arbitrarily on the diamond surface during plasma etching. Compared to Mo, Ni particles were unstable on the top of the diamond film. Therefore anisotropy etching could not be achieved successfully on the Ni-coated diamond film.

Another non-oxidizable metal gold (Au) also was used as coating material. The coating time was only 3 min because the coating rate of Au is 3 times than that of Mo. The etching process was carried out under the same conditions as those for other metals (Mo, Ni) in O_2 plasma. The result, as shown in Fig. 4.5, was that whiskers could not be formed on the Au-coated diamond film, possibly due to the high mobility of Au. This result further illustrated that non-oxidizable metals were inefficient to contribute to prevent surface from etching.

4.4 Other influential factors

Considering the influential factors on etching process, etching time was also a critical one that needed to be tested. A 10 min Fe-coated diamond film was chosen to be inspected. A high quality diamond was used in order to find whether there were some effects originated from diamond film, as shown in Fig. 2.9. The sputtering and etching conditions were the same as those for the case of Mo coating. During the entire etching process, after etching 30 min in the O_2 plasma, the sample was taken out in every 20 min and inspected with a FESEM. The results are shown in Fig. 4.6. In the first 30 minutes, it is clearly noticed that there were only some crystal surfaces remained while all grain boundaries started to be etched [Fig. 4.6 (a)]. With the time increased to 50 min, some crystal surfaces were still not etched away [Fig. 4.6 (b)]. Continuing etching for another 20 minutes, a perfect etching was achieved on the diamond surface, as shown in Figs. 4.6 (c)- (e). Whiskers of about 50 nm in diameter and 1 μm in height were unexpectedly formed, following the same locations of the diamond crystal shapes and aligned exactly with the orientations of the crystal. From above it can be found that the suitable etched time was about 60-70 min under the current

operating conditions. The crystal shape was also a potential factor influencing the distribution of the diamond whiskers.

4.5 Summary

The diamond whiskers were remarkably influenced by the type of the coating metal. Oxidizable metals, like molybdenum, aluminum, iron, *etc*., could produce metal oxide as a stable coating layer or islands on the diamond surface during etching process, contributing to the formation of high quality whiskers with lower density. Non-oxidizable metals, like nickel, gold, with poor crystallinity during RF plasma etching, could not produce efficient protecting layer, inefficiently contributed to the anisotropy etching.

For the etching on the high quality diamond film, the whiskers aligned perfectly with the crystal orientations. Therefore, it is possible to control the distribution of the whisker by controlling the crystal orientations' growth during MWPCVD deposition.

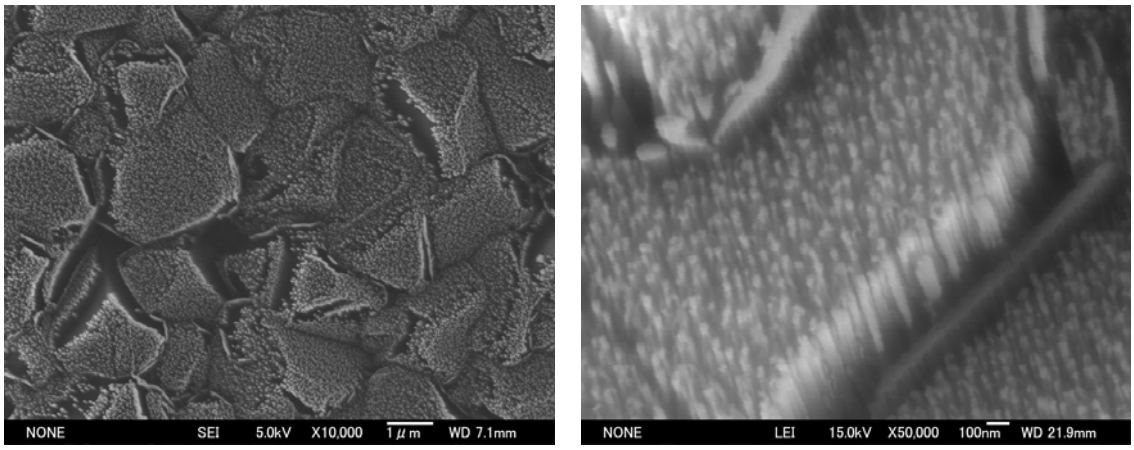

(a) (b)

Fig. 4.1. Etching of an as-grown diamond film: (a) top view and (b) perspective view.

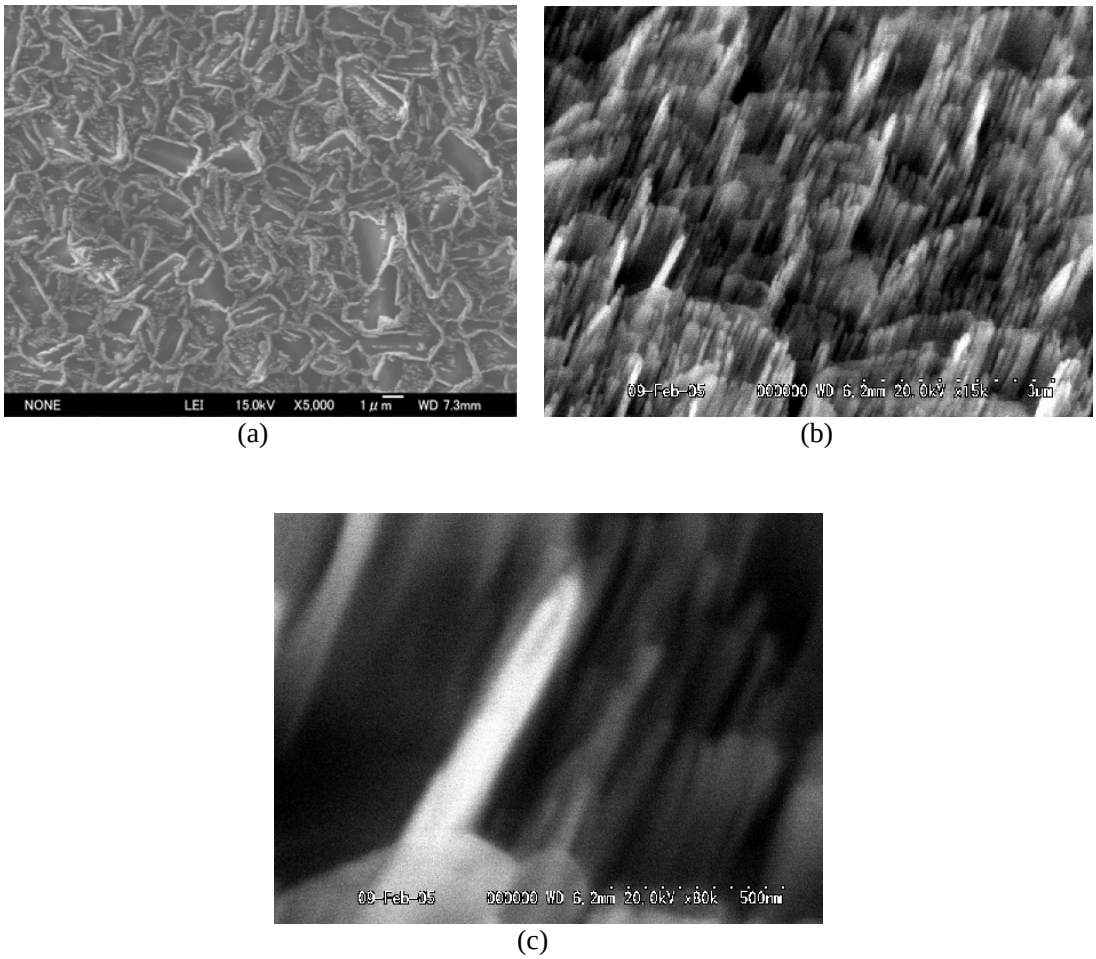

(a) (b)

(c)

Fig. 4.2. Whiskers obtained from etching 10 min of Mo-coated diamond film: (a) top view, (b) perspective view, and (c) whiskers with 50 nm in diameter and 1 μm in height were observed.

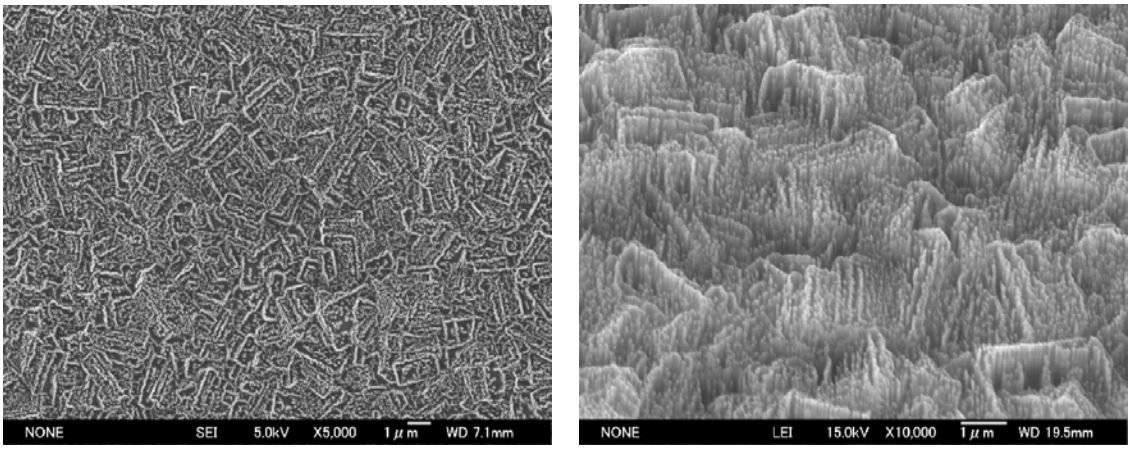

(a) (b)

Fig. 4.3. Whiskers obtained from etching 10 min Al-coated diamond film: (a) top view and (b) perspective view.

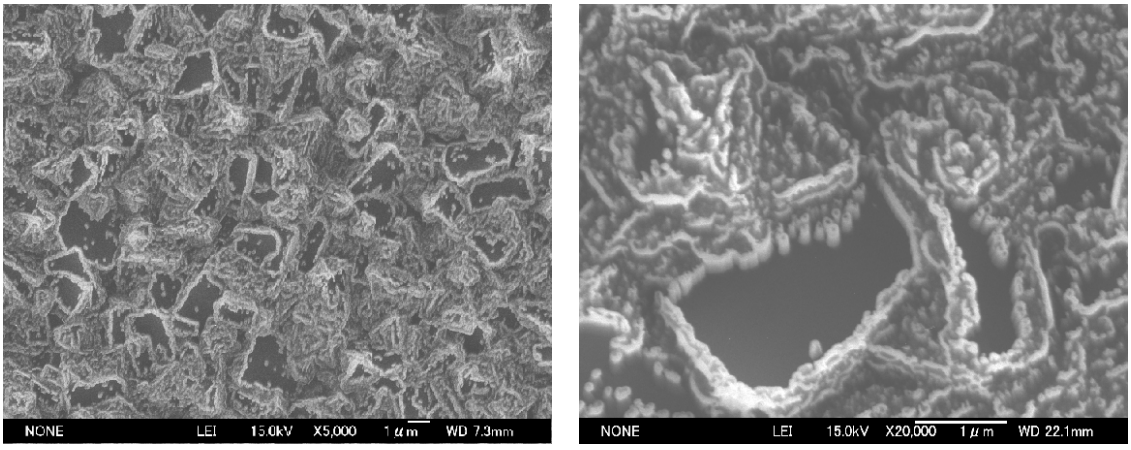

(a) (b)

Fig. 4.4. Whiskers obtained from etching 10 min of Ni-coated diamond film: (a) top view and (b) perspective view.

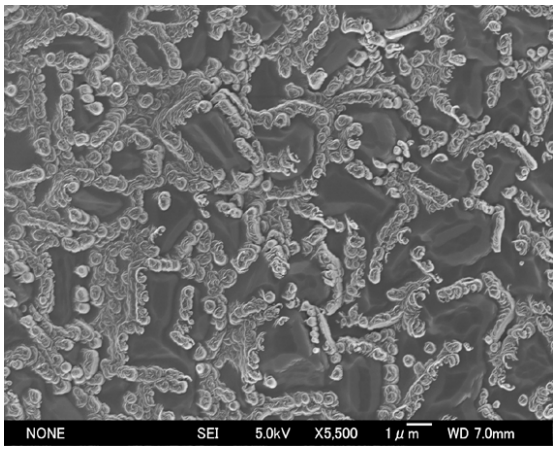

Fig. 4.5. Etching of 3 min Au-coated diamond surface.

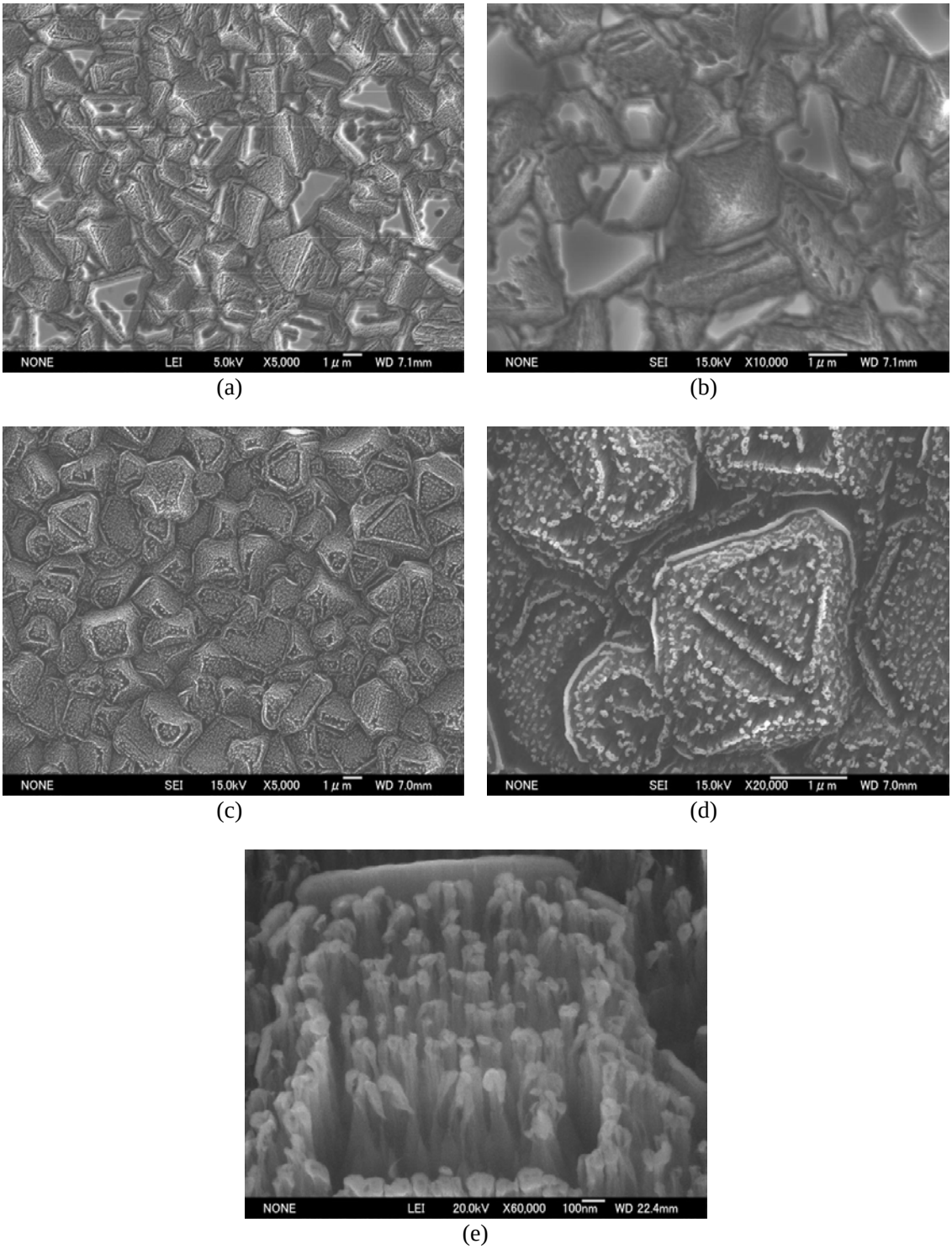

Fig. 4.6. (a), (b) and (c): Etching of 10 min Fe-coated diamond film in O_2 RF plasma for 30, 50 and 70 min, respectively; (d) the whiskers followed the same locations of diamond form; and (e) the whiskers aligned well with the same orientations of diamond crystal.

References

[1] F. J. Himpsel, J. A. Knapp, J. A. Van Vechten, and D. E. Eastman, Phys. Rev. B **20**, 624 (1979).

[2] E. I. Givatgizov, V. V. Zhirnov, A. N. Stepanova, E. V. Rakava, A. N. Kiselev, and P. S. Plekhanov, Appl. Surf. Sci. **87**, 24 (1995).

[3] Y. Nishibayashi, H. saito, T. Imai, N. Fujimori, Diamond Relat. Mater. **9**, 290 (2000).

[4] J. T. Glass, B. A. Fox, D. L. Driefus, and B. R. Stoner, MRS Bulletin **23**, 49 (1998).

[5] I. Brodie and C. A. Spindt, Adv. Electron. Electron Phys. **83**, 1 (1992).

[6] V. V. Zhirnov. E. T. Givatgizov, A. N. Stepanova, and P. S. Plekhanov, J. Vac. Sci. Texhnol. B **13**, 418 (1995).

[7] V. V. Zhirnov, J. Phys. C **5**, 107 (1996).

[8] W. J. Zhang, C. Sun, L. Bello, C. S. Lee, and S. T. Lee, JVST **17**, 763 (1999).

[9] C. Vivensang, L. F. Manin, M. V. Ravet, G. Turban, F. Rosseaux, and A. Gicquel, Diamond Relat. Mater. **5**, 840 (1996).

[10] N. S. Xu, R. V. Latham, and Y. Tzeng, Electron. Lett. **29**, 1596 (1993).

[11] M. Bernard, A. Deneuville, L. Ortega, K. Ayadi, P. Muret, Diamond Relat. Mater. **13**, 288 (2004).

[12] C. Li, and A. Hatta, Diamond Relat. Mater. **14,** 1780 (2005).

[13] C. Li, and A. Hatta**,** Trans. MRS **30**, 287 (2005).

[14] E. S. Baik, and Y. J. Baik, J. Mater. Res. **4**, 924 (2000).

CHAPTER 5

CHARACTERIZATION OF DIAMOND WHISKERS

5.1 Raman spectroscopy

5.1.1 Raman spectroscopy theory

In 1928, C. V. Raman [1] discovered an extremely faint type of electromagnetic scattered radiation. This was an amazing feat due to the small amount of scattered radiation present (about one hundred millionth part of the incident light). He would later receive a Nobel Prize for discovering this effect, which is known as the "Raman Effect."

When incident light strikes a sample, part of the light is scattered. Most of the scattered light has the same wavelength as the incident light; this is called Rayleigh scattering. Some of the light is scattered at a different wavelength; this is called Raman scattering. The energy difference between the incident light and the Raman scattered light is called the Raman shift. It is equal to the energy required to get the molecule to vibrate or to rotate. Several different Raman shifted signals will often be observed in a single sample; each being associated with different vibrational or rotational motions of molecules in the sample. The particular molecule and its environment will determine what Raman signals will be observed.

In practice, because Raman effect is so slight, a laser is used as the source of the incident light. A plot of Raman intensity *vs*. the frequency of the Raman shift is a Raman spectrum. It usually contains sharp bands that are characteristic of the functional groups of the compounds or materials. This information can be interpreted to determine chemical structure and identify the compounds present. Raman spectroscopy is a good technique for qualitative analysis and for discrimination of organic and/or inorganic compounds in mixed materials.

A Raman spectrum can be obtained from samples that are as small as 1 μm. The intensities of bands in a Raman spectrum depend on the sensitivity of the specific vibrations to the Raman effect and are proportional to concentration. Thus, Raman spectra can be used for semi-quantitative and quantitative analysis. The technique is used for identification of organic molecules, polymers, biomolecules and inorganic compounds both in bulk and as individual particles. Raman spectroscopy is particularly useful in determining the structure of different types of carbon (diamond, graphitic, diamond like carbon, etc.) and their relative concentrations. A simplified energy diagram that illustrates these concepts is given Fig. 5.1.

The energy of the scattered radiation is less than the incident radiation for the Stokes line and the energy of the scattered radiation is more than the incident radiation for the anti-Stoke line. The energy increase or decrease from the excitation is related to the vibrational energy spacing in the ground electronic state of the molecule and therefore the wavenumber of the Stokes and anti-Stokes lines are a direct measure of the vibrational energies of the molecule. A schematic Raman spectrum may appear as Fig.5.2

In the example spectrum, notice that the Stokes and anti-Stokes lines are equally displaced from the Rayleigh line. This occurs because in either case one vibrational quantum of energy is gained or lost. Also, note that the anti-Stokes line is much less intense than the Stokes line. This occurs because only molecules that are vibrationally excited prior to irradiation can give rise to the anti-Stokes line. Hence, in Raman spectroscopy, only the more intense Stokes line is normally measured.

The Raman effect is due to the interaction of the electromagnetic field of the incident radiation, E_i, with a molecule. The electric field may induce an electric dipole in the molecule, given by

$$p = \alpha E_i \tag{5.1.1}$$

where α is referred to as the polarizability of the molecule and p is the induced dipole. The electric field due to the incident radiation is a time-varying quantity of the form

$$E_i = E_0 \cos (2\pi V_i t) \tag{5.1.2}$$

For a vibrating molecule, the polarizability is also a time-varying term that depends on the vibrational frequency of the molecule, V_{vib}

$$\alpha = \alpha_0 + \alpha_{vib} \cos (2 \pi V_{vib} t) \tag{5.1.3}$$

Multiplication of these two time-varying terms, E_i and α, gives rise to a cross product term of the form:

$$\frac{\alpha_{vib} E_0}{2} [\cos 2\pi t(V_i + V_{vib}) + \cos 2\pi t(V_i - V_{vib})] \tag{5.1.4}$$

This cross term in the induced dipole represents light that can be scattered at both higher and lower energy than Rayleigh (elastic) scattering of the incident radiation. The incremental difference is from the frequency of the incident radiation, V_i, and the vibrational frequencies of the molecule, V_{vib}. These lines are referred to as the “anti-Stockes” and “Stockes” lines, respectively. The radio of

the intensity of the Raman anti-Stockes lines is predicted to be

$$\frac{I_A}{I_S} = \left(\frac{V_i + V_{vib}}{V_i - V_{vib}} \right)^4 e^{\left(\frac{-h\nu_{vib}}{kT} \right)}$$

(5.1.5)

The Boltzmann exponential factor is the dominant term in the equation, which makes the anti-Stockes features of the spectra much weaker than the corresponding Stockes lines.

5.1.2 Raman spectroscopy in analyzing diamond

The large differences in Raman spectra among the various forms of carbon make the Raman spectroscopy particularly attractive for distinguishing one form of carbon from the others. Because of the significantly large Raman cross section for graphite sp^2 bonds (5×10^{-5} $cm^{-2}\cdot sr^{-1}$) relative to diamond sp^3 bonds ($9\times10^{-7}cm^{-1}\cdot sr^{-1}$), the Raman spectroscopy allows sensitive detection of small concentrations of sp^2 bonding in diamond films.

Diamond belongs to the space group O_h with two atoms per primitive cell, it possesses one triply degenerate zone-center optical phonon with $\Gamma^{(25+)}$ (F_{2g}) symmetry [2] which is the only mode that is Raman-active in the first order. The diamond structure has no first order infrared absorption. The first order diamond Raman band appears as a singles sharp line at 1332 cm^{-1}. It is the characteristic diagnostic feature for diamond [3-5]. The line width of the first order diamond Raman line is about 1.9 cm^{-1} at room temperature, and increasing with temperature to about 3.5 cm^{-1} at 900 K. The width is solely due to lifetime broadening effect of the Raman phonon [6]. The life time effect comes from the inharmonic vibrational potential which permits the Raman phonon to decay into two acoustic modes. There is also a sharp two phonon line at 2450 cm^{-1}, which does not appear in spectra obtained by means of micro focus instrument [7]. The spectra of hexagonal diamond (also known by the mineral name, lonsdaleite) powder exhibit a single band which varies in wave number from particle to particle from 1315 cm^{-1} to 1326 cm^{-1}[7]. The Raman spectra of cut faces on natural diamond sometimes show a satellite band at 1319 cm^{-1} with the same line width as the main peak at 1332 cm^{-1} [7]. A Raman spectroscopy of a pure diamond is shown in Fig. 5.3. [8].

Most CVD films consist of small diamond crystallites surrounded by graphitic or amorphous carbon grain boundaries. These boundaries produce extra signal in the Raman spectrum that can help diagnose the crystallite size and overall “quality” of the diamond sample.

A single crystal of graphite of graphite produces a single peak at 1575 cm^{-1} [9] whereas in all other graphite materials (activated charcoal, carbon black etc.) a second feature appears at 1355 cm^{-1}. The intensity of this second peak increases relative to the first peak as (a) the amount of

"disorganized" carbon increased and (b) the graphite crystal size decrease. The 1575 cm^{-1} (called "G" peak, after crystalline graphite) is caused by breakdown of the solid-state Raman selection rules, which prevent its appearance in the spectrum of the perfect crystal, as shown in Fig. 5.4.

The absolute Raman peak intensity is affected by two important parameters—the scattering cross-section and the absorption coefficient. The ratio of Raman cross-section for diamond to graphite is about 1/ 50. Diamond is almost transparent in the visible range whereas graphite is highly absorbing material. This means, if some samples consisting of graphite and diamond regions are illuminated with a visible light, they can not be measured uniformly. The transparent regions will be totally illuminated while only the surface layer of the absorbing regions will be selectively measured. The effect of inhomogeneous absorption becomes critical when the domain size of the absorbing regions (graphite) is equal to or large the crystalline sizes of graphite (~ 20 nm). Therefore, both the concentration and the crystalline size of graphite region in diamond films have significant effects on the resulting Raman spectra.

5.1.3 Raman spectroscopy device

A Raman spectroscopy system (JASCO, NR-1800) is used to analysis CVD diamond and diamond whiskers. Fig. 5.5 shows the picture of the Raman system used in this research work. Micro-Raman spectroscopy has been carried out with a ×100 objective lens using a 514.5 nm argon ion laser (Coherent, K-70) line for excitation. With the aid of microscope which is equipped with CCD camera and TV monitor, the illuminated area can be selected and examined in situ. The block diagram of this system is shown in Fig. 5.6.

5.1.4 Experimental results

In this work, the Raman spectroscopy system introduced in last section was used to examine the bonding structures in diamond films and whiskers.

Diamond film was deposited (CH_4 in H_2 3%) on the Si substrate using the MWCVD system and the conditions introduced in Chapter 2. Before etching, Raman spectroscopy of as-grown diamond film was measured for further comparison, as shown in Fig. 5.7.

The characteristic fingerprint of diamond film at a single sharp Raman line at 1332 cm^{-1} was observed. Also, the presence of a broad and very low peak around the wave number of 1550 cm^{-1} exhibits that there was a very small amount of graphite and /or amorphous carbon in the diamond film. It illustrated that the sp^3 (as diamond) was more dominant than the sp^2 (as graphite). This diamond film was used in the sputtering and etching process whose conditions were described in Chapter 2. The nanowhiskers were formed on the diamond film surfaces by O_2 or O_2/Ar radio frequency plasma etching under different etching conditions. In order to determine the structures of

the formed whiskers and to inspect whether there was graphitic transformation of diamond during etching or not, Raman spectroscopy was performed for the samples after etchings. In order to prevent the influence from the remaining diamond film on the substrate, the whiskers were physically scraped off the substrate and collected on a piece of transparent glass, as shown in Fig. 5.8 (a) and (b). Scanning electron microscope was used to examine if there were diamond particles mixed with the whiskers, eventually no diamond particles were found in the collected diamond powders. For all of the samples, same method was used to collect the whisker for measurement.

In this experiment, Raman spectroscopy measurements were performed on three kinds of selected samples. They were nano-whiskers obtained from the Al, Mo, and Fe-coated diamond films, respectively. The etching conditions were mentioned in chapter 4.

Figure 5.9 shows the Raman spectroscopy measured from nanowhiskers obtained from etching Al-coated diamond film. Since the whiskers were fabricated on the diamond film, Raman spectra would include those from the remaining diamond film and the whiskers. The Raman spectrum from the whiskers on the diamond was almost as same as that from the diamond. It was difficult to recognize the real spectrum from the whiskers, shown as the top and middle Raman spectra. This was the reason why the whiskers were peeled. Comparing to the diamond film, the Raman spectrum from the whiskers (the bottom spectrum) was slightly changed. The spectrum also showed a typical sharp Raman at 1332 cm^{-1}. However, the ratio of the diamond peak intensity was decreased. This variation was most properly due to a small amount of crystal graphite formed in the diamond boundaries during the etching process.

Fig. 5.10 shows the Raman spectra obtained on the etched Mo-coated diamond film using O_2 radio frequency plasma. In this sample, diamond film deposited in the much high CH_4 concentration (CH_4 in H_2 5%). The Raman spectrum from the diamond film showed the typical diamond peak centered at 1332 cm^{-1} with two weak peaks: D peak at 1355 cm^{-1} and G peak at 1580 cm^{-1}. The graphite phase and diamond-like carbon might exist in a small amount due to the high ratio of introduced CH_4 during the deposition process. Theoretically, the linewidths and the intensity ratio of D band and G band vary depending on the structure of the carbons. The highly disordered carbons such as charcoal and coke show very broad bands whereas the lines are relatively narrow in glassy carbon and also in polycrystalline graphite.

Similar to the last sample, the diamond peak intensity was remarkably decreased. The peak characteristic of the diamond C-C sp^3 bonds was very prominent and appeared at 1333 cm^{-1}, which was quite close to the standard value (1332 cm^{-1}) of the as-grown diamond. However, the position and the intensity of the sp^2 bond carbon peak slight shifted to 1590 cm^{-1} with sharp intense band which had been assigned to the predicated E_{2g} C-C stretching mode [11]. It also indicates that there was graphite sheet formed during etching. Actually, the O_2 dominantly contributed to reactive ion etching to form diamond whisker, however, it also might become a menace to damage the diamond structure due to plasma bombardment. The D band also shifted to 1357 cm^{-1} band which did not

appear in large grain single crystals but does appeared in well crystallized graphite with small particle sizes. Therefore, it could be assumed that the non-diamond phase increase might be attributed to a small amount of local transformation from sp^3 to sp^2 during etching process. However, theoretically, ratio of Raman scattering cross-sections of the graphite should be 50 times higher than that of the diamond. If there were same quantities of sp^2 graphitic carbons, their peaks should be much stronger than the sp^3 diamond peak. For this sample, the diamond peak was much stronger than the non-diamond peaks, suggesting that the whiskers had not changed their bonding structures after etching. Most of the bonding structures were kept in sp^3 diamond structures during etching process. Therefore, we could conclude that the whiskers were still diamond after etching.

The third sample was the Fe-coated diamond film which was grown up with lower CH_4 ratio (CH_4 in H_2: 1%) during deposition process. The sharp peak at a wave number of 1332 cm^{-1} has very narrow full width at half maximum, which means that the diamond quality was very good, as shown in Fig. 5.11. After etching, almost no any graphite peak appeared in the Raman spectrum obtained from whiskers. However, the dominant diamond peak slight shifted to 1328 cm^{-1}. Because the etching preferentially occurred at the grain boundaries, some defect might appear with the tension strength which made the Raman spectrum to shift.

From above measurements, one can conclude that the quality of the diamond was the least varied with high quality diamond.

5.2 Energy dispersive X-ray spectroscopy

5.2.1 Energy dispersive X-ray spectroscopy theory and device

Energy Dispersive X-ray (EDX) analysis is a technique used for identifying the elemental composition of the specimen, or an area of interest thereof. The EDX analysis system works as an integrated feature of a scanning electron microscope (SEM), and can not operate on its own without the latter.

During EDX analysis, the specimen is bombarded with an electron beam inside the scanning electron microscope. The energy of the beam is typically in the range 10-20 keV. The bombarding electrons collide with the specimen atoms' own electrons, knocking some of them off in the process. A position vacated by an ejected inner shell electron is eventually occupied by a higher-energy electron from an outer shell. To be able to do so, however, the transferring outer electron must give up some of its energy by emitting an X-ray. The energy of the X-rays emitted depending on the material under examination. The X-rays are generated in a region about 2 microns in depth.

The amount of energy released by the transferring electron depends on which shell it is transferring from, as well as which shell it is transferring to. Furthermore, the atom of every element releases X-rays with unique amounts of energy during the transferring process. Thus, by measuring the amounts of energy present in the X-rays being released by a specimen during

electron beam bombardment, the identity of the atom from which the X-ray was emitted can be established.

The output of an EDX analysis is an EDX spectrum. The EDX spectrum is only a plot of how frequently an X-ray is received for each energy level. An EDX spectrum normally displays peaks corresponding to the energy levels for which the most X-rays had been received. Each of these peaks is unique to an atom, and therefore corresponds to a single element. The higher a peak in a spectrum, the more concentrated the element is in the specimen.

An EDX spectrum plot not only identifies the element corresponding to each of its peaks, but the type of X-ray to which it corresponds as well. For example, a peak corresponding to the amount of energy possessed by X-rays emitted by an electron in the L-shell going down to the K-shell is identified as a K-Alpha peak. The peak corresponding to X-rays emitted by M-shell electrons going to the K-shell is identified as a K-Beta peak. See Figure 5.12.

In this research, an EDX (EX-23000 BU) was set up with a field emission scanning electron microscope (FESEM) (JEOL JSM-7400F) together, as shown in Fig. 5.13

5.2.2 Experimental results

After etching process, EDX was carried out to determine the compounds on the etched surfaces. A sample obtained from the 3 minutes Al-coated surface was selected for investigation. Fig. 5.14 (a) is an SEM image of the obtained whiskers after etching process. Firstly, EDX mapping measurement was carried out on the same sample to determine the locations of metal particles. The results were shown in Figs. 5.14 (b), (c), and (d). Observing the intensity distribution of the individual particles, one can easily recognize that the Al and O particles were located at the same position on the diamond film. It suggests that Al coated on the surface of diamond film would react with etching gas O_2 to produce Al_2O_3 which is a stable oxide remaining on the diamond surface. The function of the Al_2O_3 was to serve as masks to protect the surface underneath due to their incomparably lower etching rate, compared to that of the carbon substrate [11].

In order to further confirm this supposition, an EDX spot measurement was performed on the same sample. The spectra show that there were Al and O on the top of the whiskers, as shown in Figs. 5.15 (a) and (b). However, no Al was found on the over-etched diamond surface (non-whiskers areas), as shown in Figs. 5.16 (a) and (b). From above measurements, the function of the coating and distribution of the whisker were well understood. The oxidizable metal reacted with O_2 to produce metal oxide which would cap on the tips of the whiskers to inhibit the etching rate and influence the distribution of the whiskers. This sample was coated with Al in DC sputtering device for only 3 min which could not form a uniform thin layer on the diamond surface. It could be assumed that the coated metal particles were preferentially adopted by the grain boundaries so that the whiskers mostly appeared in those locations. It means that the grain boundaries were

protected by metal masks, resulting in a very low etching rate.

However, when extending Al sputtering time to 10 min, a very thin metal layer was formed on the surface of the diamond film. The distribution of whiskers obtained was quite different. As shown in Fig. 5.17 the whiskers with high density were formed on the diamond film. An EDX spot measurement also performed to inspect this sample. The results are shown in Figs. 5.18 and 5.19.

The results were almost the same as that obtained from the 3 min coated diamond film. (Observed Pt particles were coated on the whiskers surface for the field emission measurement which will be used in other experiments). The Al_2O_3 capped on the tips of the whiskers and no any Al particles remained in the non-whiskers areas. This further confirmed that the distribution of the whiskers was remarkably influenced by the thickness of the coated metal. Therefore, the metal masks were a critical factor for anisotropic etching of the diamond films.

5.3 Cathodoluminescence spectroscopy

5.3.1 Cathodoluminescence spectroscopy theory and device

Electrons can be used to characterize materials in many methods [12, 13]. Interactions of keV electrons with materials lead to different signals, for instance secondary electron, backscattered electrons, X-ray and photons in the ultraviolet, visible and infrared spectral range. The last process is called cathodeluminescence (CL) and can be defined as the emission of light as a result of electron (Cathode ray) bombardment [14].

CL can achieve a high spatial resolution comparing to other forms of luminescence. The typical diameter of an electron beam is in the order of nanometers and the interaction volume of such a beam is in the order of 100 nm, which is at least one order of magnitude smaller than the spot of a typical laser beam. By varying beam energy one can also obtain depth resolved information, as the range of the electrons is directly proportional to the beam energy.

CL has a wide variety of applications, in geology it is used for the investigation of rock compositions. In material science CL can be used to characterize the defects of the materials and the high resolution makes CL an idea tool in nanosciences [15, 16], for example, to investigate the properties of nanostructures.

CL spectroscopy is a vitally important technique for characterizing the defects in diamond. It is a powerful tool to obtain information about optical centers existing in the near-surface region. The luminescence from diamond has been studied extensively about 50 years. Most of the early works were carried out using ultraviolet radiation or X-ray as excitation photons. The use of a focused electron beam to simulate lumininescence in diamond was pioneered by Raph [17] using firstly a converted electron microscope and later, a custom-built cathodoluminescence equipment. Electron-beam excitation is simply a very convenient method for producing a high concentration of

electron-hole pairs. Electron and holes may recombine in a variety of different ways. In very pure diamonds, an electron and a hole can recombine directly to give the free exciton “edge emission”, in diamonds containing donor and acceptor, such as nitrogen and boron, radiative recombination can happen between an electron trapped to a donor and a hole trapped to an acceptor; in addition, many vibronic center may capture an exciton and subsequently be de-excited to produce an oscillatory luminescence.

In this research work, cathodoluminescence measurement was carried out using a Topcon 350 type scanning electron microscope. Monochromatized light was detected by a Humamatsu R928 photo-multiplier tube for imaging and a Roper LN/CCD-400EB-GI for collecting the spectra. The device and the schematic diagram of the CL measurement system are shown in Fig. 5.20.

5.3.2 Experimental results

Cathodoluminescence measurement was performed on the diamond surface where two components were present: diamond and whiskers, for each sample. Under the SEM these two parts could be easily observed. As an example, SEM images obtained from the Mo-coated samples are shown in Fig. 5.21. In Fig. 5.21 (a) the separate line between the Mo-coated diamond film and the whiskers parts is clearly observed. Figs. 5.21 (b) and (c) present the enlarged SEM images of diamond film and whiskers.

In Chapter 4, the effects of different coating metals on the formation of diamond whiskers were compared. The metals were classified into two types: oxidizable and non-oxidizable. CL measurement was chosen to analyze functions of these two kinds of metal coatings. The Mo-coated and Ni-coated diamond films were used as representative samples, respectively.

The CL spectra were taken at 21 points along a line crossing the boundary between the whiskers and the diamond, an interval of 20 μm between the investigated points was considered.

Fig. 5.22 shows the CL measurement on the Mo-coated diamond film. The arrow direction illustrates the examination points from diamond to whiskers part.

From the CL spectrum of the Mo-coated sample, it was found that the dominant diamond peak was band-A centered at 425 nm. At the beginning of the etching process, the coated Mo reacted with O_2 to produce molybdenum oxide which would converge to form islands on the surface of diamond film, which was attributed to the quite different surface tension strengths between the Mo and carbon, making it easy for the islands to form. Although Mo also could react with carbon to form molybdenum carbide, its amount was small due to the lower substrate temperature. Both of them would contribute to form a protecting monolayer on the top of whiskers, restraining further etching underneath. The average luminescent intensity of the whiskers was almost the same as those of the as-diamond. Therefore, it could confirm that Mo coating contributed to form well needle-like whiskers.

However, in the case of Ni-coated diamond film, as shown in Figs. 5.23, the situation was significantly different. Compared to the bright part which corresponded to the diamond, the luminescent intensity was dramatically decreased, showing in the dark area in Fig 5.23 (a).

In Chapter 4, it was not found any regularity of the distribution of the whisker obtained from the Ni-coated diamond film. The distribution of the whiskers did not correspond to that of the Ni particles. One reason might be that non-oxidized Ni is conductive, during the sputtering process, nickel particles can be diffused on the diamond surface by ion bombardment, resulting in forming a continuous thin coating layer which is difficulty to be etched. Another reason is might be the significantly decrease of Ni melting point produced nano-balls which had higher flow ability to move to the grain boundaries during plasma etching. Another effect factor should be considered is the similar surface tension strengths between Ni and carbon so that Ni easily coalesced to form a very thin metal layer to cover the diamond surface. Contrast with Ni, Mo is oxidized metal which will be insulating presenting at molybdenum oxide which will charge up to form reflected ions during the sputter process. The molybdenum oxide will form some islands on the diamond surface. Therefore, Ni particles were not stable on the top of the diamond film, which significantly influenced the anisotropic etching of the diamond film. Therefore, high quality whiskers could not be formed on the diamond surface with nickel coating. The CL results also confirmed the assumption that the quality of the whiskers was lower and perhaps damages were induced during the etching process due to the poor crystallinity of Ni in RF plasma etching.

In order to further investigate, the Fe-coated film was also examined using the same method. The results are shown in Figs. 5.24 (a)–(c). Like the case of the Mo-coated film, the average luminescent intensity of the whiskers was almost the same as those of the as-diamond. The quality of the diamond did not change before and after etching process. The explanation should be similar to that of the Mo-coated diamond film.

5.4 Summary

In this chapter, the characteristics of diamond whiskers were analyzed by Raman spectroscopy, Energy dispersive X-ray spectroscopy and Cathodoluminescence spectroscopy measurements, respectively.

Raman spectroscopy measurement showed that the strongest diamond peak was centered at 1332 cm^{-1}, the sp^3 bonding structure of the whiskers was still dominant though there were slight G or D peaks appearance. Therefore, the quality of the diamond film did not changed after radio frequency etching process. The whiskers are still diamond.

EDX measurement confirmed the effects of the metal coating. The metal particles would cap on the tips of the whiskers after etching. No metal particles were found on the non-whiskers area. The distribution of the whiskers also was remarkably influenced by the thickness of the coating metal.

The high number density of the whiskers was due to the unformed metal coating layer. However, the metal particles or islands contributed to the formation of lower number density whiskers.

The functions of two kinds of metal coating—oxidizable and non-oxidizable metal were examined with CL measurements. The results showed that the first kind of metal coating did not change the luminescent intensity of the diamond. However, the luminescent intensity dramatically decreased on latter metal coating film. Therefore, oxidizable metal contributed to the formation of better diamond whiskers, non-oxidizable metal deteriorate the quality of the diamond film during etching process.

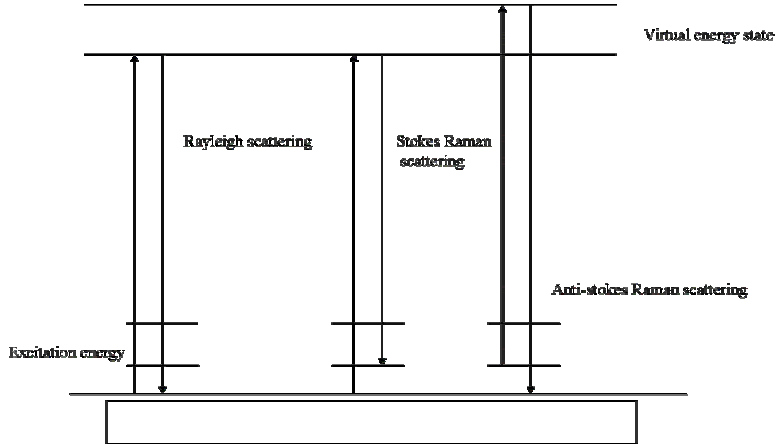

Fig. 5.1. A simplified energy diagram that illustrates Raman effect.

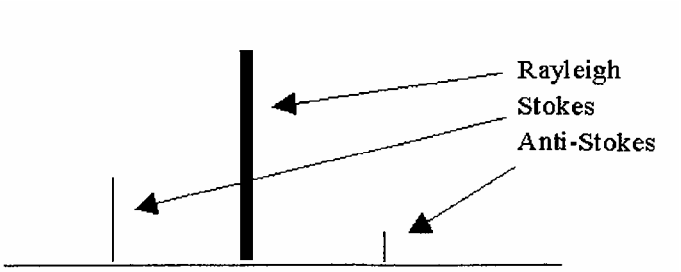

Fig. 5.2. A schematic of Raman spectrum may appear as intense Stokes line.

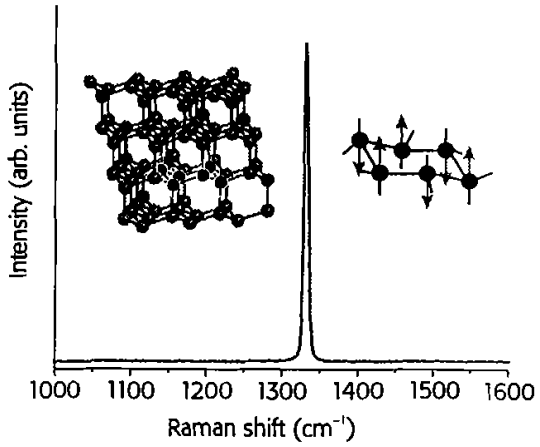

Fig. 5.3. Raman spectrum of a diamond single crystal, inset shows a cartoon of the nuclear displacements associated with this vibration. In the bulk crystal the vibration propagates throughout the lattice.

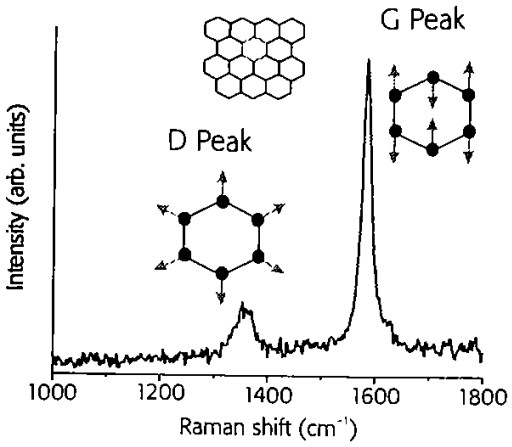

Fig. 5.4. The 514 nm Raman spectrum of highly orientated pyrolitic graphite, with inset cartoons of the nuclear displacements associated with each vibration.

Fig. 5.5. A photo of Raman spectroscopy system (JASCO, NR-1800) used in this research work.

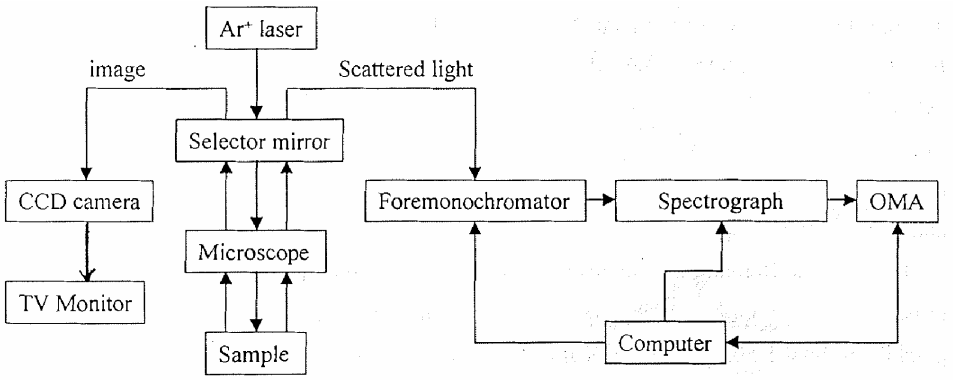

Fig. 5.6. Block diagram of Raman spectroscopy system.

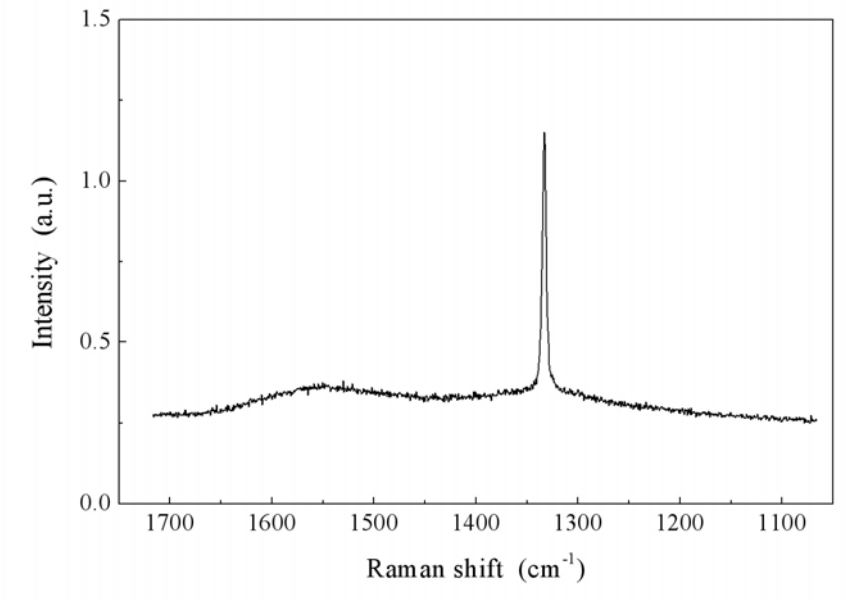

Fig. 5.7. Raman spectrum of as-grown diamond film deposited on the Si substrate using MWCVD system (CH_4 in H_2 3%).

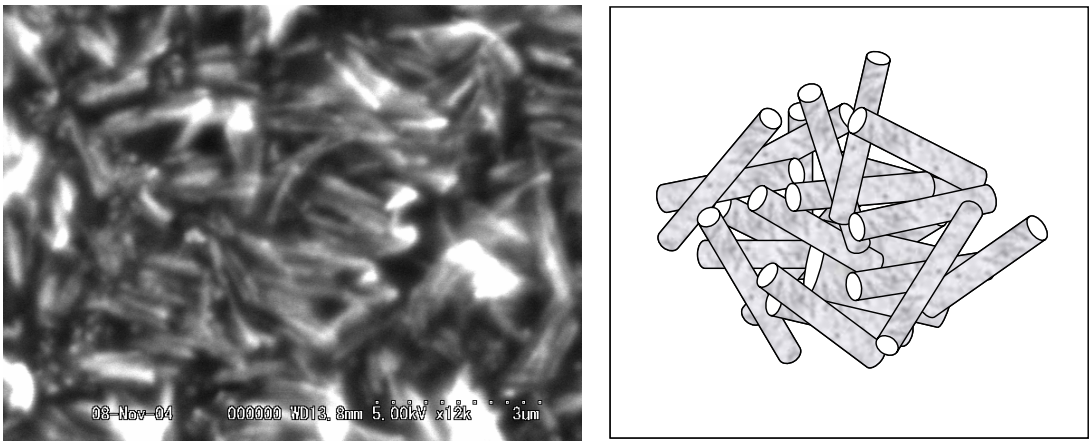

(a) (b)

Fig. 5.8. (a) An SEM image of scratched diamond whiskers on a transparent glass, and (b) the schematic of collected diamond whiskers.

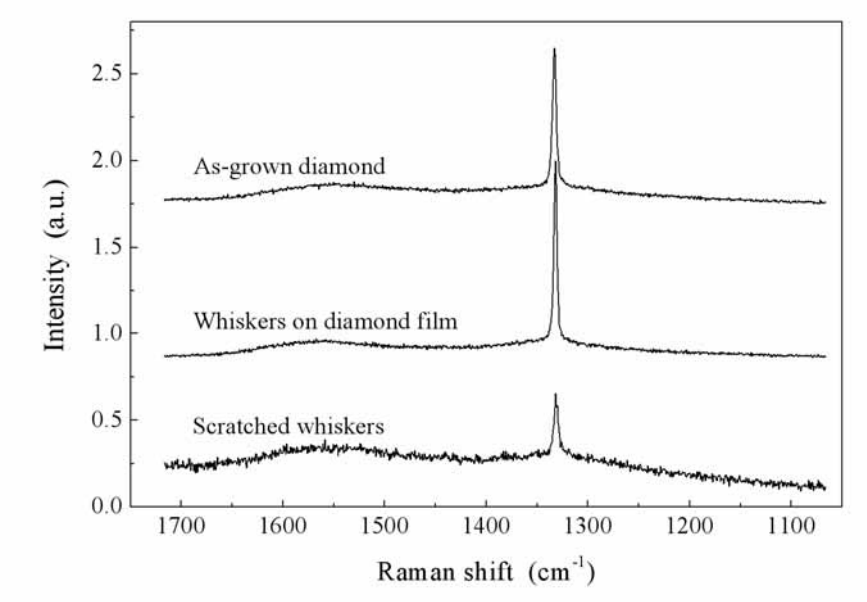

Fig. 5.9. Raman spectroscopy measured from nanowhiskers obtained from etching 10 min Al-coated diamond film.

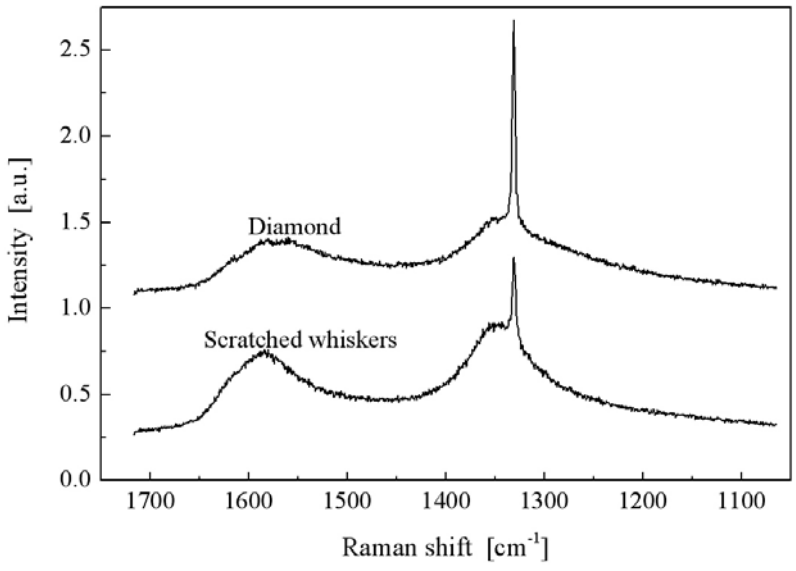

Fig. 5.10. Raman spectroscopy measured from nanowhiskers obtained from etching 10 min Mo-coated diamond film.

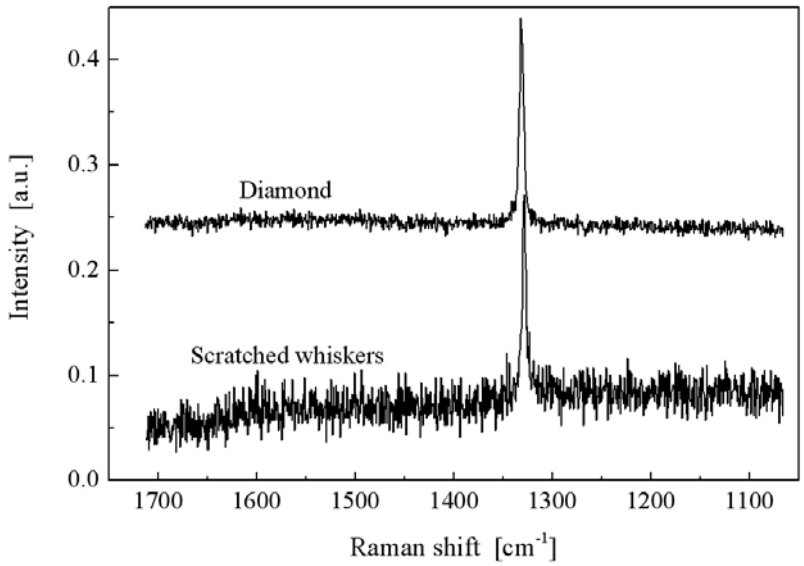

Fig. 5.11. Raman spectroscopy measured from nanowhiskers obtained from etching 10 min Fe-coated diamond film.

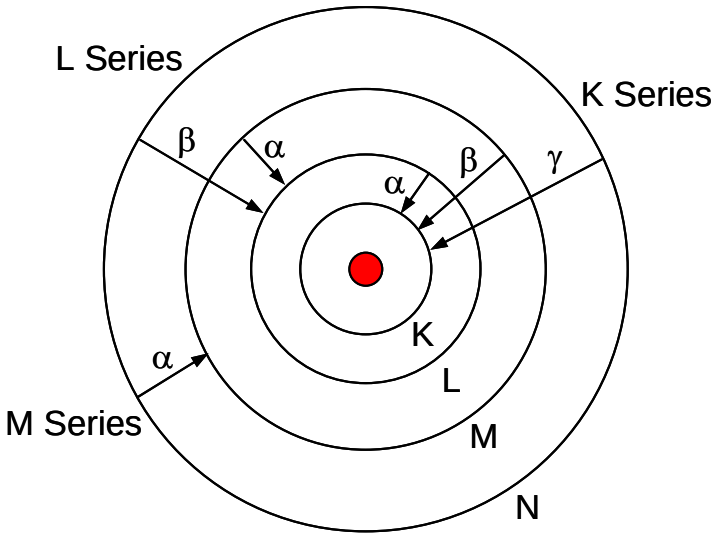

Fig. 5.12. Elements in an EDX spectrum are identified based on the energy content of the X-rays emitted by their electrons as these electrons transfer from a higher-energy shell to a lower-energy one.

Fig. 5.13. Energy Dispersive X-ray Spectroscopy (EX-23000 BU) combines with a Field Electron Emission Microscope (JEOL JSM-7400).

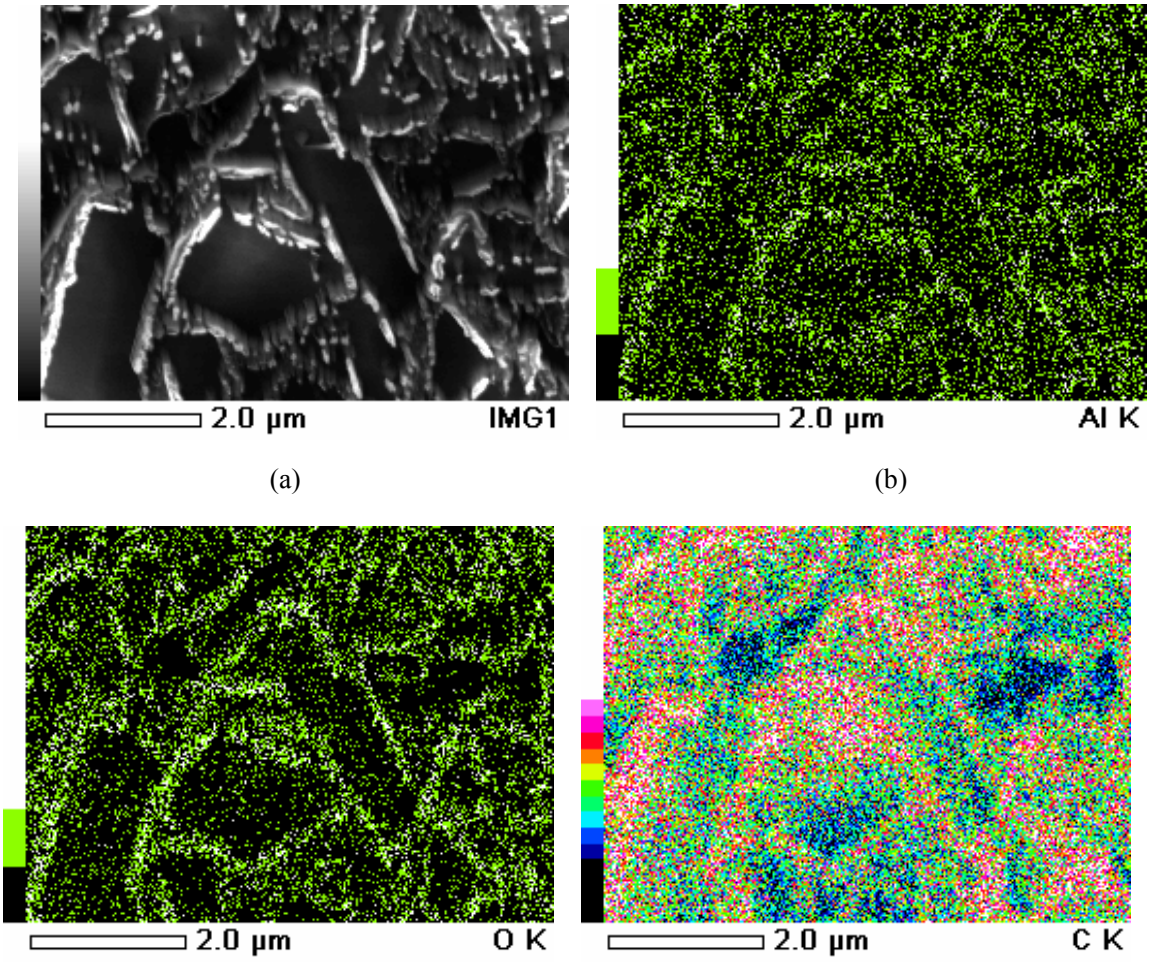

(a) (b)

(c) (d)

Fig. 5.14. EDX mapping measurement of whiskers obtained on 3 min Al-coated diamond film.

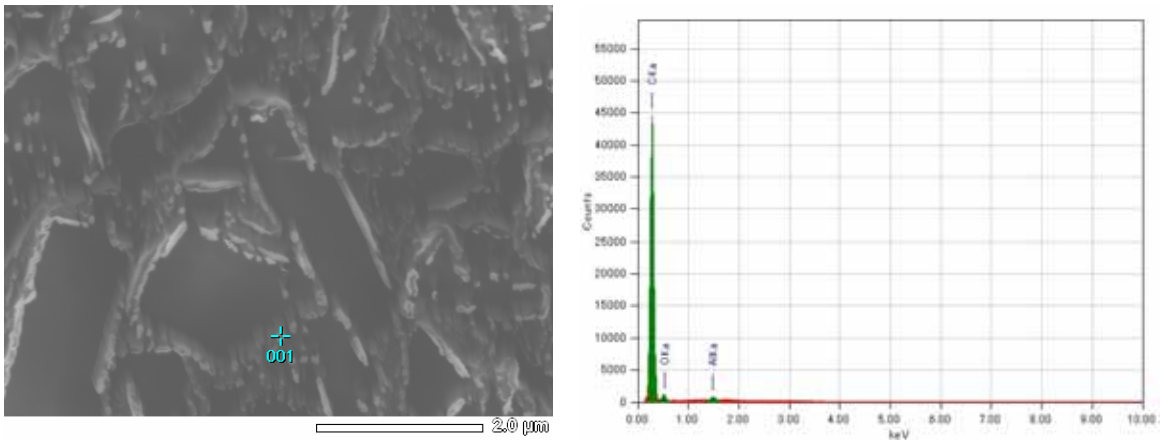

(a) (b)

Fig. 5.15. EDX spot measurement of whiskers obtained on 3 min Al-coated diamond film, tip of the whisker.

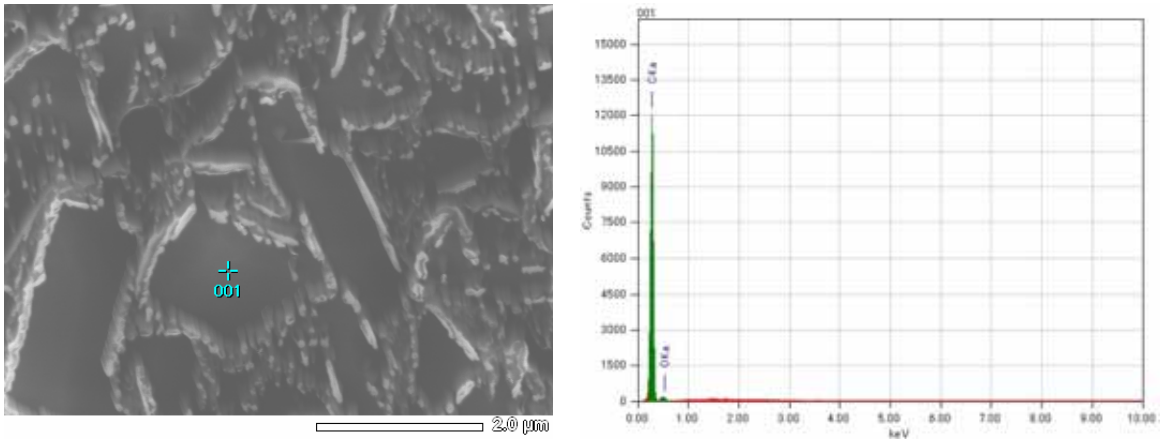

(a) (b)

Fig. 5.16. EDX spot measurement of whiskers obtained on 3 min Al-coated diamond film, non-whiskers point.

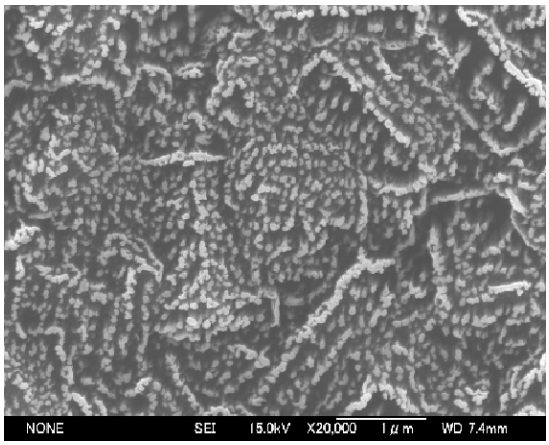

Fig. 5.17. SEM image of whiskers obtained on 10 min Al-coated diamond film.

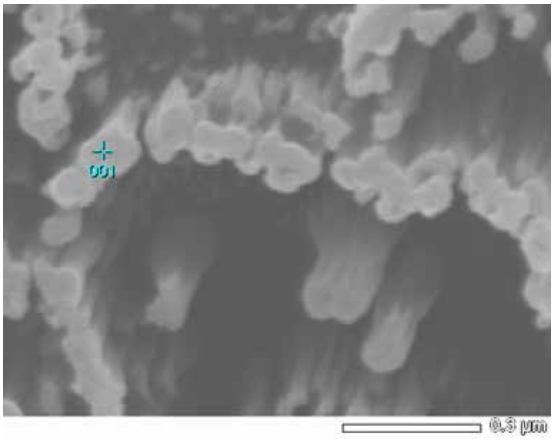

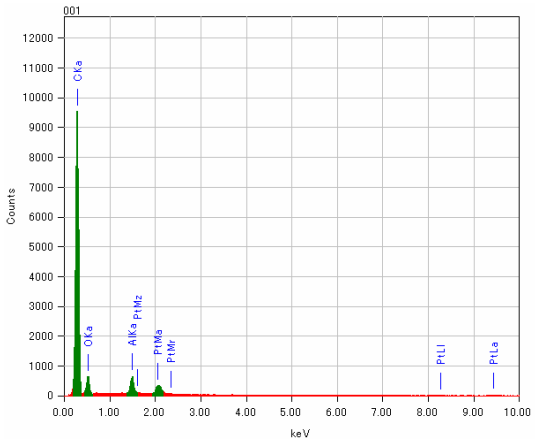

(a) (b)

Fig. 5.18. EDX spot measurement of whiskers obtained on 10 min Al-coated diamond film, tip of the whisker.

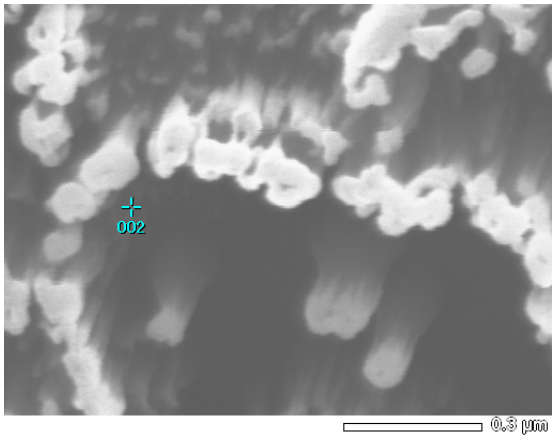

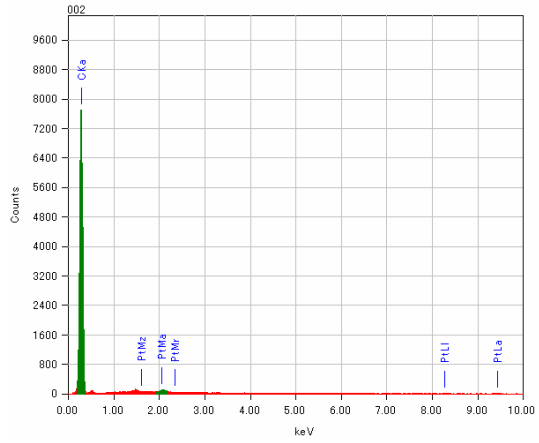

(a) (b)

Fig. 5.19. EDX spot measurement of whiskers obtained on 10 min Al-coated diamond film, non-whiskers point.

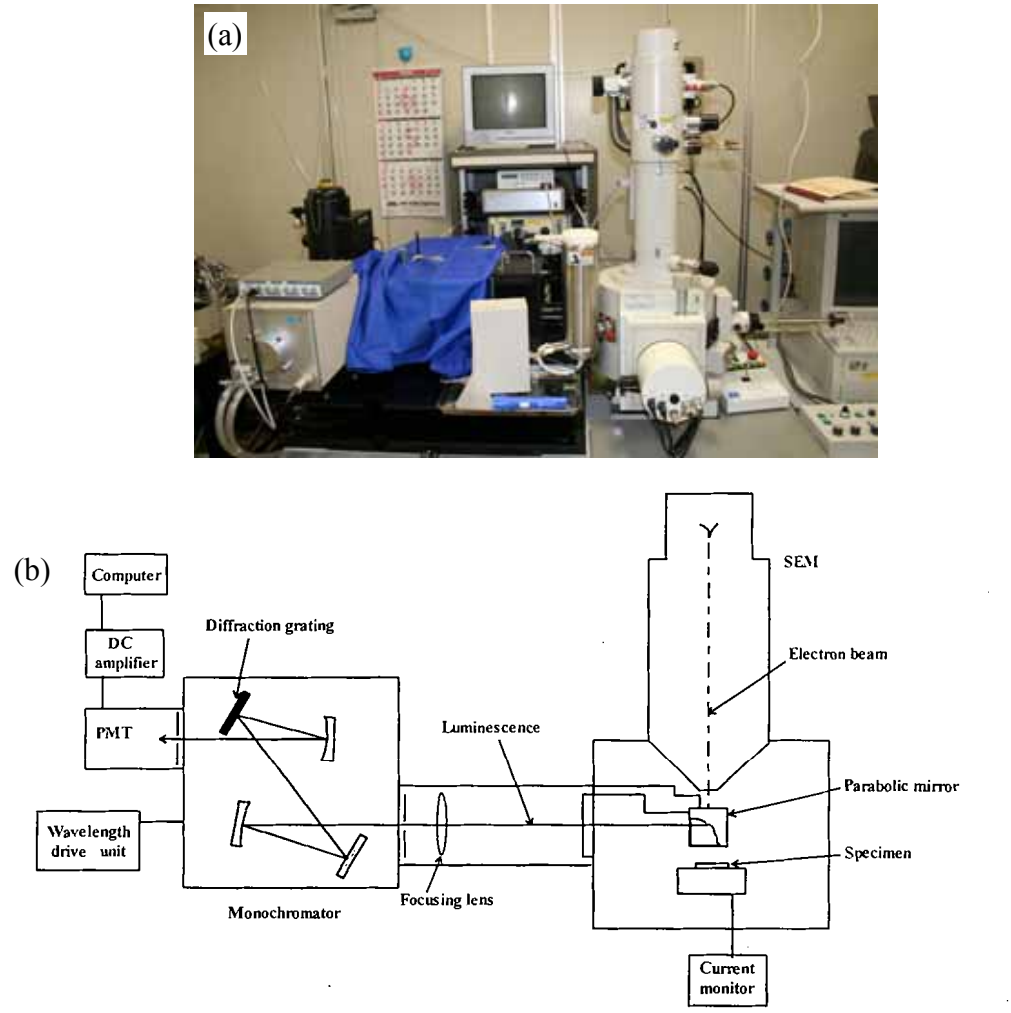

Fig. 5.20. (a) A Topcon 350 type scanning electron microscope used for cathodoluminescence spectroscopy in this research, and (b) a schematic diagram of the Cathodoluminescence spectroscopy measurement system.

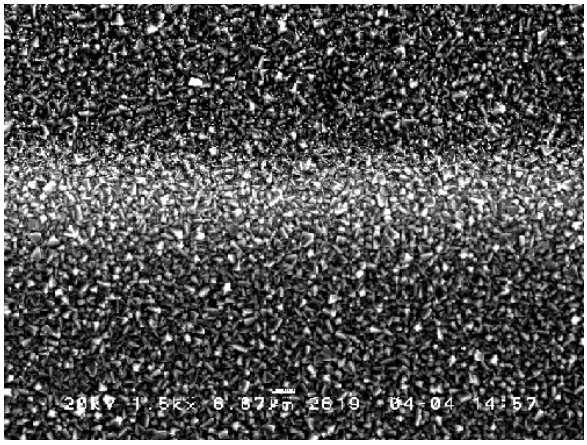

(a)

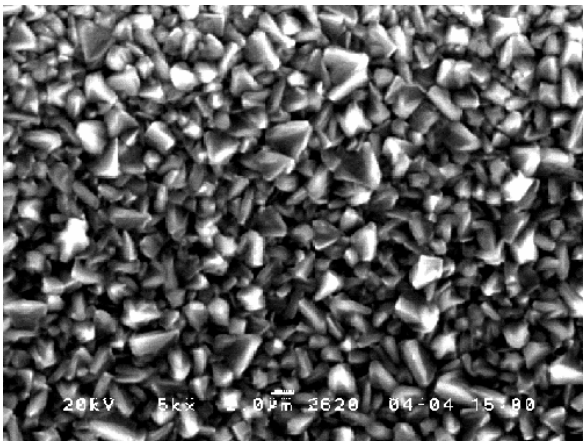

(b)

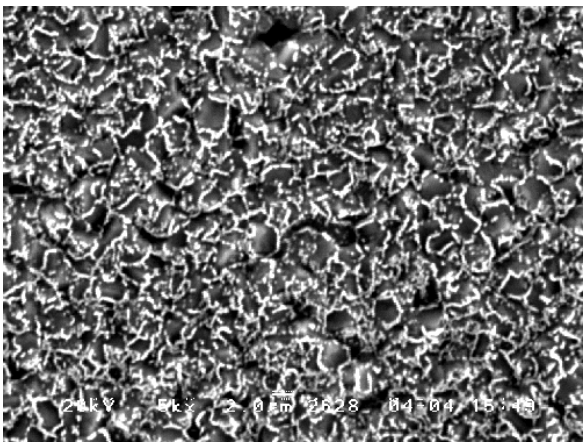

(c)

Fig. 5.21. SEM images of 10 Mo -coated diamond film. Half of the sample was etched (a) A separated line between diamond and whiskers can be observed clearly, (b) diamond part and (c) whiskers part.

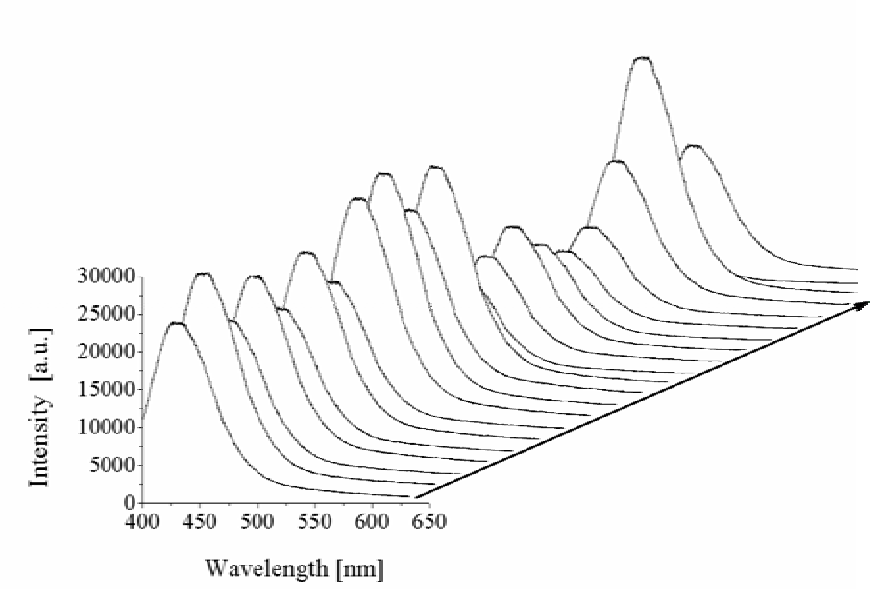

Fig. 5.22. CL measurement on the Mo-half coated diamond film. The arrow direction illustrates the examination points from whiskers to diamond part.

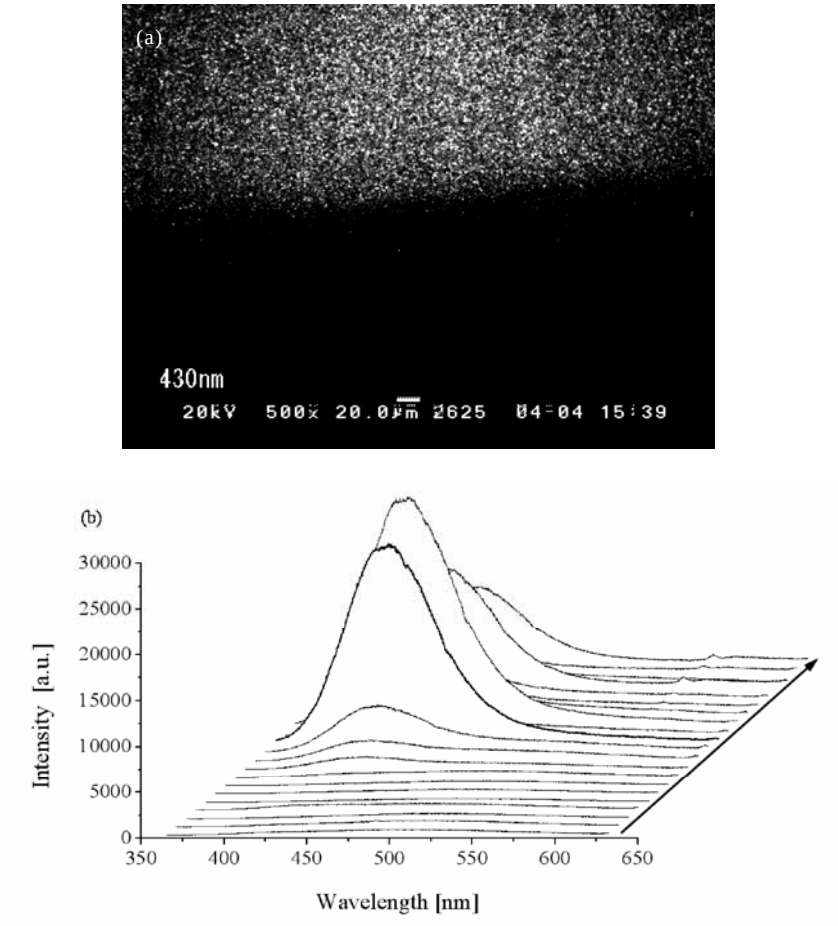

Fig. 5.23. CL measurement on the Ni half-coated diamond film. The arrow direction illustrates the examination points from whiskers to diamond part.

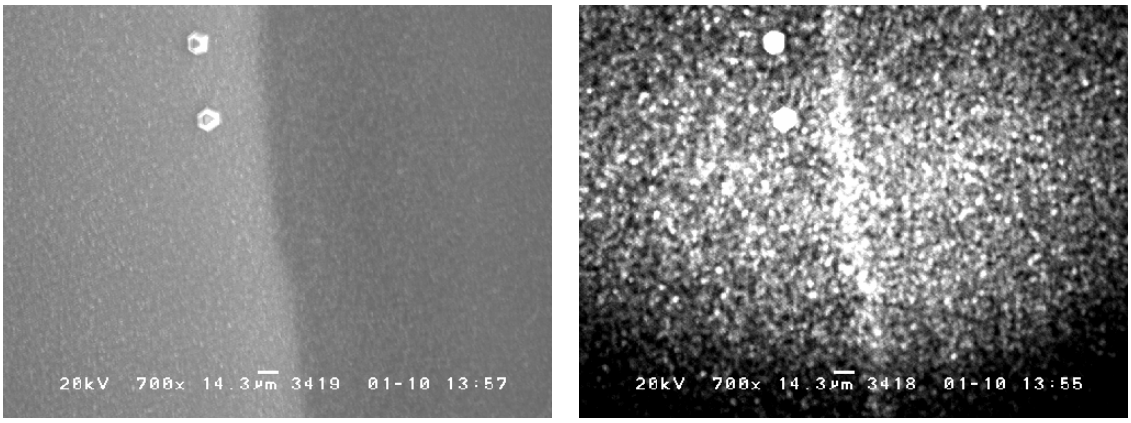

(a) (b)

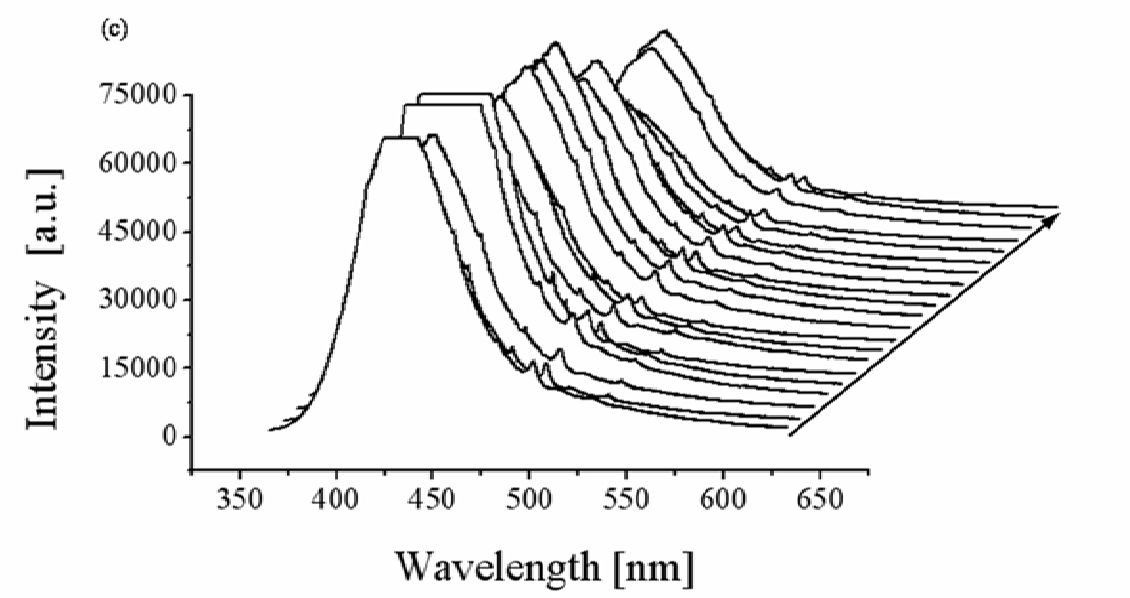

Fig. 5. 24. CL measurement on the Fe half-coated diamond film. The arrow direction illustrates the examination points from whiskers to diamond part.

References

[1] C. V. Raman and K. S. Krishnan, Nature **121**, 521 (1928).

[2] S. A. Solin and A. K. Ramdas, Phys. Rev. B **1**. 1687 (1970).

[3] L. H. Robins, E. N. Farabaugh, and A. Feldman, J. Mater. Res. **5**, 2456 (1990)

[4] A. M. Bonnot, Phys. Rev. B **41**, 6040 (1990).

[5] S. A. Stuart, S. Prawer and P. S. Weiser, Appl. Phys. Lett. **62**, 1227 (1993)

[6] G. Davies, P.A. Thrower, Chemistry and Physics of Carbon, Marcel Dekker Inc., New Yok, 1 (1977).

[7] M. C. Tobin, Laser Raman Spectroscopy, Wiley (Interscience), NY (1971)

[8] J. Filik, Spectroscopy Europe **17,** 11 (2005).

[9] F. Tuinstra and J. L. Koenig, J. Chem. Phys. **53**, 1126 (1970).

[10] D. S. Knight and W. B. White, J. Mater. Res. **4**, 385 (1989).

[11] J. Tessmer, and D. L. Dreifus, Appl. Phys. Lett. **62**, 1803 (1993).

[12] B. G. Yacobi and D. B. Holt, Cathodoluminescence Microscopy of Inorganic Solids, Plenum, 292 (1990).

[13] A. S. Marfunin, Spectroscopy, Luminescence, and Radiation Centers in Minerals, Springer-Verlag, 1979.

[14] B. G. Yocobi and D. B. Holt, J. Appl. Phys. **59**, R1 (1986).

[15] F. A. Ponce, D. P. Bour, W. Gotz and P. J. Wright, Appl. Phys. Lett. **68**, 57 (1996).

[16] H. J. Fan, F. Bertran, A. Dadgar, J. Christen, A, Krost, and M. Zacharias, Nanotech. **15**, 1401 (2004).

[17] J. E. Ralph, Proc. Phys. Soc. London **76**, 688 (1960).

CHAPTER 6

ELECTRON FIELD EMISSION CHARACTERISTICS OF DIAMOND WHISKERS

6.1 Introduction

There has been theoretical interest in diamond's electronic properties since the beginning of the semiconductor age. The "diamond emission era" started in 1991. There were 3 papers, firstly, reported unexpectedly high electron emissivity from diamond [1-3]. After that many groups paid more attention to the electron emission from diamond materials.

As mentioned in the Chapter 2, diamond has many unique properties. Among them one of the more unusual and important properties is its presentation of a rather small barrier to the emission of electrons into the vacuum. This barrier has been reported to be as low as 0.05 eV [4]. Comparing to other materials, diamond has remarkable advantage, such as behaving as a refractory material that does not melt but rather sublimes at 3550 ℃ and has an associated low vapor pressure ($<< 10^{-11}$ Torr at 100 ℃). This combination of a low barrier to electron emission in an otherwise stable, robust material has attracted attention from electronic researchers. The motivations for this increasing activity are prospective applications in vacuum microelectronics that is vacuum emission devices fabricated by modern microelectronic technologies. Experts expect that combining the physical advantages of emission devices and the technological progress in solid-state microelectronics will result in the development of an entirely new generation of high-performance electronic devices-among them, for instance, flat-panel display and miniature microwave tubes [5].

6.2 Theory of field emission from diamond

6.2.1 Explanation of electron emission

The various semiconductor emission processes are illustrated in Fig. 6.1 [6]. Electrons inside a solid cannot escape into vacuum under equilibrium conditions because of the potential barrier at the surface. The barrier must always be positive for equilibrium electrons because of the requirement for stability. In order to overcome this barrier, external energy is required to excite the electrons

(e.g. thermionic, photo-and secondary electron emission, or emission through a p-n junction.) to create metastable nonequilibrium states (exoemission) or to apply high electric fields to the surface (field emission).

The theory of electron emission from a solid was originally developed by Richardson [7] based on the thermodynamic theory of vapor pressure. The electrons were treated as a substance that escapes from the solid state into a vacuum. Some of these electrons are absorbed again eventually equilibrium is established. The equilibrium between these two rates changes with temperature. As the temperature of the system increases, electrons escape into the vacuum faster than they find their way back to the surface and become reabsorbed.

The Richardson-Dushman equation relates the current density of a thermionic emission to the work function and temperature of the emitting material:

$$j_s = AT^2 \exp(-W / kT), \tag{6.1}$$

where

j_s is the current density of the emission (mA/mm^2);

A is Richardson's constant (approx. 1202 mA/mm^2K^2);

T is temperature (K);

W is the work function of the cathode material (J);

k is the Boltzmann constant ($1.38066E^{-23}$ J/K).

Only those electrons at the highest energy levels allowed by their probability distribution have the energy to escape. At room temperature, the average energy is about 0.025 eV. The energy necessary to overcome the barrier to emission is typically about 4.0-4.5 eV for most materials of interest. At room temperature, a vanishingly small percentage of electrons have the energy necessary to clear hurdle.

The simplest way to change this situation is to modify the statistics to increase the number of electrons that will have the energy to clear the hurdle and escape. This can readily be done by heating the emitter–that is to heat the filament that emits electrons to excite the cathodoluminescent color phosphors. This technique works well and is used in electron guns in cathode-ray tube (CRT). However, the disadvantage is the high power consumption and thermal shock effect due to the start up and shutdown transients.

One way early performed by Heinrich Hertz and Wilhelm Hallwachs [8, 9] demonstrated the electron can be removed from a solid when its surface is irradiated by ultraviolet light, whereas no charge was observed for positive charge, which is the basic foundation of photoelectric effect, which can be explained by the fundamental photoelectric equation [10], the maximum kinetic

energy $E_{kin}^{\max}$ of the emitted electrons is:

$$E_{kin}^{\max} = h\gamma - \Phi_0 \tag{6.2}$$

Where h γ is the photo energy, Φ_0 is work function.

There is another way to exploit the energy-probability statistics to increase electron from a source. From the quantum mechanical tunneling theory, if under the normal condition, a disappearingly small percentage of electrons will tunnel through the energy barrier provided by the interface between an emitter and vacuum. It can presume, from this theory, that an electron is more likely to go through the more narrow width of the energy barrier. The width can be varied by supplying a very large electric field at the surface. The governing equation for field emission is the Fowler-Nordheim equation [11]

$$J = a\frac{(BF)^2}{\phi}\exp\left(-\frac{b\phi^{\frac{3}{2}}}{\beta F}\right). \tag{6.3}$$

where ϕ(eV) is the barrier height, F is the applied field, β is the field enhancement factor, and *a* and *b* are constants. The local field at the emission site is βF.

The Fowler-Nordheim theory is the most commonly used model for the emission of cold electrons from a metal under a strong applied field. When ln (I/V^2) is plotted versus 1/V (F-N plot), one should obtain a straight line, implying the emitters show characteristics of field emission.

Over 80 years, the theory and finding of Fowler and Nordheim has been used to explain and analyze the field emission phenomenon.

6.2.2 Diamond field emission

Comparing to other materials, diamond possesses very strong bonding as demonstrated by its high melting temperature, low vapor pressure, extraordinary hardness, and high thermal conductivity. Diamond has been shown to have a negative electron affinity (i.e., the conductive band is above the vacuum level) and a low work function [12-14]. Fig. 6.2 shows the band diagram for diamond.

Note in this diagram that the band gap is about 5.5 eV and the conduction band (E_c) is about the vacuum level (E_{vac}). The difference between the conduction band and the vacuum level is the electron affinity χ. For hydrogen terminated diamond, the affinity is negative. This relationship is such that an electron in the conduction band near the surface would "prefer" to leave the crystal. However, the current predicted is not very high. The free carrier concentration in a perfect diamond crystal is very low due to the high energy band gap. It was found the primary source of free carriers in diamond comes from the graphitic phase which exists in not only highly crystalline diamond but also polycrystalline, because it has been confirmed that high concentration free carriers remain in the material with poor crystalline quality [5].

As most results of low field emission are from CVD diamond of both n and p types, with poorly characterized surfaces, it now seems clear that negative electron affinity (NEA) is not fully responsible for the process. In fact, there is a wide range of models such as the defect model [12], the conducting channels in insulting diamond [15], dielectric breakdown [16-19], tip emission [20], tunneling [21] and hot electron injection [22], that attempt to explain low field emission.

However, as mentioned in last section, the electron emission relies on electrons with enough energy to clear the hurdle presented by the surface, or on the use of an electric field to thin the barrier to the extent that comparatively unenergetic electrons can escape through tunneling. Therefore, these two kinds of emission from diamond still dominated:

(1) Fowler-Nordheim field emission: electrons tunnel from a metal into either a vacuum level or the conduction band of a negative electron affinity (NEA) diamond surface.

(2) Surface conduction emission (SCE): electrons tunnel into surface states existing at the interface between a NEA diamond surface and vacuum.

Emission from the diamond is sensitive to surface treatments. Much better emission was achieved for "rough" substrates [20]. The results can be explained by emission from sharp protrusions at the diamond or interface of diamond and substrate. Hence, many groups attempted to make the diamond surface roughly or shape diamond surface with sharp structures which so called whiskers, rods, pillars, *etc*.

One new method of preparation of diamond whiskers on diamond single crystal substrate was reported as early as 1968 [23]. However, progress in this direction was not made, probably due to limitation of micro manufacture technique. It was difficult to control the whiskers dimensions. With the developing of integrated circuit, in recent years, the micro-, nano diamond technique was considered as one important research field [24-28].

From the early cold emission studies of diamond, two approaches, as shown in Figs. 6.3 (a) and (b) [6], were formulated that originated from different research fields. The first approach assumed that only the material properties (low work function, negative electron affinity, etc) were keys to controlling emissivity. This approach resulted in the development of "planar" cold cathodes, as shown in Fig. 6.3 (a), that were to become revolutionary generation electron emission devices

replacing “classical” field emission tips-Spindt tip (as shown in Fig. 6.4 [29]). It was postulated that flat structures could be manufactured cheaply and that an efficient electron source could be produced by a process not requiring submicron scale techniques, a drawback of sharply point field emitters.

In another approach, the cathode geometry was always considered a key factor and the cathodes were fabricated by deposition of thin diamond coating onto the ends of sharply pointed field emission tips, as shown in Fig. 6.3 (b). The emission threshold, maximum current density, current stability, and reproducibility of emission parameters are all improved comparing to Si tips [30].

However, with the development of microfabrication technique, A new generation of the field emitter using nanostructure was expected. In this research, the field emission cathode is replaced by needle-shaped diamond whiskers. The fabrication processes of the whiskers were described in Chapters 3 and 4.

6.3 Experimental Method

6.3.1 Sample preparation

The CVD diamond films were deposited onto Si (100) substrates (previously abraded with 5-12 μm diamond grit) by a MWPCVD systems (ASTeX) using a mixture of methane and hydrogen. During the deposition, the microwave power was 5 kW and the pressure was 124 Torr, the substrate temperature was kept during 850-930 ℃. The surfaces of diamond films were free or coated with different metals (Mo, Al, Fe) using the DC sputtering system. The conditions were dependent on the metal targets, as referred in Chapter 3.

The etching was performed using the 13.56 MHz radio frequency reactor and the O_2 as the sole process gas. The process pressure was 22 Pa and the RF power was 100 W (DC self bias voltage was -510V). The etching conditions were set up for different samples, as mentioned in Chapters 3 and 4. The different types of diamond whiskers were formed as a result of etching.

The samples before field emission measurement were treated in the hydrogen plasma for 10 min. The hydrogen treatment effects [31] are:

(1) Clean the diamond surface by removing contaminants such as carbonaceous and oxygen-or nitrogen-containing materials and preferentially etches away graphitic or amorphous carbon presented on the surface or along the particulate boundaries.

(2) Saturates dangling bonds on the diamond surface with hydrogen, leading to a hydrogenated NEA surface.

(3) Improve particles-to-particles bonding through vapor transport and diffusional reactions. The surface property of negative or low electron affinity coupled with the inherent defective structure was considered to be the main factor making the diamond as a good

field emitter.

6.3.2 Field emission measurement apparatus

In this research a field emission measurement system was installed in an SEM observation chamber, as shown in Figs. 6.5 (a) and (b): Fig. 6.5 (a) is a picture of the field emission measurement system, and Fig. 6.5 (b) is an inside structure of the anode and cathode (sample) structure, respectively.

The characterization of field emission properties was performed in a specially designed vacuum chamber by controlling the distance (d) and parallelism between the anode and cathode (samples) surfaces using a precisely combined XYZ-angular micrometer stage, as shown in Fig. 6.5 (c). The advantage of this kind of measurement is that the sample surface can be observed before and after measurement. The emission site can be defined precisely to micro area (the diameter of the anode is 12 μm). The distance between the anode and the cathode can be adjusted precisely.

The field emission characteristics of the films were tested using a diode configurations consisting of a cathode (the diamond whiskers under test) and an alloy tip anode (cylinder shape, 12 μm diameter) mounted on a substrate holder in an SEM vacuum chamber system, as shown in Fig. 6.5 (b) in last section.

The tip-sample distance was adjustable at 5, 10, and 20 μm. A needle gap image is shown in Fig. 6.6. A high voltage source current meter (KEITHLEY 6517A) was applied to the cathode using a power supply system and current measurement, as shown in Fig. 6.7.

During the test, it was found necessary to ramp the voltage up and down several times in order for the I-V curves to stabilize and become reproducible. This conditioning or activation effect has been reported previously [32], and is often accompanied by morphological changes on the surface of diamond film.

The structure and morphology of the diamond film and whiskers were inspected at high resolution using a JEOL 7400 FSEM, both before and after field emission measurements.

6.4 Experimental results and discussion

Figures 6.8–11 show the results of the field emission measurement obtained on the Al, Mo, Fe coated diamond films. The emission current (I) was measured as a function of anode-to-cathode voltage in an SEM vacuum chamber.

From the I-V curves of these samples, it can be found that when the applied voltage was 1000 V for every sample, the emission current reached 10^{-5}~10^{-4} A for Al, Fe coated samples. A largest emission current of 1 mA was obtained from the Mo coated diamond film. The emission currents were improved more than that from the original CVD diamond. By plotting the I-V data as a

Fowlor-Nordheim diagrams which are small insets in the each I-V curves of Fig.6.8-11 for a fixed cathode-anode distance (d) of 5 μm, there is good linearity in the ln (I/V^2) versus 1/V plot. It clearly found that all samples showed the field emission characteristic.

Analyzing the above field emission results, the field emission current density can be calculated (An example: whiskers obtained from Mo-coated sample) by anode diameter (12 μm) and the maximum emission current. The current density obtained from the whiskers (about 10^{-5} A/ μm^2) is much larger that from the original diamond film (about 10^{-7}A/ μm^2) although the threshold voltage is almost same about 60 V/ μm when the applied voltage is approach 1000 V. The field emission measurement points were uniformed selected on the etch sample surface. The field emission results are stable, which illustrated the reproducibility of the field emission.

After the field emission measurement, the samples were examined by FESEM. One unexpected phenomenon was that damage was found on the original diamond surface, as shown in Fig. 6.12. However, one interesting phenomenon is that no damage was found on the diamond whiskers after the same emission measurement. The nature and appearance of damaged sites varied depending upon the properties of the film and the testing conditions. These damage sites were believed to occur as a result of an extremely high local current density in the vicinity of the emission sites, causing dielectric breakdown of the surface, followed by rapid heating and vaporization of the surface layer [33]. Considering the thermal conductivity, the diamond film is apparent much larger than the diamond whiskers. However, the whiskers on the diamond surface fabricated much higher density emission sites than the only boundaries of diamond films. It is easier to presume that the same high current on the whiskers which obtained from the same area of diamond will be dispersed by different emission sites, which is the reason why no damage sites occurred on the diamond whiskers.

The results illustrated that the diamond whiskers has much better thermal conductivity than that of the diamond film. Therefore, the nanostructures of the diamond can improve thermal conductivity of diamond.

6.5 Summary

Field emission characteristics of the diamond film and metal (Al, Mo, Fe) coated diamond films were investigated. The results show the improved field emission property obtained from the diamond whiskers. The highest emission current was obtained from whiskers fabricated on the Mo coated diamond film. The emission current density (about 10^{-5}A/ μm^2) is much larger that from original diamond film. The emission measurement is reproducible because the uniformed surface measurement. There was no damage site found on the surfaces of diamond whiskers due to the higher density emission site dispersed the high current. It can help to prevent the cathode emitter from damaging due to the high emission current.

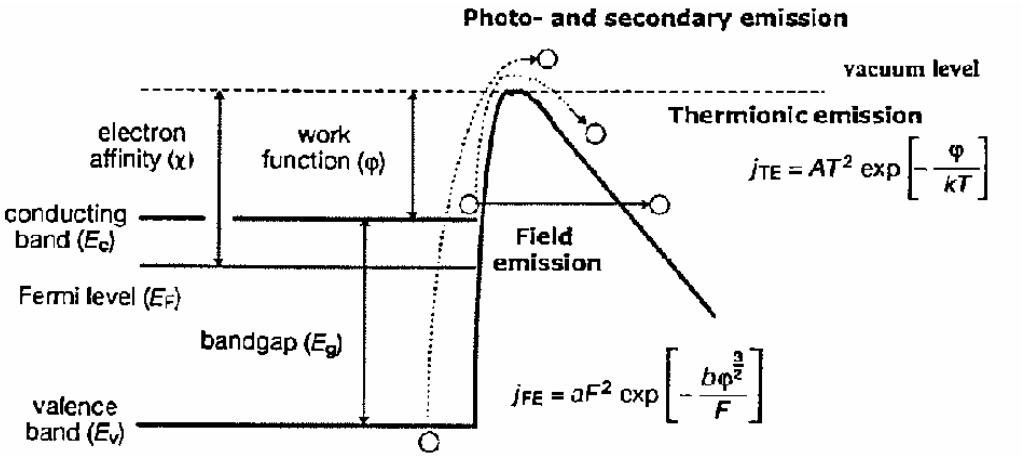

Fig. 6.1. The various electron emission processes [6].

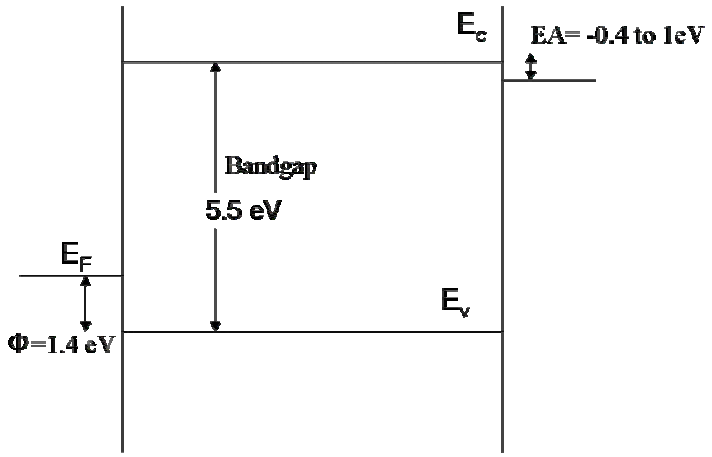

Fig. 6.2. The band diagram for diamond.

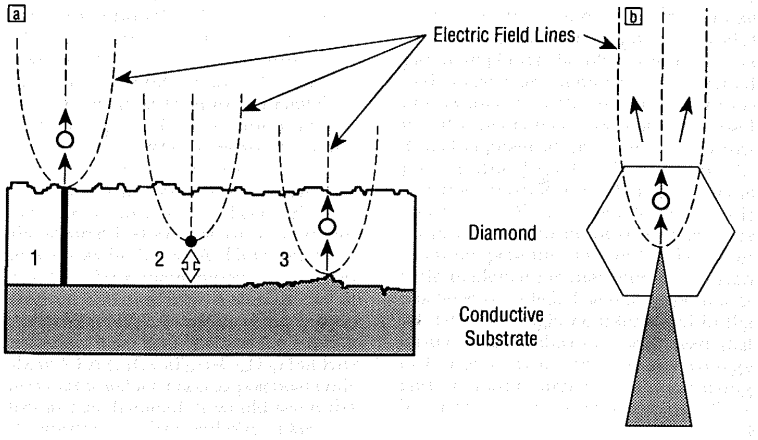

Fig. 6.3. Illustration of two cold emission mechanisms: (a) planar, and (b) coating diamond thin film onto "classic" field emission tips.

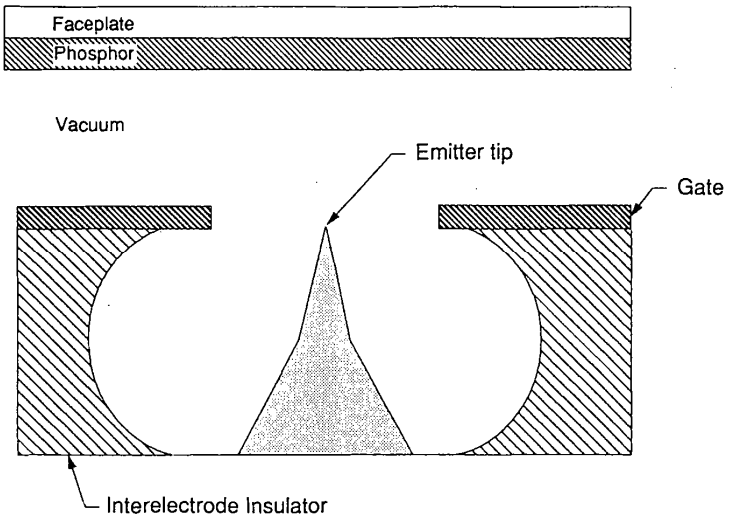

Fig. 6.4. "Classic" field emission tips—Spint tips using as a field emitter.

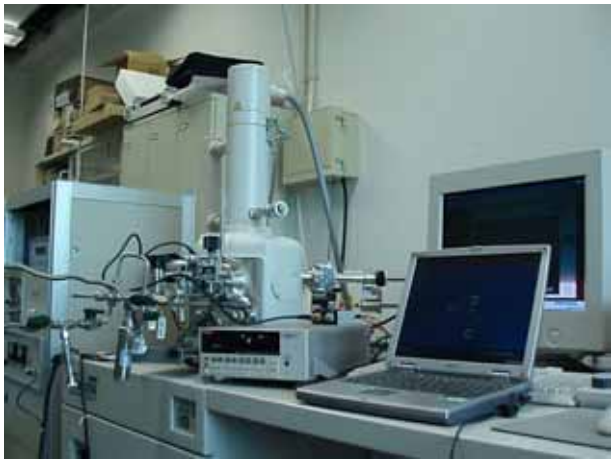

(a)

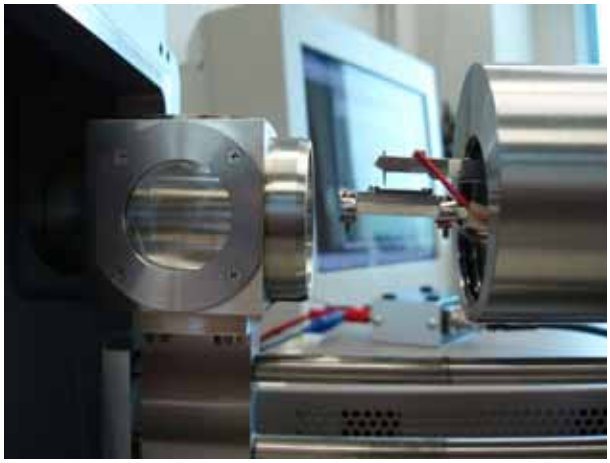

(b)

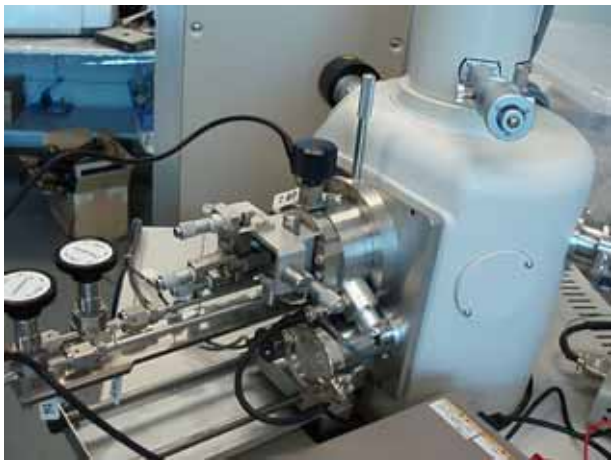

(c)

Fig. 6.5. (a) A picture of the field emission measurement system, (b) an inside structure of the anode and cathode (sample), and (c) field emission measurement stage.

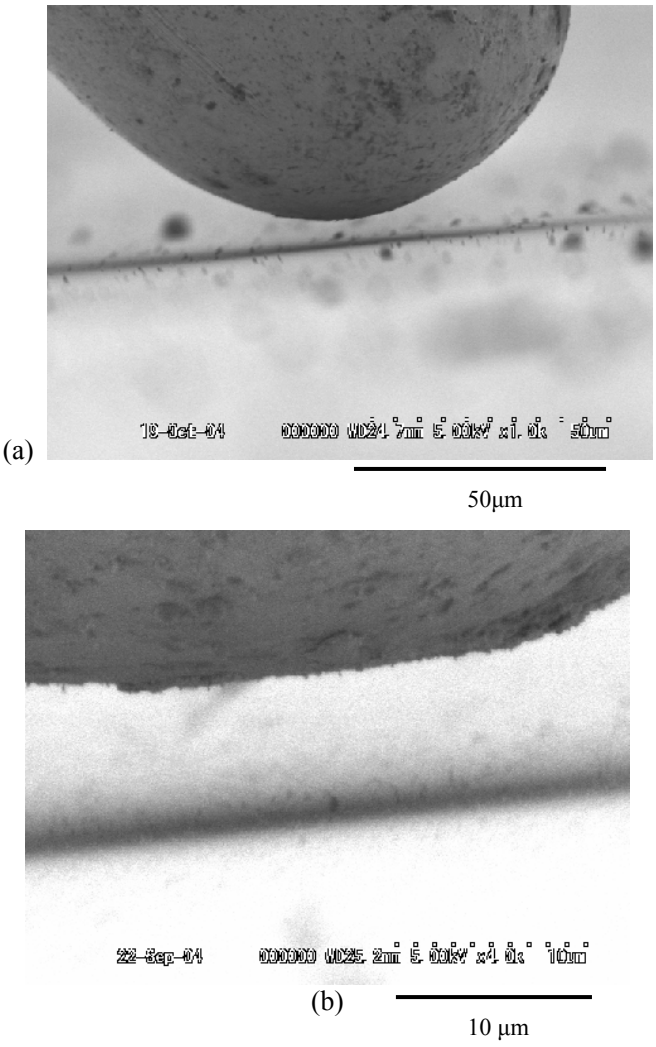

Fig. 6.6: Needle gap images: (a) alloy anode and diamond cathode and (b) 10 μm distance.

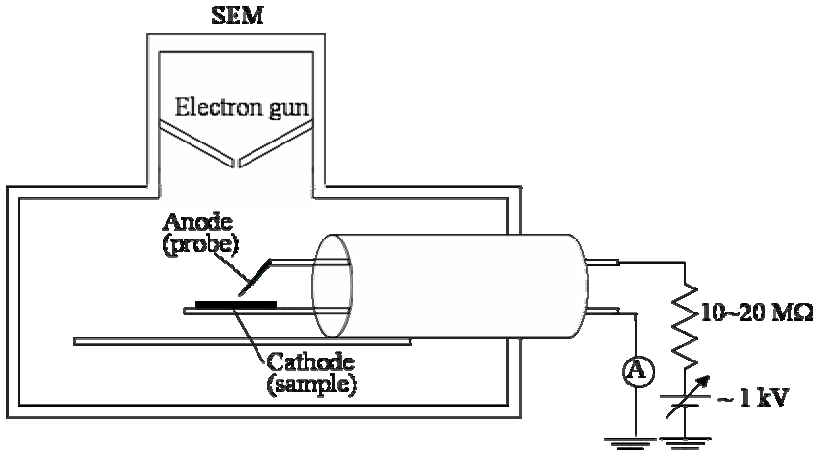

Fig. 6.7. A schematic of the field emission measurement system.

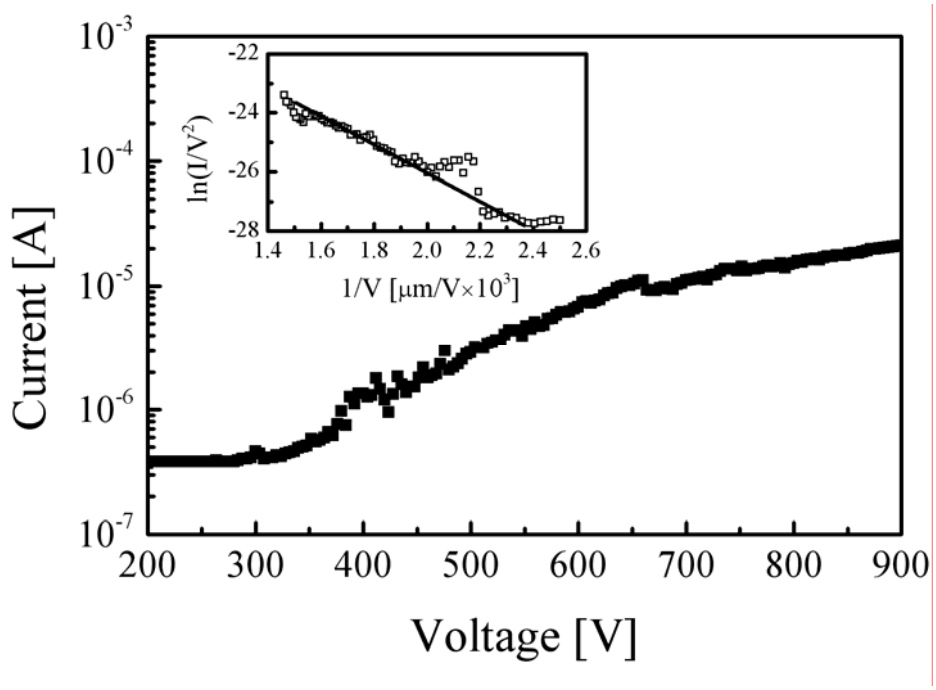

Fig. 6.8. Field emission measurement of original diamond film: I-V curve and insert of F-N plot.

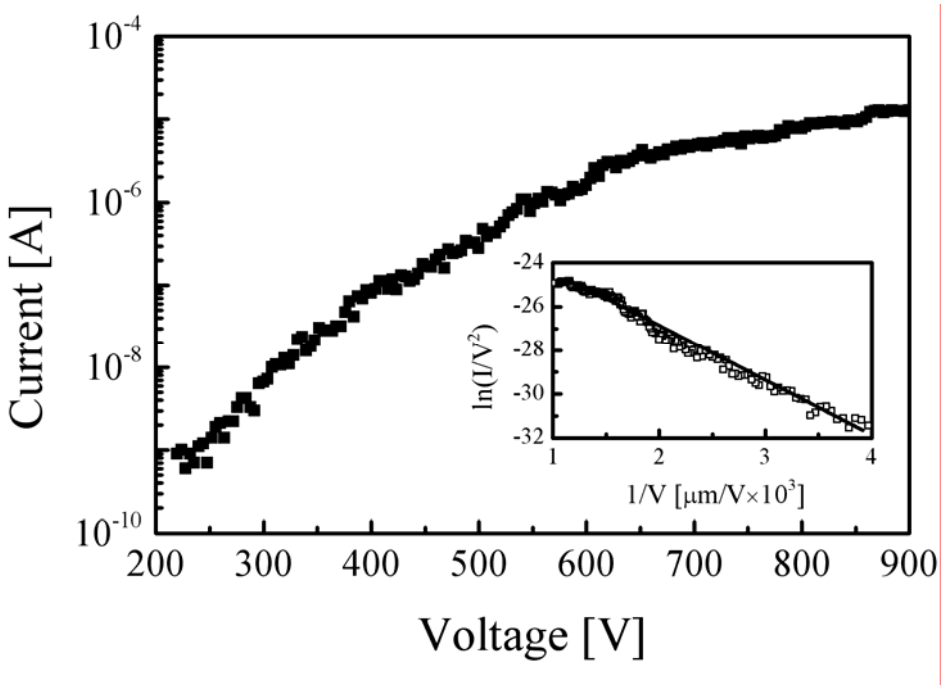

Fig. 6.9. Field emission measurement of whiskers obtained from Al coated diamond film: I-V curve and insert of F-N plot.

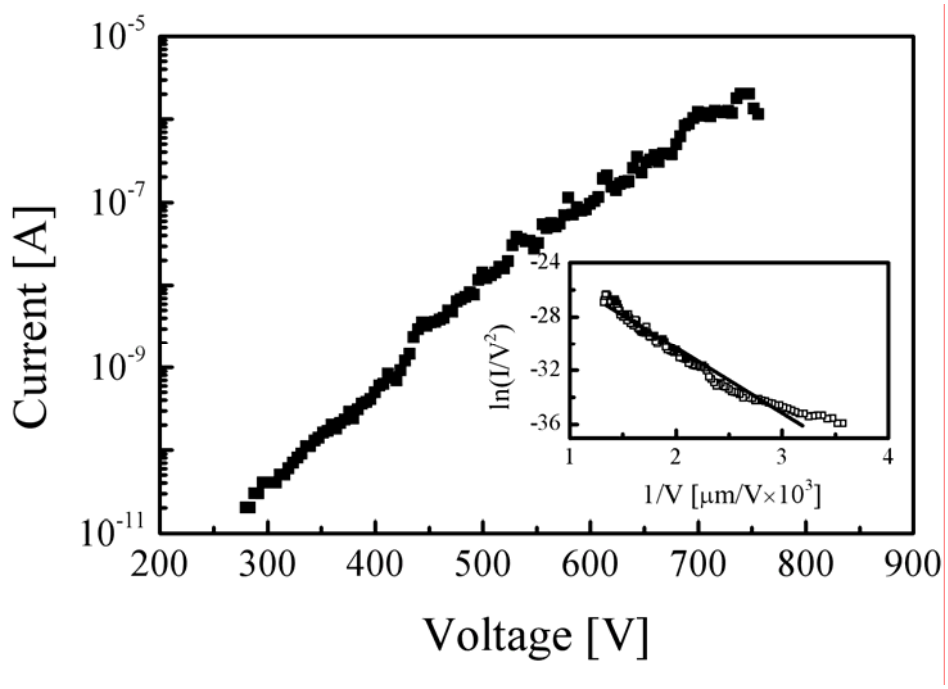

Fig. 6.10. Field emission measurement of whiskers obtained from Fe coated diamond film: I-V curve and insert of F-N plot.

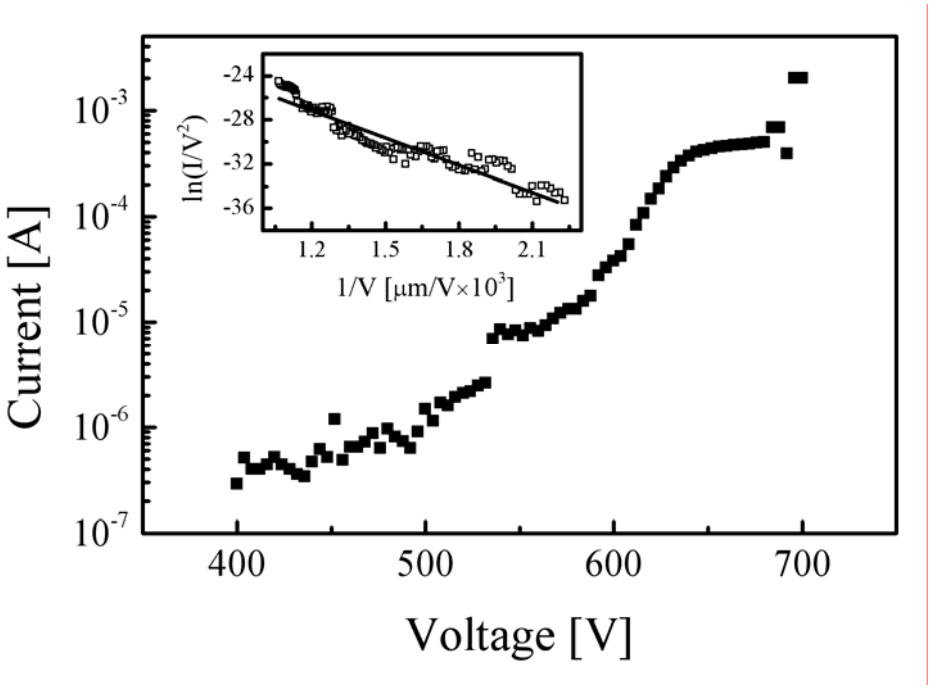

Fig. 6.11. Field emission measurement of whiskers obtained from Mo coated diamond film: I-V curve and insert of F-N plot.

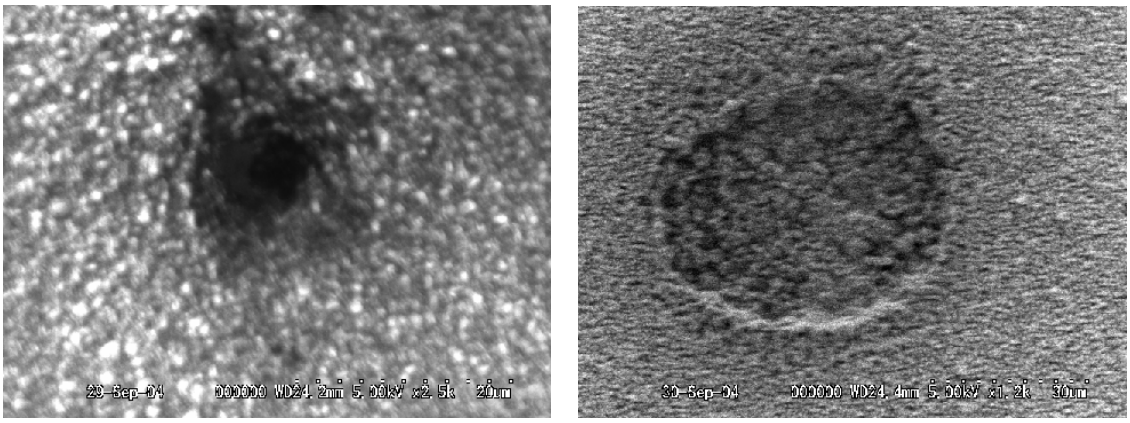

(a) (b)

Fig. 6.12. SEM images of the damage site on the diamond surface after field emission measurement.

References

[1] B. C. Djubua and N. N. Chubun, IEEE Trtans. Electon Devices **38**, 2314 (1991).

[2] C. Wang, A. Garcia, D. C. Ingram, and M. E. Kordesh, Electron. Lett. **27,** 1459 (1991).

[3] M. W. Geis, N. N. Efremov, J. D. Woodhouse, M. D. McAleese, M. Marchywka, D. G. Socker, and J. F. Hochedez, IEEE Electron Device Lett. **12**, 456 (1991).

[4] G. A. J. Amaratunga and S. R. P. Silva, Proc. of Inter. Conf. on Amorphous Semiconductors **4**, 39 (1995).

[5] J. E. Jaskie, MRS Bulletin **21**, 59 (1996).

[6] V. V. Zhirnov and J. J. Hren, MRS Bulletin **9**, 42 (1998).

[7] P. W. Bridgeman, The Thermodynamics of Electrical Phenomena in Metal (Macmillan, New York, 1934).

[8] H. R. Herz, Physik und Chemie, **31,** 983-1000 (1887).

[9] W. Hallwachs, Physik und Chemie, **33**, 301 (1888).

[10] A. Einstein, Ann. Phys. **17**, 132 (1905).

[11] R. H. Flower and L. Nordheim, Proc. Roy. Soc. Lond. **119**, 13 (1928).

[12] B. B. Pate, W. E. Spicer, T. Ohta, and I. Lindau, J. Vac. Sci. and Technol. **17**, 1087 (1980).

[13] N. Eimori, K. Maeashi, A. Hatta, T. Ito, and A. Hiraki, 3rd Int. Symp. Diamond Mater., 934 (1993).

[14] C. Xie, C. N. Potter, P.L. Fink, C. Hilbert, A. Krishnan, D. Eichman, N. Kunar, H. K. Schmidt, B. Baker, D. Patterson, and W. Brookover, Int. Vac. Microelectronics Conf. Pro. **271**, 229 (1994).

[15] W. Zhu, G. P. Kochanski, S. Jin, and L. Seibles, J. Vac. Sci. Technolol. **14,** 2011 (1996).

[16] N. S. Xu and R. V. Latham, J. Phys. **19**, 477 (1986).

[17] O. Groning, O. M. Kuttel, E. Schaller, P. Groning, and L. Schlabach, Appl. Phys. Lett. **69**, 476 (1996).

[18] R. Hessmer, M. Schreck, S. Geier, and B. Strizker, Diamond Relat. Mater. **3**, 951 (1994).

[19] W. N. Wang, N. A. Fox, T. J. Davis, D. Richardson, G. M. Lynch, J. W. Steeds, and J. S. Lee, Appl. Phys. Lett. **69**, 2825 (1996).

[20] M. W. Geis, J. C. Twichell, and T. M. Lyszczarz, J. Vac. Sci. Technol. **14**, 2060 (1996).

[21] M. W. Geis, J. C. Twichell, J. Macaulay, and K. Okano, Appl. Phys. Lett. **67**, 1328 (1995).

[22] Z. H. Huang, P. H. Cutler, N. M. Miskorvsky, and T. E. Sullivan, Appl. Phys. Lett. **65**, 2562 (1994).

[23] B. V. Derjaguin, D. V. Fedoseev, V. M. Lukyanovich, B. V. Spitzin, V. A. Ryabov, A. V. Lavrentyev, J. Cryst. Growth **270**, 1179 (1968).

[24] K. Okano, T. Yamada, H. Ishibayashi, S. Koizumi, J. Itoh, Appl. Phys. Lett. **70**, 2201 (1997).

[25] H. Shiomi, Jpn. J. Appl. Phys. **36**, 7745 (1997).
[26] O. Kornienko, P. T. A. Reilly, W. B. Whitten, J. M. Ramsey, Anal, Chem. **72**, 559 (2000).
[27] T. Ito, Nonmember, IEICE Trans. Electron. **5,** 797 (2003).
[28] J. L. Davidson, W. P. Kang, A. Wisitisora-At, Diamond Relat. Mater. **12**, 429 (2003).
[29] C. A. Spindt, I. Brodie, L. Humphrey, and E. R. Westerberg, J. Appl. Phys. **47**, 5248 (1976).
[30] V. V. Zhirnov, E. I. Givargizov, A. V. Kandidov, B. V. Seleznev, and A. N. Alimova, J. Vac. Sci. Technol. **15**, 446 (1997).
[31] N. A. Fox, W. N. Wang, T. J. Davis, J. W. Steeds, and P. W. May, Appl. Phys. Lett. **71**, 2337 (1997).
[32] W. Zhu, G. P. Kochanski, S. Jin, Science **20**, 1472 (1998).
[33] R. Hessmer, M. Schreck, S. Geier, and B. Sritzker, Diamond Relat. Mater. **3**, 951 (1994).

CHAPTER 7

CONCLUSIONS

A novel method to fabricate nanowhiskers on polycrystalline diamond films using radio frequency plasma etching has been demonstrated in this research work. The factors affecting the fabrication of diamond whiskers were investigated systematically. It was found that the diamond distribution was highly related to the concentration of O_2 in the O_2/Ar RF plasma. Different metals, firstly classified into oxidizable and non-oxidizable, were introduced to the etching process to investigate their effects on the formation of diamond whiskers.

As mentioned in chapter 1, the theory on fabrication of nano-sized diamond structures is still not clearly. In this research, whiskers have been characterized using Raman spectroscopy, Cathodoluminescence spectroscopy, and energy dispersive X-ray spectroscopy. Through the detailed analysis, the mechanisms of fabricating whiskers became more clearly.

For the purpose of using diamond nanowhiskers as field emitter in field emission devices, particularly in field emission display, field emission properties of the nanowhiskers were investigated. The results opened up a brilliant prospect for applying diamond whiskers in next generation field emitter replacing the traditional use of metal tips.

The main conclusions of this research are summarized as following.

Chapter 2. Synthesis of diamond film using microwave plasma chemical vapor deposition

Diamond film was deposited on Si substrate using microwave plasma chemical vapor deposition method. The temperature and the CH_4 concentration were the critical factors influencing the quality of the diamond. The quality of CVD diamond film could be controlled by adjusting the CH_4 concentration in H_2. The quality of the diamond film increased with decreasing CH_4 concentration. High quality diamond film could be obtained in CH_4 less than 1% and in optimum deposition conditions.

Chapter 3. Fabrication of diamond whiskers using Ar/O_2 radio frequency plasma etching

Diamond whiskers were firstly fabricated by etching diamond films in O_2 and O_2/Ar radio frequency plasma. The effect of etching gas ratio on the properties of whiskers was investigated. It was found that the number density of the whiskers increased with the O_2 concentration. During the etching process, O_2 contributed to both reactive ion etching and physical etching, whereas Ar only contributed to physical etching. A suitable Ar and O_2 molar ratio could efficiently increase the

etching rate. Whiskers with 30 nm in diameter and 1 μm in height were formed in the pure O_2 etching process. It was also found that Al coating was an important factor contributing to anisotropic etching. Al would react with O_2 to produce aluminum oxide remaining on the top of the diamond surface, serving as mask to protect further etching of the diamond surface.

Chapter 4. Effects of metal coating on formation of diamond whiskers in O_2 radio frequency plasma etching

The diamond whiskers were remarkably influenced by the type of coating metal. Oxidizable metals, like molybdenum, aluminum, iron, *etc*., could produce metal oxide as stable coating layer or islands on the diamond surface during etching process, contributing to the formation of high quality whiskers with lower density. Non-oxidizable metals, like nickel, gold, with poor crystallinity and higher flow ability during radio frequency plasma etching could not produce efficient protecting layer, inefficiently contributed to the anisotropy etching.

For etching on high quality diamond film, the whiskers aligned perfectly with the crystal orientations. Therefore, it is possible to control the distribution of the whisker by controlling the crystal orientation growth during MWPCVD deposition.

Chapter 5. Characterization of diamond whiskers

The diamond whiskers were characterized by Raman spectroscopy, Energy dispersive X-ray spectroscopy and Cathodoluminescence spectroscopy measurement. Raman spectroscopy measurement showed that the predominated diamond peak was centered at the 1332 cm^{-1}, the sp^3 bonding structure of the whiskers was still dominant though there were slight G or D peak appearances. Therefore, the quality of diamond film was almost not changed after radio frequency etching process.

EDX measurement confirmed the functions of metal coating. The metal particles would cap on the tips of the whiskers after coating. No metal particles were found on the non-whiskers area. The distribution of the whiskers was also remarkably influenced by the thickness of the coating metal. The high number density of the whiskers was due to the uniformly distributed metal coating layer. However, the metal particles or island contributed the lower number density.

CL measurement results made it possible to compare the functions of two kinds of metal coatings: oxidizable and non-oxidizable metals. The results showed that the oxidizable metal-coated films did not change the intensity quality of the diamond. However, the luminescent intensity dramatically decreased on non-oxidizable metal-coated films. Therefore, oxidizable metals contributed to the formation of well oriented diamond whiskers, non-oxidizable metals deteriorated the quality of diamond film during etching process.

Chapter 6. Electron field emission characteristics of diamond whiskers

Field emission characteristics of the diamond film and metal (Al, Mo, Fe) coated diamond films were investigated. The results show that improved field emission property was obtained from the diamond whiskers. The emission current density (about $10^{-5}A/\mu m^2$) is much larger that from original diamond film. The emission measurement is reproducible because the uniformed surface measurement. There was no damage site found on the surfaces of diamond whiskers due to the higher density emission site dispersed the high current. It can help to prevent the cathode emitter from damaging due to the high emission current.

Therefore, it is possible to use diamond whiskers as field emitter in next generation field emission display.

LIST OF PUBLICATIONS

A) Paper in first name:

1. Preparation of diamond whiskers using Ar/O_2 plasma etching
   Chaoyang Li and Akimitsu Hatta
   Diamond and Related Materials, 14 (2005) 1780-1783.

2. Fabrication of diamond nano-whiskers by reactive ion etching
   Chaoyang Li, Hiroaki Yoshimura, Akimitsu Hatta
   Transactions of the Materials Research Society of Japan, 30 [1] (2005) 287-290.

3. Effect of metal coating on the formation of diamond whiskers in O_2 RF plasma
   Chaoyang Li and Akimitsu Hatta
   Diamond and Related Materials, 15 (2006) 357-360.

4. Function of aluminum coating on fabrication of nanowhiskers in radio frequency plasma etching
   Chaoyang Li and Akimitsu Hatta
   Diamond and Related Materials, 15 (2006) 1122-1125.

5. Properties comparison of diamond nanowhiskers obtained from etching diamond films with different metal coatings in radio frequency plasma
   Chaoyang Li and Akimitsu Hatta
   Japanese Journal of Applied Physics, Vol. 45, No.10B

6. Whiskers formation mechanism in radio frequency Ar/O_2 plasma etching of polycrystalline diamond films with Al sputtering.
   Chaoyang Li and Akimitsu Hatta
   Thin Solid Films, in press

7. Electron and structural properties of nanowhiskers fabrication on iron-coated diamond film by radio frequency O_2 plasma etching
   Chaoyang Li and Akimitsu Hatta
   Journal for New Material for Electrochemical Systems, (submitted)

B) Other Publications

1. Fabrication of Nano-structures of Silicon and Diamond Using Plasma Processing
   Akimitsu Hatta, Hiroaki Kanakusa, Hiroaki Yoshimura, **Chaoyang Li** and Hiroyuki Fujimori
   Journal of the Surface Finishing Society of Japan (in Japanese), Vol. 56, No. 12, (2005) 121-126.

C) International Conferences

1. The 7th Asia Pacific Conference on Plasma Science and Technology Symposium on Plasma Science for Materials (APCPST): Study of Field Electron on Emission from Diamond Films Etched by RF Plasma (Poster presentation)
   Kyushu, Japan, 28/ 6/ 2004-2/ 7/ 2004.

2. The 10th International Conference on New Diamond Science and Technology (ICNDST-10): Preparation of Diamond Whiskers Using Ar/O_2 Plasma Etching (Poster Presentation)
   Tsukuba, Japan, 11/ 5/ 2005-15/ 5/ 2005.

3. The 8th Applied Diamond Conference NanoCarbon 2005 (ADC 2005): Effect of Metal Coating on the Formation of Diamond Whiskers in O_2 RF Plasma (Poster Presentation).
   Chicago, US, 15/ 5/ 2005—19/ 5/ 2005.

4. The 17th International Symposium on Plasma Chemistry (ISPC 17): Fabrication of Diamond Whiskers Using Reactive Ion Etching (Oral Presentation).
   Toronto, Canada, 7/ 8/ 2005-12/ 8/ 2005.

5. The 16th European Conference on Diamond, Diamond –Like Materials, Carbon Nanotubes, and Nitrides (Diamond 2005): Radio Frequency Plasma Etching of Diamond in O_2 and O_2/Ar Plasma (Poster Presentation).
   Toulouse, France, 11/ 9/ 2005-16/ 9/ 2005.

6. The 6th International Conference on Reactive Plasma and 23rd Symposium on Plasma Processing (ICRP6): Properties Comparison of Diamond Nano-rods Obtained from Etching Diamond Films with Different Metal Coatings in Radio Frequency Plasma (Poster presentation).
   Matsushima/ Sendai, Japan, 24/ 1/ 2006-27/ 1/ 2006.

7. The 11th International Conference on New Diamond Science and Technology and The 9th Applied Diamond Conference NanoCarbon 2006 (ICNDST&ADC 2006): Synthesis and Characterization of Diamond Nanowhiskers by Etching Iron-coated Films in O_2 Radio Frequency Plasma (Poster presentation).
North Carolina, U.S, 12/ 5/ 2006-18/ 5/ 2006.

8. The 8th Asia Pacific Conference on Plasma Science and Technology Symposium on Plasma Science for Materials (APCPST): Radio Frequency Plasma Etching of Metal Coated Diamond Films for Fabrication of Diamond Whiskers for Field Emission Application (Poster presentation).
Queen Island, Australia, 2/ 7/ 2006-5/ 7/ 2006.

9. New Materials for Electrochemical Systems (New Materials 2006): Electron and Structural Properties of Nanowhiskers Fabricated on Iron-coated Diamond Film by Radio Frequency Etching (Oral presentation).
Montreal, CA, 9/ 7/ 2006 -12/ 7/ 2006.

D) Domestic Conferences

1. The18th Diamond Symposium: Fabrication of Diamond Whiskers and Measurements of Electron Field Emission (Oral presentation).
Tsukuba, Japan, 18/ 11/ 2004-21/ 11/ 2004.

2. The 15th Symposium of the Materials Research Society of Japan: Fabrication of Diamond Nano-whiskers by Reactive Ion Etching (Oral Presentation).
Tokyo, Japan, 24/ 12/ 2004-26/ 12/ 2004.

3. Plasma Science Symposium 2005 (PSS 2005): Fabrication of Diamond Whiskers by RF Plasma Etching (Poster Presentation).
Aichi, Japan, 26/ 1/ 2005-28/ 1/ 2005.

4. The 18th Symposium on Plasma Science for Materials (SPSM-18): Nanowhiskers formation mechanism by radio frequency Ar/O2 plasma etching diamond film with an aluminum coating (Oral Presentation)
Tokyo, Japan, 28/ 6/ 2005-29/ 6/ 2005.